



BAKİ ALİ NEFT MƏKTƏBİ
BAKU HIGHER OIL SCHOOL

PETROLEUM ENGINEERING DEPARTMENT
FIELD DEVELOPMENT PROJECT
GROUP 2

Geology	Javidan Ibrahimli
Reservoir Engineering	Amil Huseynov
Drilling Engineering	Turkan Aliyeva (Team Leader)
Production Engineering	Amil Huseynov
Health, Safety and Environment	Kanan Allahverdiyev
Economics	Mahammad Mikayilov

Supervisor: **Elkhan Ahmadov**

Date of Submission: **January 14, 2021**

DECLARATION OF AUTHORSHIP

We hereby declare that the submitted report is entirely our own original work. All the external sources used for this project (methods, ideas, tables, figures, scientific papers, books, software packages, online programs etc.) have been listed properly in the References section and demonstrated within the report at their point of use. We are aware of the regulations set by university regarding the plagiarism and understand our responsibility.



Turkan Aliyeva



Javidan Ibrahimli



Kanan Allahverdiyev



Mohammad Mikayilov



Amil Huseynov

Date: December 21, 2020

ACKNOWLEDGEMENTS

Firstly, we would like to thank to our supervisor, Mr. Elkhan Ahmadov, for his continuous support, insightful feedbacks and excellent methodology. During the project, his valuable assistance and deep technical knowledge helped us to make significant progress.

Then, we would like to express our special thanks to Mr. Javid Shiriyev for his invaluable efforts for our team in terms of Reservoir Engineering section. We highly appreciate his remarkable expertise and guidance for the part of this project.

Table of Contents

EXECUTIVE SUMMARY.....	6
1. OVERVIEW.....	7
1.1. Project Description.....	7
1.2. Objectives.....	7
1.3. Mind map.....	8
1.4. Project Schedule.....	9
2. GEOLOGY	10
2.1. Introduction – Basin Evaluation	10
2.2. Structural configuration	11
2.3. Petroleum play components.....	13
2.4. Reservoir architecture and stratigraphy.....	14
2.5. Depositional Environment	15
2.6. Core Analysis.....	16
2.7. Log Interpretation	18
2.8. Log Correlation	21
2.9. RFT Analysis	23
2.10. Cross Sections.....	25
2.11. Porosity and Saturation Calculations	27
2.12. Permeability Analysis.....	32
2.13. Reservoir Heterogeneity	33
2.14. Shale Volume Calculation	34
2.15. Evaluation of Net Sand/Gross Interval.....	35
3. Reservoir Engineering.....	40
3.1. Gross Rock Volume (GRV) Calculation	40
3.2. STOIP Calculation.....	42
3.2.1. Deterministic STOIP Calculation.....	42
3.2.2. Probabilistic STOIP Calculation	43
3.3. STOIP Sensitivity Analysis	44

3.4. Drive mechanism and Reserves Estimation.....	46
3.4.1. Drive Mechanism.....	46
3.4.2. Recovery Factor (RF) Estimation	46
3.4.3. Reserve Estimation & Its Sensitivity Analysis	47
3.5. Special Core Analysis	47
3.6. Fractional Flow Evaluation	50
3.6.1. Water Injection Analysis	50
3.6.2. Fractional Flow Analysis	51
3.7. PVT Analysis	54
3.8. Reservoir Property Distribution Maps	62
3.9. Number & Location of Production and Injection Wells	64
3.9.1. Number of Production Wells	64
3.9.2. Number of Water Injection Wells	65
3.9.3. Location of Injector and Producer Wells	65
4. Drilling Engineering	66
4.1. Drilling Rig Selection & Location	66
4.2. Pressure Profile	68
4.3. Casing Design.....	70
4.3.1. Preliminary Casing Design	70
4.3.2. Detailed Casing Design	72
4.4. Cementing Design	76
4.5. Drilling Fluid Design.....	77
4.6. Drill Bit Design	79
4.7. Directional Drilling	80
4.8. BHA Design.....	81
4.9. BOP Design.....	83
4.10. Drilling Risks.....	83
4.11. Drilling Schedule	85
4.12. Lower Completion Design.....	86
4.11. Perforation Design.....	87
REFERENCES	90

Geology & Formation Evaluation	90
Reservoir Engineering	91
Drilling Engineering.....	91
 APPENDIX.....	 94
Appendix A. Geology & Formation Evaluation.	94
Appendix A1. Composite Well Logs	94
Appendix A2. Core Porosity and Permeability graphs.....	96
Appendix A3. Determination of cut-offs (core calibration method).....	97
Appendix B. Reservoir Engineering.....	100
Appendix B1. STOIIP Calculation	100
Appendix B2. PVT Analysis Tables	101
Appendix C. Drilling Engineering.....	108
Appendix C1. Pressure Profile	108
Appendix C2. Casing Design	111
Appendix C3. Cementing Design	114
Appendix C4. Directional Drilling	115
Appendix C5. Perforation Design	117

EXECUTIVE SUMMARY

The introduced report presents the outcomes of the group project dedicated to the field development planning of the X-field located in the Central North Sea and block UKCS 22/12. It is approximately 210km east north east of mainland Britain and in the water depth of 81m. In total, six appraisal wells have been penetrated into the oil containing Jurassic reservoir to obtain a wide range of data sets in order to evaluate the commercial feasibility of this project. The detailed investigation of regional geology and available data from well logging, core sampling, seismic etc. allowed us to state the detection of two reservoir sands: thick main reservoir sand and thinner Ribble sand layer which is not continuous over the entire formation. The significant amount of hydrocarbon accumulation has been discovered in this field as being supported by the presence of all the key petroleum play components. With the help of elaborate formation evaluation, two compartments of the X-field have been detected, namely south and north compartments. Their communication has been hindered by the presence of main sealing fault leading to two different oil-water contacts. At the end of the separate evaluation of these compartments, deterministic and probabilistic STOIP values have been calculated as 854 MMSTB and 839 MMSTB respectively with the slight deviation of 1.74%. After making reasonable recovery factor estimation, sensitivity analysis has been performed for reserve calculation. It concluded that the amount of reserves might change between 449 MMSTB and 673 MMSTB with 40%-60% recovery factor. As it was stated in the overview file, water aquifer support for this field is weak as just after a year of production, reservoir pressure declined by 1000 psi. Therefore, the main driving force for the X-field comes from expansion drive mechanism. This necessitates the drilling of water injection wells to provide pressure maintenance and effective voidage replacement. Based on our initial estimation, 10 production and 10 water injection wells will be drilled; however, these numbers may be subjected to changes after building dynamic reservoir modelling. For the drilling operations, a single fixed-type steel jacket platform has been selected based on the water depth, number of wells planned to drill and harsh weather conditions in the North Sea just to name a few. It has been decided to drill deviated wells to increase the formation exposure and reach reservoir targets from single platform. Well configuration typical for the North Sea – Central Graben wells has been applied to the wells of X-field as well. Based on the stratigraphy of nearby analogous Fulmar field, relevant drilling fluid and bit design were carried out.

In the 2nd semester, proper field development scenarios will be proposed and after assessing their technical and economic viability, one of them will be selected as the best development option. Heath, safety and environmental aspects will be considered as well combined with discussions concerning the sustainable development. Elaborate analysis on the evaluation of the project economy will also be included in the scope of work for the 2nd semester.

1. OVERVIEW

1.1. Project Description

This field development planning (FDP) project is dedicated to the development of the X-field located in the Central North Sea in the block of United Kingdom Continental Shelf (UKCS) 22/12. The provided overview file dictates that six appraisal wells have been drilled into the oil bearing Jurassic reservoir from 10126ft to 11175ft. The data collected from this appraisal stage have been utilized in the development of this field.

In general, oil & gas field development projects carry high risk owing to the geological, technical and economic uncertainties. The extra complication arises when there is lack of data collect at the appraisal stage and in turn, this situation requires making an elaborate evaluation of the data present and taking reasonable assumptions where needed. After assessing the technical and economic viability of the project, it can be further developed via choosing relevant FDP scenarios and making investments.

Our team – “Group 2”, consisting of 5 students, has been assigned to work on this FDP project. Although group members have agreed to take the responsibility of the particular section, all students had special contributions to each section by trying to protect the workload balance among team members.

1.2. Objectives

The key objectives of the FDP project for the first semester have been listed below:

- ❖ Meticulous analysis of the data from appraisal stage provided in the overview document;
- ❖ Careful geological analysis of the field by referring to nearby fields and various sources;
- ❖ Estimating the amount of STOIP and reserves;
- ❖ Making initial prediction for the number and location of the wells;
- ❖ Planning the typical drilling activities for one of the development wells;

It has been planned to perform the operations below for the second semester:

- ❖ Recommending the technically and economically viable FDP scenario for maximizing the amount of recoverable hydrocarbons;
- ❖ Ensuring the compliance with health, safety and environmental regulations of the UK;
- ❖ Discussing the positives and negatives of the selected FDP program concerning sustainability;
- ❖ Making efforts to reduce risks and uncertainties of the project;
- ❖ Achieving the favorable Net Present Value (NPV) of the project;

1.3. Mind map

The mind map illustrated beneath provides the clear information related to the scope of this project and lists the performed activities for separate sections:

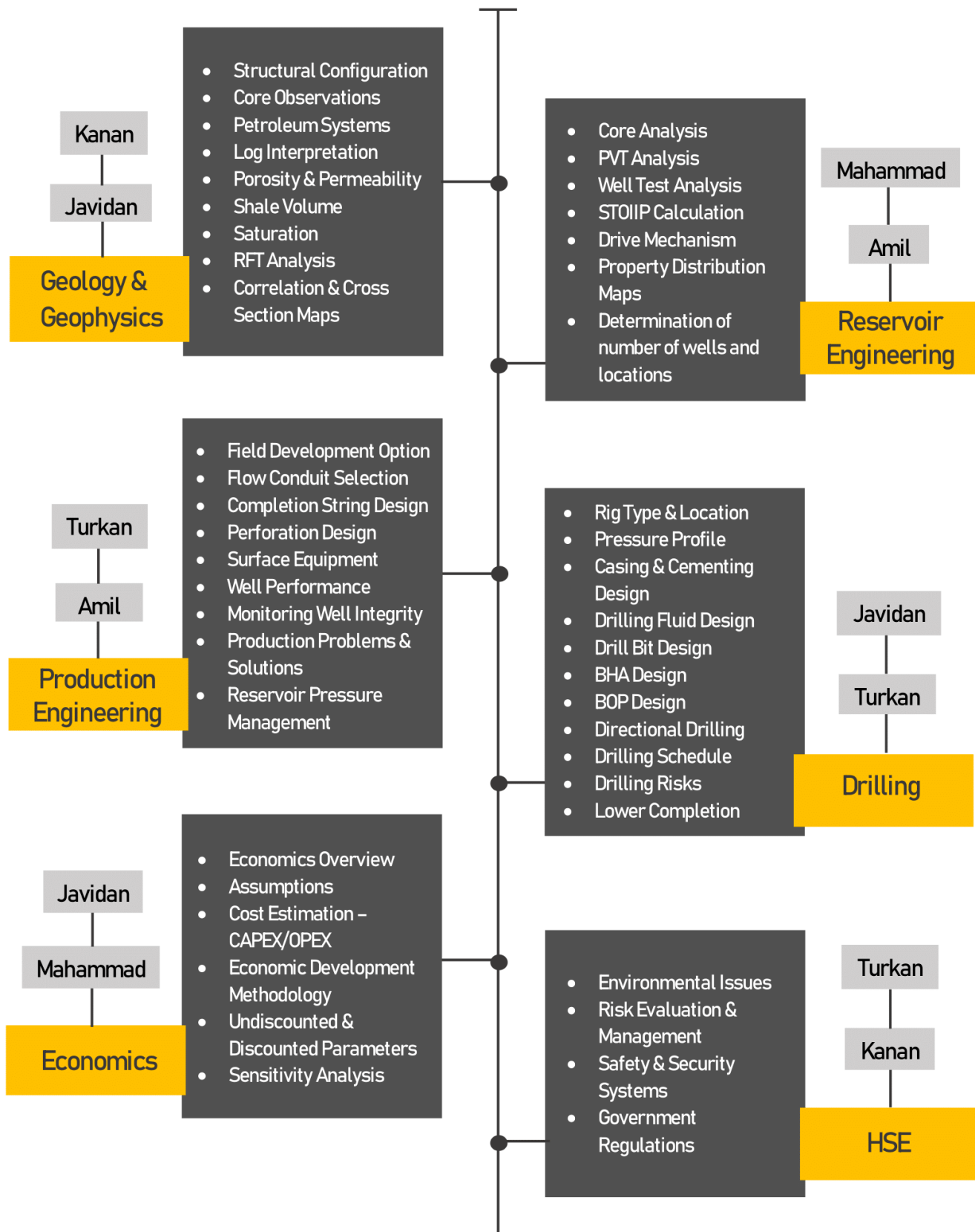


Figure 1.1. Mind Map and Workload Distribution

1.4. Project Schedule

The table and chart provided in this section gives information about the project schedule and the delivery time in total. It is worthy to note that the project deadline for the 1st semester was set as January 14, 2021. Based on the constructed chart, the project was delivered half month before the project deadline. All group members have made considerable efforts to catch up with internal team deadlines and deliver the project even well before the deadline.

PROJECT SCHEDULE

PROJECT NAME	SEMESTER START DATE		
Field Development Planning	Tuesday, September 15, 2020		
PROJECT EXECUTIVES	SEMESTER END DATE		
GROUP 2	Thursday, January 14, 2021		
TIMELINE			
PHASE TITLE	START DATE	END DATE	DURATION in days
Geology & Formation Evaluation	21.09.2020	21.10.2020	31
Reservoir Engineering	21.10.2020	16.11.2020	27
Drilling Engineering	17.11.2020	15.12.2020	29
Final Report Preparation	16.12.2020	31.12.2020	16

Table 1.1. Project Schedule

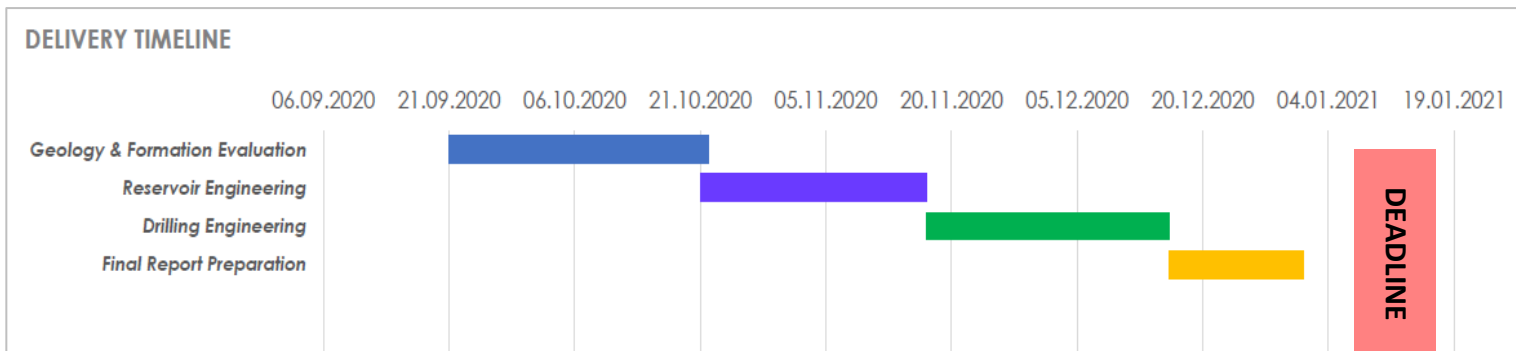


Figure 1.2. Delivery Timeline Chart

2. GEOLOGY

2.1. Introduction – Basin Evaluation

X-field is a small triangular, partly eroded domal anticline with steeply dipping flanks, located on a fault terrace within the western margin of the South West Central Graben. Mainly, the field is formed by three tectonic processes: (1) halokinesis, (2) syndepositional reactivation of Caledonian basement faults; and (3) syndepositional through post-depositional displacements along the nearby Auk Horst Boundary Fault. The tectonic processes and failed rifting during earliest Cretaceous and the latest Jurassic are essential for evaluating oil and gas accumulation in the North Sea fields. Over the course of later Jurassic and late Cretaceous periods, three main rifting systems including Viking Graben, Moray Firth and Central Graben were formed by uplifting and crustal extension of the North Sea Oil province. The geological history of Central Graben can be divided into three rifting periods, which play crucial role in the generation of hydrocarbons [5]:

Pre-rift:

This period encompasses time interval between late Triassic and early Jurassic during which deposition of oldest formations occurred. During Triassic time, siltstone formations and Smith Bank mud were accumulated above the salt. Marine transgression created a stable link between Boreal Sea and Tethys which resulted in Triassic sedimentation patterns within latest Triassic and earliest Jurassic timeframe. Over the course of Early Jurassic, shallow-marine depositional environment existed over most parts of the North Sea Basin. Sea level rose in Early Jurassic creating space for deposition of marine shales. Middle Jurassic period was accompanied by volcanic activities, uplifting, and extensive erosion of Late Triassic – Early Jurassic depositions. This unconformity was then overlain by fluvial and estuarine sediments. The North Sea Dome is an extensional uplift, which centered near the junction of the Central Graben, shed sediment to incipient rift basins adjacent to the Moray Firth/Witch Ground and Central Graben, where thin sequences of coal-bearing fluvial sandstone accumulated. In the Central Graben, as much as 1,000 m of nonmarine rocks was deposited, while a clastic wedge advanced southward into the southern North Sea [6].

Syn-rift:

Syn-rift events – contains late Jurassic and early Cretaceous timeframes. Syn-rifting had a major control on source rock, reservoir, and seal formations, and hydrocarbon entrapment. Late Jurassic play is specific to high-quality sandstone formations which are distributed over the Viking and Central Graben systems. Kimmeridge clay following massive sandstone depositions acts as both source rock and seal for the entire play. Distributions and behaviors of reservoir in this play are controlled by depositional

environments and creation of accommodation space. Due to sea level change depositional environment divides succession into shallow marine (Fulmar formations) and deep marine sandstones (Magnus formations). Creation of accommodation space varies throughout the entire basin. Syn-rift play is controlled by two contrasting sandstone reservoirs named submarine and retrogradational shelf sandstones with various thicknesses.

Post-rift:

These activities are chiefly related to late Cretaceous and Paleocene timeframes. The Late Cretaceous play is represented by Chalk group deposits which covers Southern North Sea up to Central Graben. Chalk deposits plays a main role in forming effective top seal for Central Graben hydrocarbon bearing zones including Fulmar, Argyll, and Auk reservoirs. Hydrocarbon bearing Chalk Group reservoirs include Tor and Ekofisk formations but other rare occurrences are also found in older Hod Formations. Due to its naturally formed fractures, Chalk group deposits have increased permeability being effective particularly for dual porosity-dual permeability modeling systems [7].

Since steep geothermal gradients connected with the extensional tectonics decayed, the regional pattern became one of gradual cooling and associated subsidence where post-rift sediments accumulated to greatest thickness. Salt tectonics in the Central Graben occurred due to the process of the great iso-static differences resulting from erosion of uplifted blocks and accompanying rapid sedimentation in sub-basins which continued into the Holocene.

2.2. Structural configuration

After analysis of top structural map and 2D cross sectional view at the direction from NW to SE, it is determined that possible amount of hydrocarbons is more likely to accumulate at the dome-shaped anticline. It can be easily defined from the map that top point of anticline-shaped structure is approximately 9800 m. From top to bottom direction, this structure expands. Because of variety of inclination angle at the flanks of structure, flank between north-west and south-west inclines steeply, while other

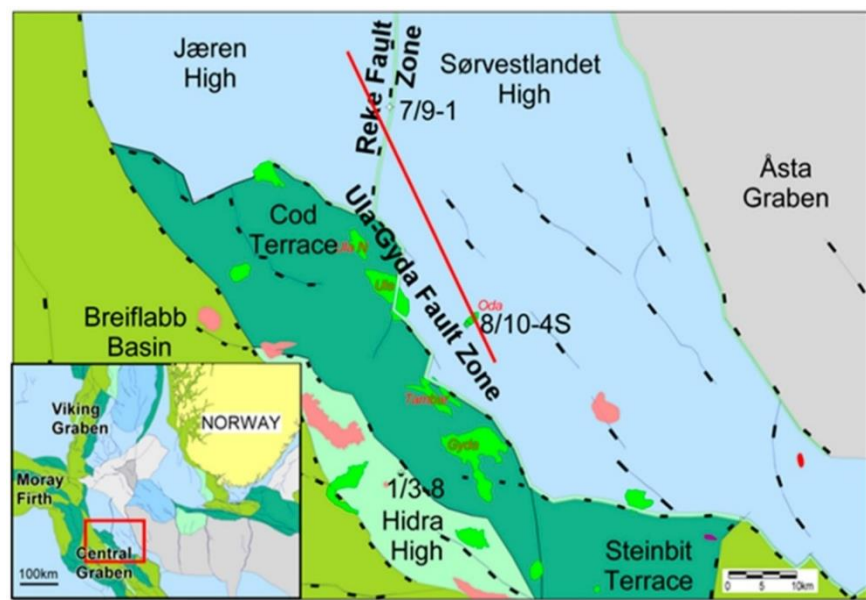


Figure 2.1. Central Graben faulting zones

flanks have a big longitude, not having steep configuration. Total area of this field is around 64 square km (8 equivalent length and width). After analysis of well testing data, it is predicted that parallel or intersecting faults should exist around exploration well 2 and 5. Although data from well 3 and 6 do not show the possibility of faults around them, it is assumed that there are a lot of faults in the field. Because of poor well testing and noisy data, it is less likely to be possible to define exact location and orientation of faults. From general view of Central Graben in North Sea in term of faults, it can be determined that massive number of big faults with strike in north-west direction exist in this location and therefore assumption of reservoir division by fault to two or more parts can be possible (**Figure 2.1**). From 2D cross sectional view, different layers are observed (**Figure 2.2**). However, Faults cannot be noticed (**Figure 2.3**). Although in the middle layer, there are certain fault-shaped fractures, they are not faults. Because the top end of fractures ends in layer and for faulting, both fracturing and movement of parts of layer against each other are required. However, faults may exist also. More data and analysis are required for exact fault determination. After analysis of formation with logging data, we can determine existence of faults with more accuracy.

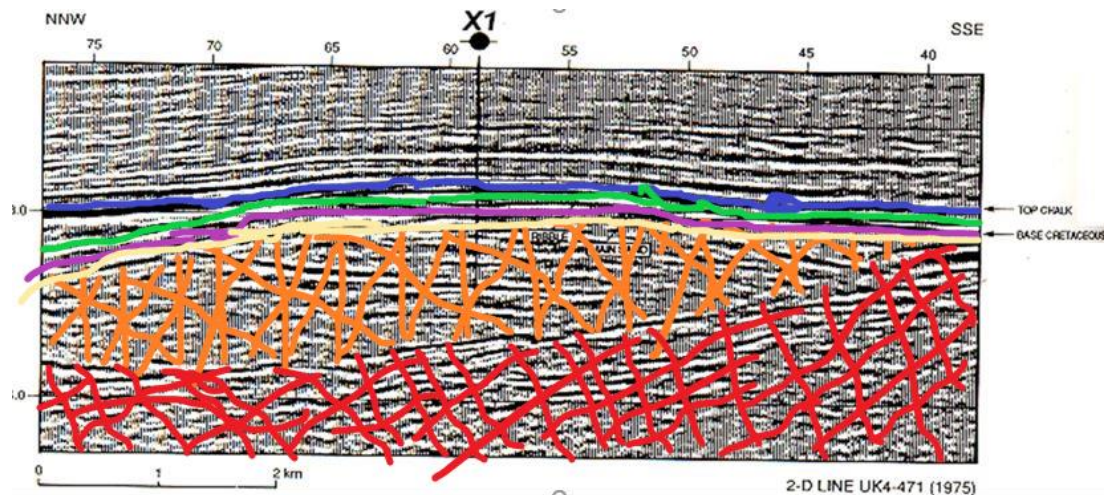


Figure 2.2. 2D seismic cross section

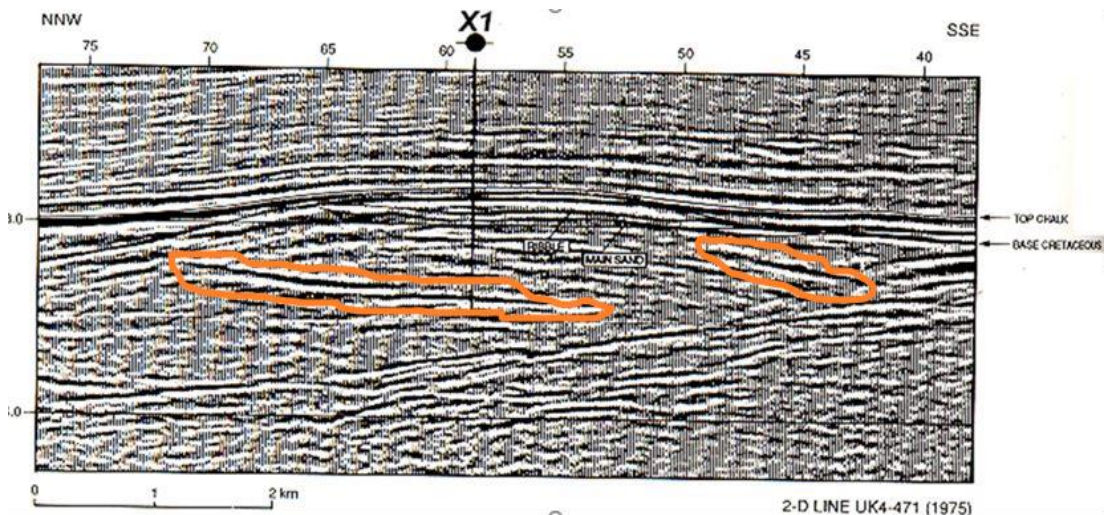


Figure 2.3. Initial fault analysis over seismic cross section

2.3. Petroleum play components

In general, the prevalence of similar lithologic character and a narrow stratigraphic interval contribute to the definition of a single petroleum system. The Kimmeridgian Shales Total Petroleum System is defined to comprise all the oil – prone regions of the North Sea Graben, including Central North Sea where X – field has been located [18].

Source rock

As it was previously mentioned, the mature shales of Kimmeridge Clay Formation are the source of the oil in the Central North Sea fields. The Kimmeridge Clay is the upper Jurassic marine mudstone or its stratigraphic equivalents. These black shales are considered highly radioactive and organic – rich (average TOC: between 3% and 8%). Hydrogen to carbon ratio is about 1.1. The Kimmeridgian Shales contain typical “type II” mixed kerogen. By taking amount of TOC and kerogen type into account, it can be said that the fields in this area are good source potential for hydrocarbon. Global sea-level rise, coupled with high organic productivity and increasing water depths, caused anoxic bottom waters in areas of closed bathymetric basins.

Reservoir rock

In terms of reservoir quality and connectivity in the North Sea fields like Piper & Forties fields, minor controls are the limited lateral continuity of sands, also decrease in porosity and permeability by diagenetic cements and the presence of clay-lined fractures reducing permeability. Here reservoir happens in thick Upper Paleocene sands whose deposition is sequence of a major sand rich submarine fan. Besides it, the reservoir contains stacked sandstone bodies.

Reservoirs are mainly found in strata with ages ranging from Devonian to Eocene. Pre-rift reservoirs can be of any age prior to the Late Jurassic. Subsequently, syn-rift reservoirs include rocks of Late Jurassic to earliest Cretaceous age. When it comes to post-rift reservoirs, they range in age from Early Cretaceous to Eocene.

Seal

Reservoir seal in nearby fields such as Fulmar & Nelmos contains Upper Cretaceous chalks (can be straightforwardly identified from their low gamma-ray values on logs) that produce unconformable lie on the top of the formation in the North & East and the Kimmeridge Clay (easily identified by their extremely high gamma-ray values on logs) in the South & West. For current case (X – field) Kimmeridge Clay may be seen in the 1st, 2nd and 3rd wells while Upper Cretaceous chalks correspond to Wells 4, 5 and 6.

Seals are diverse, depending upon the structural setting and reservoir age. Pre-rift reservoirs commonly have seals formed by fine-grained, post-rift sedimentary sequences that drape the Late Jurassic to earliest Cretaceous structures. Contemporaneous shales such as the Kimmeridge Clay seal many syn-

rift reservoirs. Fields with post-rift reservoirs generally require seals in fine-grained rocks which belong to Tertiary time zone.

Trap

The shallow oil – water contact in the north parts of the fields appears to be limited to a fault-bounded block. This OWC is interpreted as a perched contact resulting from a combination of fault juxtaposition of reservoir. Migration of oil happened throughout the early to middle Tertiary from the deeper parts of the Central Graben.

Timing

In almost all areas of the Central North Sea Graben, source rocks have undergone almost continuous subsidence and burial since their deposition. In definite restricted regions of greatest subsidence and most rapid accumulation of sediments, the Kimmeridgian source rocks reached thermal maturity with respect to oil generation as early as Cretaceous time. By Eocene time, oil generation was widespread. Subsidence and burial of the source rocks still continue to this day in most of the Central North Sea Graben, source rocks are at their maximum temperature and burial depth at present. In some areas of continuous burial, source rocks have exceeded the temperature interval for oil generation and attained thermal maturity with respect to gas during Neogene to Holocene time [19] [20].

2.4. Reservoir architecture and stratigraphy

Based on the investigation of nearby fields in Central Graben, it can be estimated that X-field is highly analogous to Fulmar field due to the presence of “Ribble” and “Main Sand” as given in 2D seismic. Therefore, stratigraphic configuration of Fulmar field was used as a key to identify major stratigraphic units in X-field and this data will then be supported with the help of logging interpretation and seismic cross section.

As mentioned earlier, the reservoir is consisted of shallow marine sandstones from Upper Jurassic. There was a major transgressive event leading to the end of deposition of main reservoir sands and beginning of deposition of Kimmeridge Clay formation. In addition to main sand formations, there was a series of turbiditic sandstones named Ribble sand, which was deposited near the base of Kimmeridge Clay. Ribble sand is relatively thinner and interrupted with shale layers. Another essential geological event to be stressed is associated with the Base Cretaceous unconformity, which truncated a huge section of the reservoir on the eastern and northern flanks of the field [11]. It is considered that this vital event acted as a boundary between syn-rifting and post-rifting events. Finally, Upper Cretaceous chalks overlie Ribble & Kimmeridge Clay formation as proven by 2D seismic cross section. Overall, it can be stated that the reservoir section of this field primarily contains fine to medium grained, shallow marine sandstones that were probably derived from Triassic sediments. The figure 2.4 below shows that how

stratigraphic interpretation of nearby field is matched with the given 2D seismic profile of X-field in order to ascertain depositional timeframe and define the zones that have not been logged before.

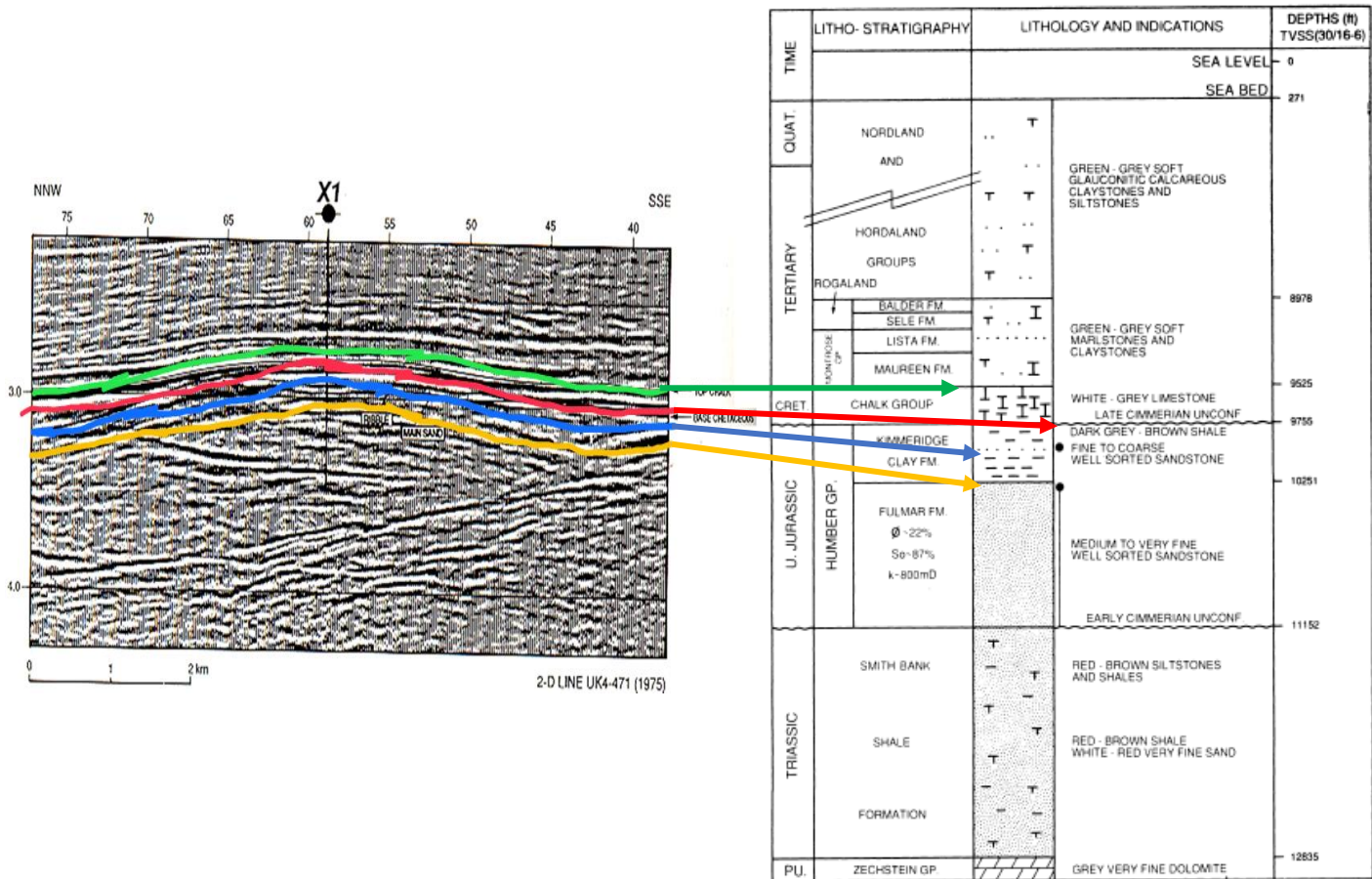


Figure 2.4. Interpretation of seismic cross section with stratigraphy of Fulmar field.
 Green – top of chalk; Red – base Cretaceous unconformity; Blue – top of Ribble sand;
 Yellow – top of Main Sand;

2.5. Depositional Environment

By having a precise diagnosis of depositional environment, information about the quality of reservoir and vertical & lateral continuity of the rock units in the reservoir can be gathered. Moreover, in well spacing and further reservoir management issues, the accurate determination of depositional environment plays a crucial role.

To figure out the depositional environment, the team used data available from logs, core sample pictures, and nearby Central Graben fields [19] [25]. Core sample photos were only present for Well X-5 located in the northern part of the field. Detailed analysis of core samples will be illustrated in the next section particularly being dedicated to core analysis however, quick observations in order to understand environment of deposition have been given here as well. The literature review proves that depositional

environment of nearby field Fulmar was shallow marine and considering the analogous features of X-field with Fulmar field, it is more likely to observe the same depositional environment in X-field also. Due to the reasons listed below, X-field is considered to be deposited in shallow marine environment:

- Coarsening in upward direction as GR log presents;
- Presence of bioturbation, slumps, and mud clasts;
- Deposition of similar Fulmar field in shallow marine environment;

Then it is possible to state that reservoir has a good quality accompanied by the lateral continuity of sand layers with approximate thickness ranging between 500-1000ft. The thickness of sand interval is relatively thinner in the well X-6 compared to others being quite thick. Ribble sand is not considered to be the main producing sand as it is a part of Kimmeridge formation deposited in the deep marine environment resulted by sea level transgression. Additionally, Ribble sand observed in well X-1 and X-2 has always disrupted by shale layers.

2.6. Core Analysis

Evidently, core sampling is an expensive process that can be performed during drilling phase with the aim of obtaining as much information as possible about the reservoir. Therefore, core samples and resultant measurements are available only for wells X-1, X-4, and X-5. Additionally, students are provided with the core sample photos belonging to well X-5 for further analysis. Data gained from core samples are also priceless in terms of obtaining clues about reservoir quality and depositional environment. Examination of the pictures state that cores are taken from specific depth interval of 10940ft – 10976ft. A wide range of information, such as grain size, sorting, colors and depositional environment can be gathered very easily. Taking a quick glance at the pictures, it is obvious that reservoir pay zone is highly consolidated. Another verification that the pictures provide is about the presence of slumps, bioturbation, and mud clasts that have been marked by colorful circles. Summarizing all findings coming from core analysis, following statements below can be made:

- ❖ Grains are **moderate to well-sorted** and **fine to medium-sized**;
- ❖ Formation color is changing from **grey to brown**;
- ❖ Primary sedimentary structures (occurring during rock formation) include **low angle laminations** being indicator of low energy environment;
- ❖ Secondary sedimentary structures (occurring after rock formation) include **bioturbation, slumps, and mud clasts** formed probably formed by storm waves being indicator of marine environment;
- ❖ Depositional environment is much likely to be **shallow marine environment** based on the findings from core samples and features of analog Fulmar field;



● SLUMP
● BIOTURBATION



● LAMINATION



● MUD CLAST

Figure 2.5. Core sample pictures for well X-5

2.7. Log Interpretation

Overall, there are six wells penetrated into the oil bearing Jurassic reservoir of X field: wells X-1 and X-2 are vertical while remaining four wells are deviated up to 25 degrees. With the purpose of obtaining detailed and accurate information about the formation, a wide range of wireline logging tools, including Gamma Ray (GR), Neutron (CNL), Density, Sonic, and Resistivity (LL9S, LL9D, and RT) were employed. Log interpretation was performed by utilizing the software called "Techlog 2015" offered by Schlumberger. Separate projects were initiated in Techlog in order to generate logging sheets for each well. Below, the results of log interpretation for each well have been reported elaborately where the lithology, top & bottom of the reservoir, its thickness, presence of formation fluids, and fluid contacts have been highlighted [\[2\]](#) [\[8\]](#) [\[9\]](#) [\[23\]](#). As an example, all drawings for the aforementioned parameters have been shown on the log sheet for well X-1 and remaining ones will be presented in Appendix part.

Well X-1.

Initially, by looking through the Gamma Ray log lithological features of given well can be clarified. Beginning from very top till 10250 ft TVDSS and between 11150 ft and 12050 ft TVDSS intervals correspond to shale layers as the GR value is high. Taking inferiority of resistivity log figures into account it may be stated that the aforementioned zones are not desirable for production. However, within these ranges Ribble sand is observed in 10160 ft – 10190 ft. This type of sand is not continuous and mostly substituted by shale formation. The remaining parts, specifically 10250 ft – 11145 ft belongs to main sand in which the value of GR log is relatively low. Although the depth interval of 10250-10350ft corresponds to relatively higher GR readings, which would normally be interpreted as, clay/shale, high value of resistivity log and density & neutron logs confirm that there is hydrocarbon here. The reason could be the malfunction of GR log as its value shift around 100ft. Thereafter, a decrease in resistivity log figure occurs which is principal signature of water. Turn to density & neutron logs, no large gaps between density and neutron log have been observed which means there is not a butterfly effect indicating the absence of gas. Although the density log value reduces there, the neutron porosity number is almost stable all over the log. Last but not least, investigation of resistivity log highlights that OWC places at 10831 ft TVDSS since the resistivity value descends significantly starting from that point.

Well X-2.

In the case of Well X-2, the examination of GR log indicates that starting from 10220ft to 10358ft, there is a Ribble Sand layer interrupted by a wide range of shale layers as it was illustrated previously in the report related to the investigation of 2D seismic cross section. However, aforementioned sand layer is not a productive zone as proven by the reading of resistivity log since low and equal resistivity values (LL9D, LL9S, and RT) show less permeable zones and low invasion. The main reservoir section starts at 10620ft and ends up at 11510ft as given by lower gamma ray reading. It is evident from the resistivity

logs that when reservoir section just starts to appear in GR log, there is a following increasing trend in resistivity log as well which proves the presence of hydrocarbon there since high resistivity readings correspond to the hydrocarbons. As opposed to that, relatively low resistivity readings indicates the presence of water as it is more conductive and less resistive compound. Analysis of neutron and density logs helps us to state that the productive zone does not contain gas as there is no any butterfly effect (lower density but higher neutron log reading causing to have a great gap between two logs) being observed. Finally, commenting on the oil-water contact (OWC), a sudden drop in resistivity log readings has occurred at 10860ft depth, which means there is a transition from oil to water zone. As a result, OWC has been ascertained to be at 10860ft. After the end of sand zone (11510ft), there is a continuous shale layer until 11950ft.

Well X-3.

Having a look at well 3, it can be clearly seen from Gamma Ray log that reservoir section corresponds to 10550 ft- 10930 ft interval due to relatively low value of GR log. Additionally, high resistivity readings in these sections confirm presence of HCs. As gamma ray values at 10036ft – 10175 ft range is too low for sand zone, it can be considered as chalk layers. When it comes to shale layers, higher values of GR log in 10175ft-10270ft and 10425ft-10500 ft ranges represents mainly shale formations. Between these two shale sections there is small interval starting from 10270 ft and ending at 10425 ft which demonstrates Ribble sand layer. Turning to density and neutron logs, since there is not huge gap between corresponding logs, reservoir does not contain any gas bearing formation. Finally, by analyzing resistivity logs, OWC can be determined at 10855 ft depth due to sharp decrease in resistivity values at this point.

Well X-4.

In terms of well 4, due to very low GR readings starting from 9452 ft there are chalk layers which continues up to 10225 ft. After this point, GR values start to significantly increase which clearly indicates small shale zone corresponding to 10225 ft-10330 ft interval. Following this, according to relatively low readings of GR log, sand layers can be vividly observed starting from 10330 ft and ending at 11362 ft depth. In the range of 10330 ft- 10840 ft section, presence of HCs can be confirmed by referring to high values of resistivity logs. In this particular interval, again there is not any gas bearing formation as butterfly effect cannot be seen. After 11362 ft, high values of GR log represent beginning of shale section which concludes at 11526 ft depth. The last noteworthy detail to mention is that OWC corresponds to 10840 ft where there is considerable descend in resistivity values.

Well X-5.

In terms of lithology, starting from top until 10115 ft TVDSS chalk layer is seen since GR readings are too low for it to be main sand. Later, chalk layers are being followed by thin clay layer which ends at

10250 ft. Starting from 10250 ft, there are main sand layers which cover the depth interval of 10250 ft and 10870 ft TVDSS interval. This is because of lower value of GR log that also allows the reader to say that within this zone reservoir interval can be set. Relatively higher resistivity log values are evident for availability of hydrocarbon within that interval. The range of 10870 ft – 11200 ft TVDSS is relate to shale formation. Despite the fact that there is not enough data for resistivity log in order to declare OWC more precisely, RFT analysis can be examined for reaching the target. The graph of RFT analysis for well – 5 clearly displays that OWC is at 10620 ft depth. Meaningfully, if resistivity log continued in deeper parts, it would face with sharp reduction at that TVDSS which corresponds to water region below it.

Well X-6.

Looking at logs of Well X-6, it can be obviously seen that chalk layer is located in 9896-10100 ft interval being differentiated according to the lowest readings of GR log. Shale layer which has thickness of 509 ft starting at 10600 ft TVDSS and ending at 11009 TVDSS ft is not productive layer, being determined with higher value of API at GR log. There is also main sand layer between chalk and shale zones in the range of 10100-10600 ft. It has relatively lower reading of GR log than shale zone. Due to higher resistivity at the log in the interval of 10100-10550 ft, hydrocarbons are more likely to accumulated at this part of main sand layer. CNL, density and SONIC logs should be analyzed in order to find type of hydrocarbon. Over interval of main sand, SONIC and density logs demonstrate approximately the same readings and determination of hydrocarbon type cannot be performed with them. CNL log mainly shows lower values at gas zones. However, readings of CNL log at the reservoir section and shale zone are the identical. If gas exists in the reservoir section, reading of CNL should decrease and demonstrate lower values than that of shale zone. Therefore, oil accumulated in this section. From the logs, OWC is determined around 10550 ft TVDSS after which there is a sharp drop in resistivity log values.

The table 2.1 below indicates all outcomes obtained through the log interpretation. Additionally, graphical illustration given right after the table shows the key markers on the log sheet itself for well X-1. Please refer to the Appendix part for the logging illustrations of the other wells.

Wells	Top of reservoir (ft)	Bottom of reservoir (ft)	Reservoir thickness (ft)	OWC (ft)	Oil column thickness (ft)
X-1	10250	11145	895	10831	581
X-2	10620	11510	890	10860	240
X-3	10550	10930	380	10855	305
X-4	10330	11362	1032	10840	510
X-5	10115	10870	755	10620	505
X-6	10100	10600	500	10550	450

Table 2.1. Initial fault analysis over seismic cross section

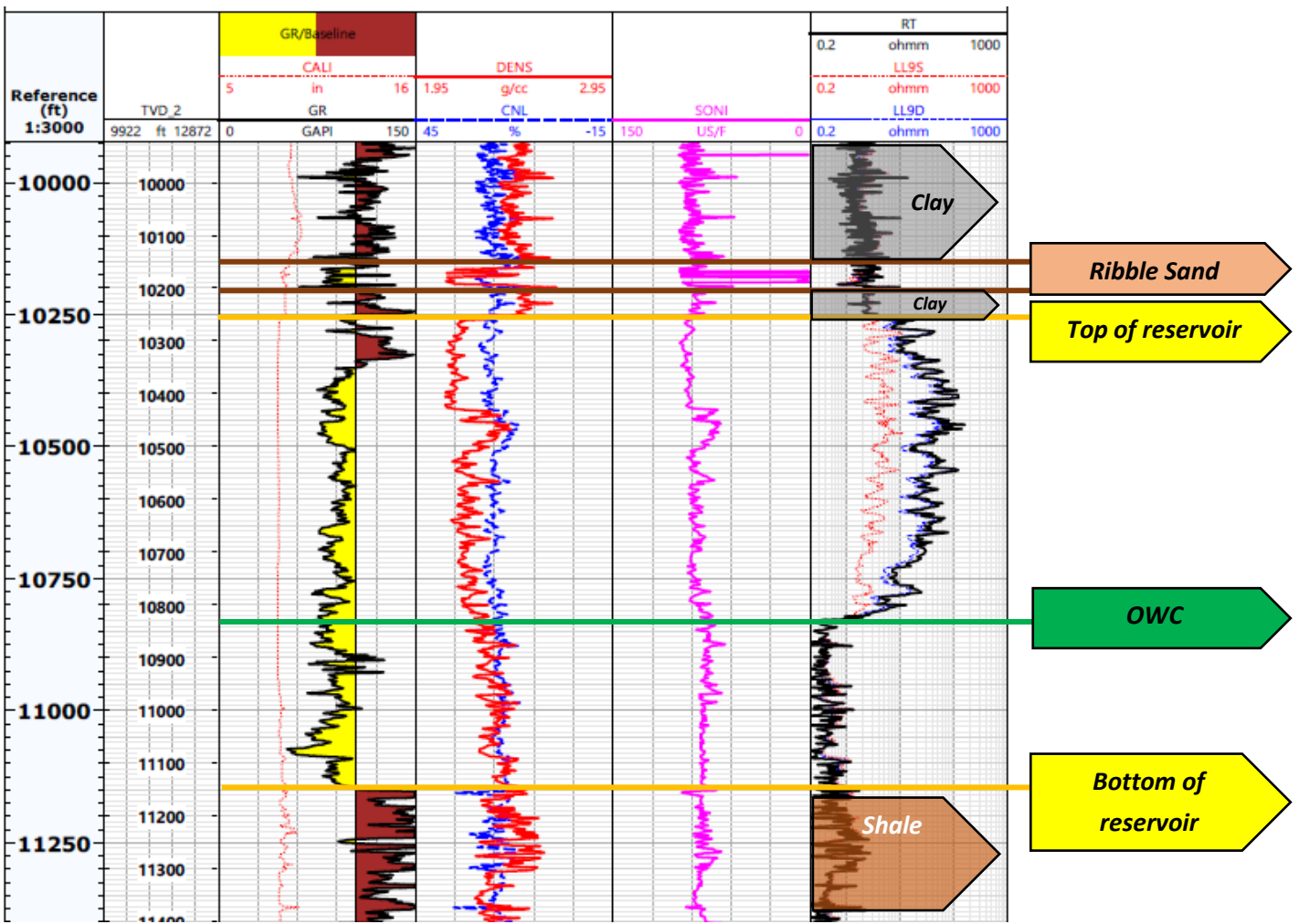


Figure 2.6. Log analysis for well X-1

2.8. Log Correlation

Since log interpretation has been performed together with determination of reservoir boundaries, fluid contacts, and lithology, now it is time for correlating the wells. Correlation is necessary to understand the lateral continuity of the layers and draw geological cross sections. Instead of correlating all wells together, the team decided to group wells and correlate them separately. For the ease of process, wells X-1, X-2, and X-5 were correlated together as they lie almost on the same line. Subsequently, the correlation for the 2nd group of wells was carried out.

Wells X-2 / X-1 / X-5 correlation [27].

To begin with, the chalk layer is not observed in some logs however, as it was captured in 2D seismic cross section, and also explained in “stratigraphy” section of this report, it is decided to include chalk layer into the geological cross section which will be drawn later. The presence of thick shale layers is evidently seen from all three wells as emphasized in log interpretation section so, it can be easily correlated and become key geological marker for the correlation. Additionally, there is a thin Ribble sand

layer in well X-1 and X-2 being absent in well X-5. Moreover, in well X-5, there is a chalk layer till 10100ft which is absent in the case of X-1 and X-2 (Figure 2.7).

Wells X-4 / X-6 / X-3 correlation [27]. There are 3 main layers for correlation (chalk, shale and main sand layer). The top chalk layer is quite continuous and thick being observed in all three wells. Therefore, it is considered to be a key geological marker. Sand layer is main productive layer, as it is thick and continuous (it can be seen at all wells). While big shale below main sand layer can be detected at well X-4 and X-6, being absent in well X-3 (Figure 2.8).

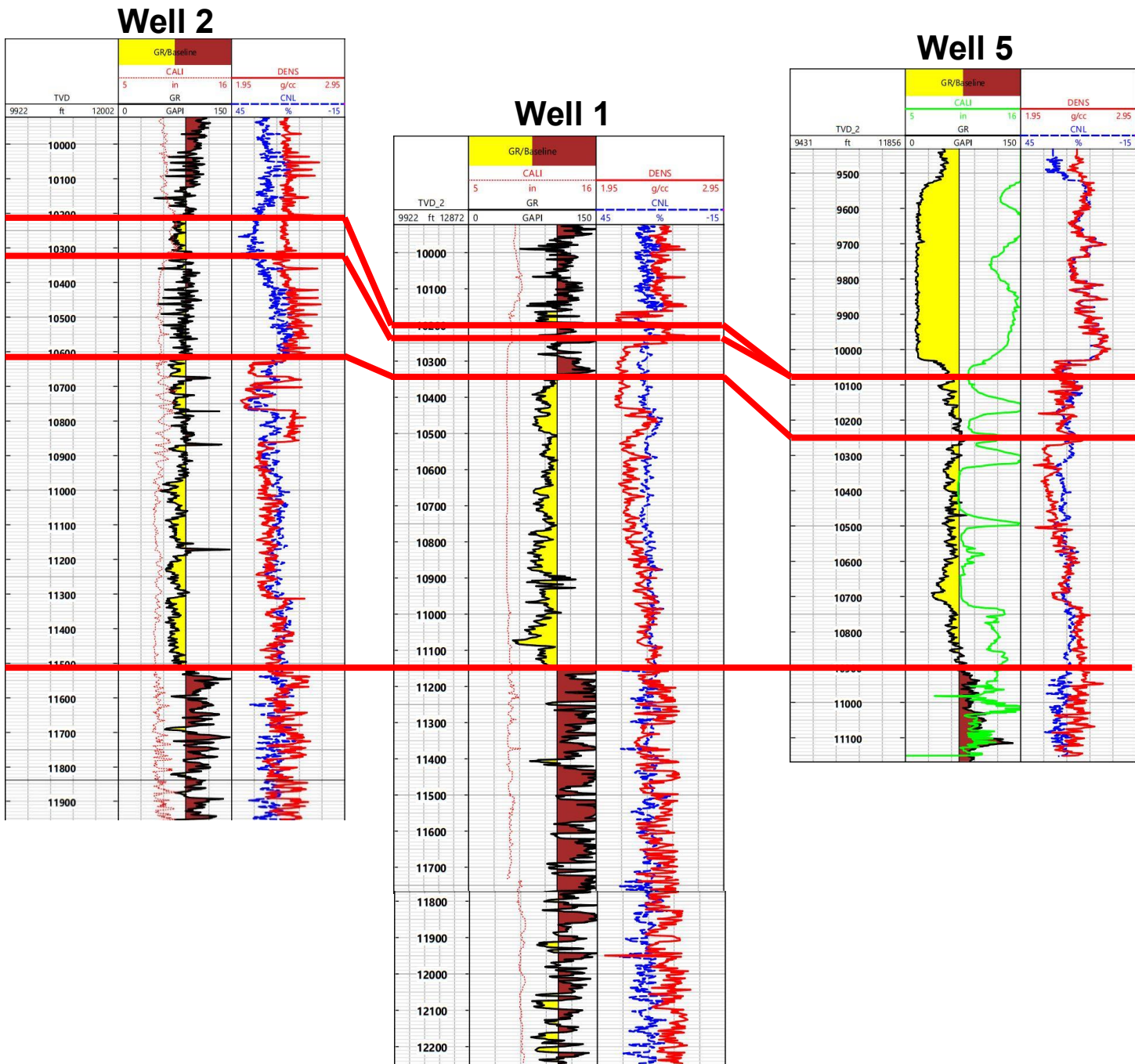
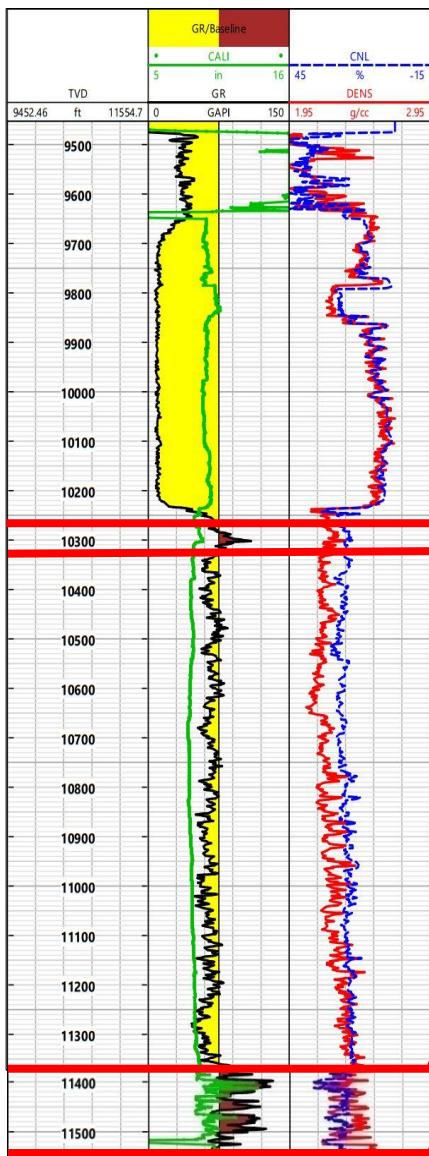
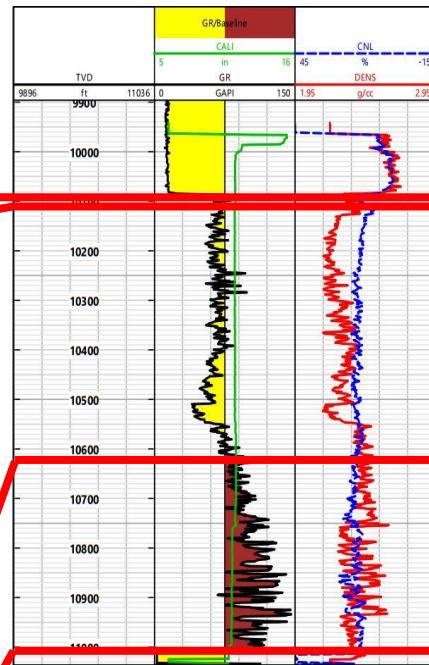


Figure 2.7. Correlation for wells X-2, X-1, and X-5

Well 4



Well 6



Well 3

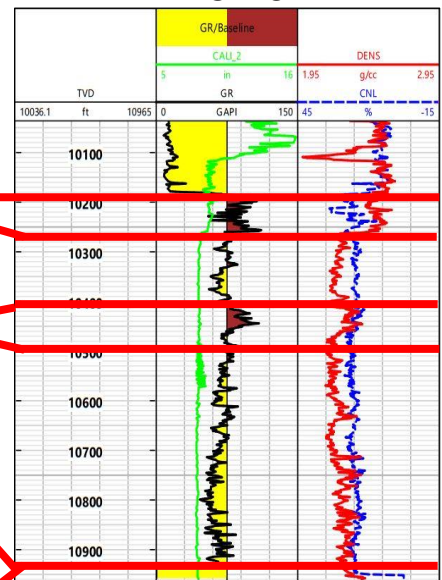


Figure 2.8. Correlation for wells X-4, X-3, and X-6

2.9. RFT Analysis

Repeat Formation Tester (RFT) is a device employed with the aim of ascertaining formation pressure at certain depth. By taking advantage of RFT, fluid types and contacts can be identified as well with the help of difference in pressure gradients. In the case of X field, RFT data only for well X-1, X-2, and X-5 have been provided. However, utilizing RFT data for well X-1 and X-2, it is impossible to plot RFT graphs. Because data for them is inadequate and incorrect. Therefore, only RFT plot (**Figure 2.9**) for well X-5 is created [28].

X-5		X-2		X-1	
TVDSS (ft)	Pressure (psi)	TVDSS (ft)	Pressure (psi)	TVDSS (ft)	Pressure (psi)
10,500	5,550	10,280	5,640	10,450	5,650
10,100	5,570	10,550	5,705	10,600	5,720
10,200	5,600	10,780	5,780	10,700	5,775
10,400	5,650	10,828	5,790	10,800	5,820
10,500	5,685			10,828	5,845
10,565	5,710				
10,565	5,710	10,828	5,790	10,828	5,790
10,700	5,720	11,900	5,920	11,075	5,900
10800	5,820				
11,100	5,920				

Table 2.2. Provided RFT data

OWCs cannot be found from RFT plot for well 1 and 2 due to reasons which are aforementioned, while log analysis will be more reliable to determination of OWCs for them. As opposed to well X-1 and X-2, well X-5 has relatively accurate data and after plotting, it is determined that oil gradient (0.28 psi/ft) is smaller than water gradient (0.45 psi/ft) (Figure 2.9), having normal values. OWC for well 5 has been observed at the depth of 10620 ft. It should also be mentioned that there is again incorrect value (red cell in the table) in data of well X-5 (same depth (10500 ft) has two pressure values (5500 and 5685 psi)). Therefore, before RFT plotting, incorrect value is removed.

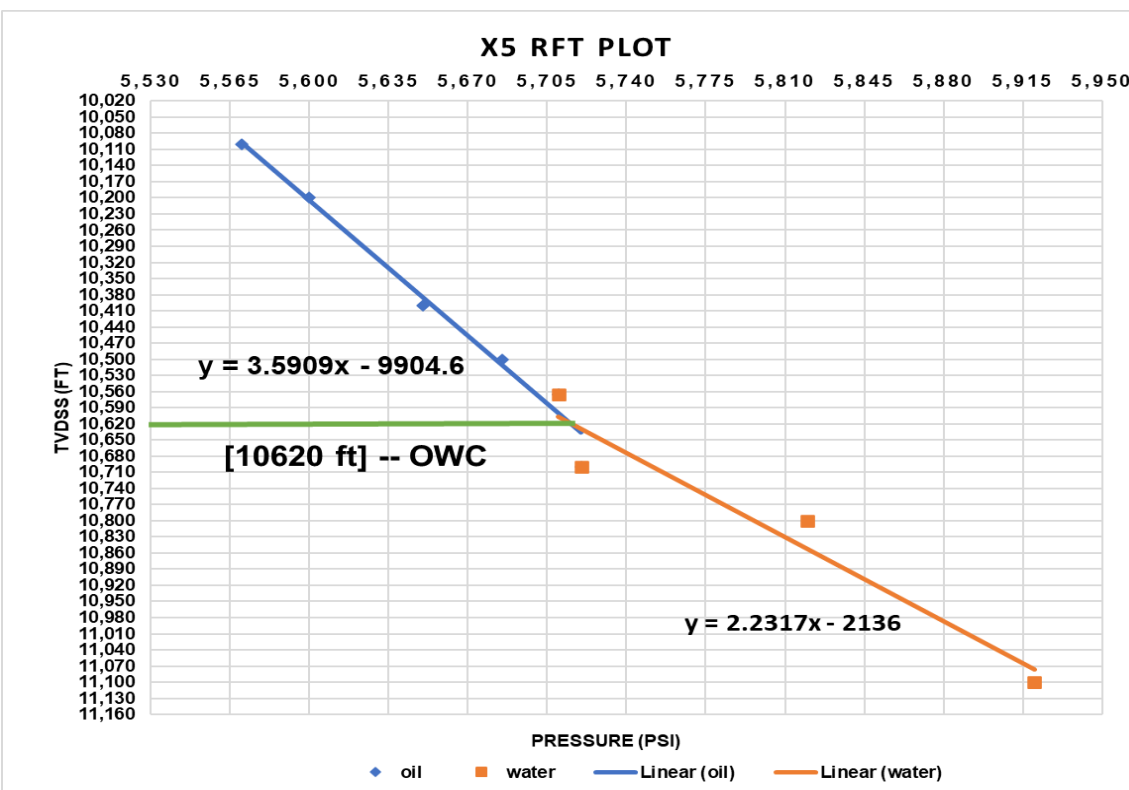


Figure 2.9. RFT plot for well X-5

2.10. Cross Sections

Utilizing wells X-2/X-1/X-5 correlation, cross sectional view (Figure 2.12) was generated. It can be easily seen that OWC-s from Well X-2 and Well X-1 have approximately equal depths at the left section of main sand, while OWC from Well 5 (right section of main sand) is located at upper zone of subsurface. This difference between depths of OWC-s demonstrates that there should be fault between zones where Well X-2&X-1 and Well X-5 pass through.

Utilizing Wells X-4/X-6/X-3 correlation, cross section (Figure 2.13) was prepared. This cross section demonstrates U-shaped or intersecting faults in the subsurface. This type of faults is mainly generated by compression. Due to faulting process, zone between intersection faults has moved in upper direction and therefore OWC from Well X-6 is located at upper part (middle section of main sand layer) than that of Well X-4&X-3. Although Well X-4 and Well X-3 are drilled through different section of subsurface in the field, both of OWC-s are located at approximately same depths at left and right sections of main sand layer.

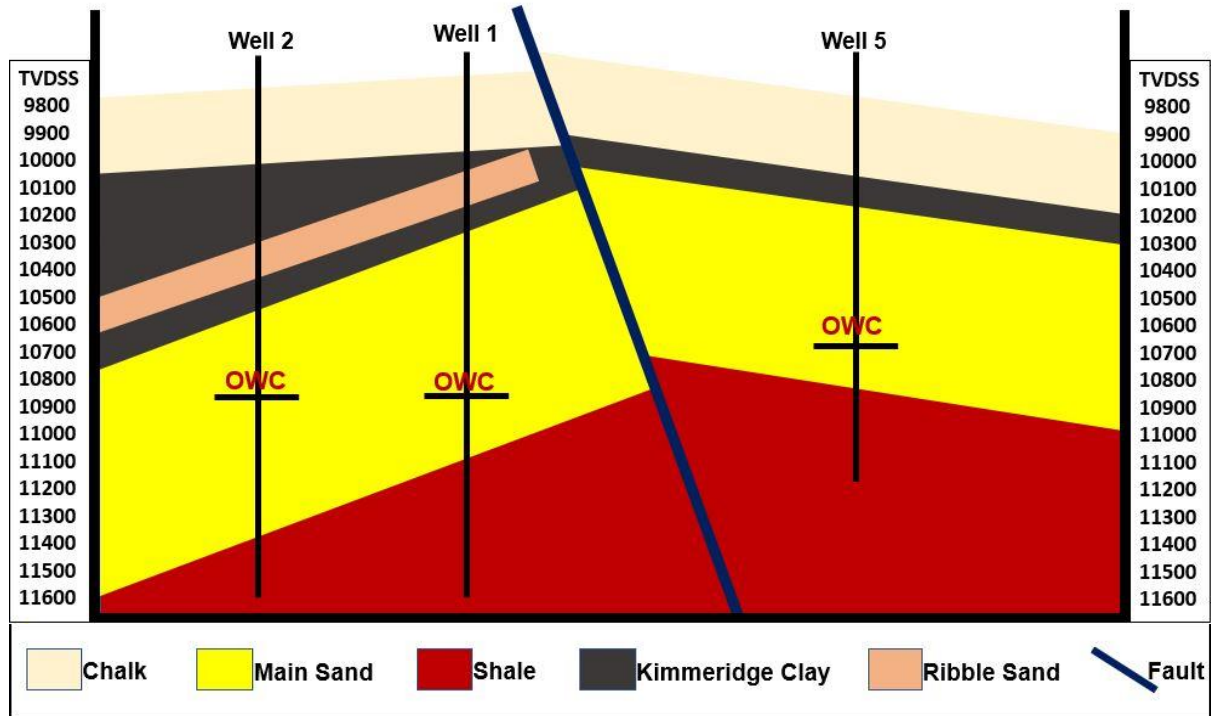


Figure 2.12. Cross section map for wells X-1, X-2 and X-5

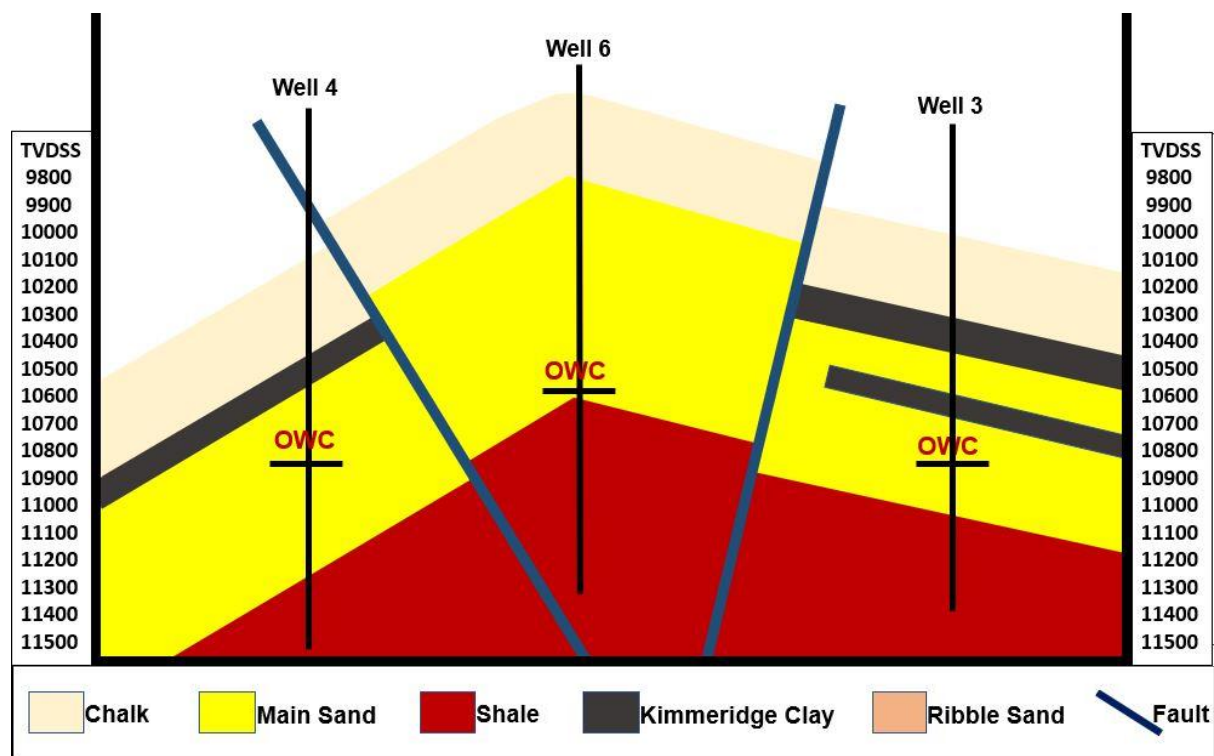


Figure 2.13. Cross section map for wells X-3, X-4 and X-6

While Figure 2.12 has only one of these faults, both of them are detected in Figure 2.13. It should also be mentioned that they are sealing faults due to difference in depths of OWCs.

These faults can be also demonstrated at the **top structural map (Figure 2.14)**. From the map, it can be determined that intersecting (sealing) faults have caused to compartmentation in the field. There are also several faults in the field. However due to less data (orientation and location and so on) about them, they cannot be displayed in the map. They also can be defined with extra well drilling and analysis, being taken into account economics of the field.

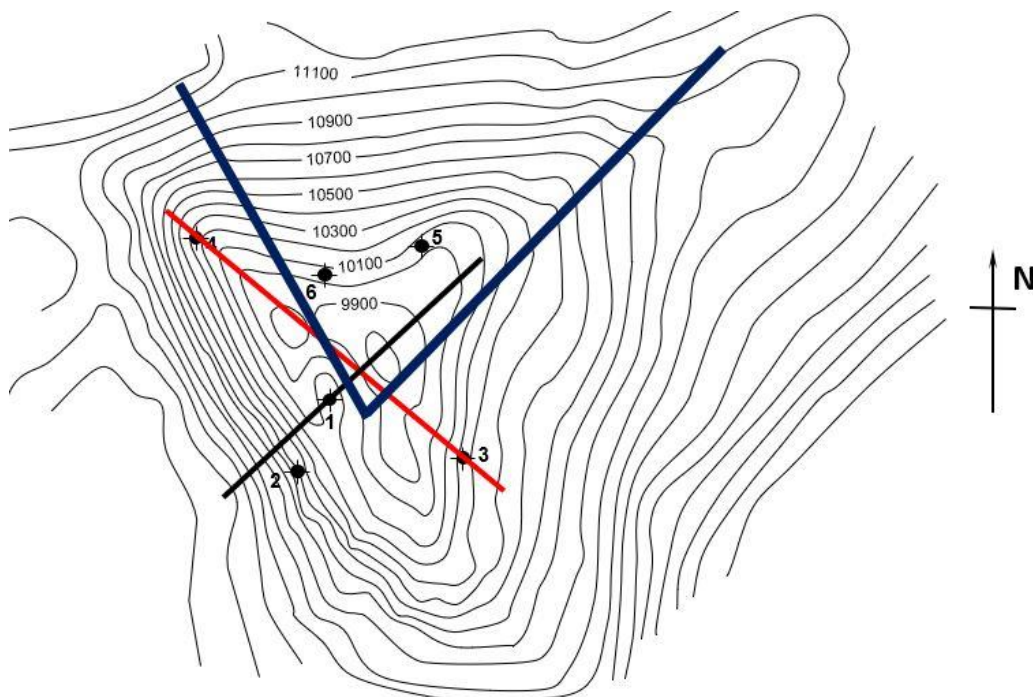


Figure 2.14. Top structural map showing faults

In the map above,

- **Black line** - Top view of cross section line of Well X-2/X-1/X-5
- **Red line** – Top view of cross section line of Well X-4/X-6/X-3
- **Intersecting Blue lines** – Top view of intersection fault lines

2.11. Porosity and Saturation Calculations

Porosity calculations. The major source of data for porosity calculation is considered to be logging and core sample measurements. Mainly, three types of logging tools – density, neutron, and sonic log are employed with the aim of porosity calculation. However, in our case, the team decided to take advantage of the density log as it is much more straightforward to compute porosity values for all six

wells. It is essential to highlight that core sample measurements are also provided for well X-1, X-4, and X-5, which is another factor affecting our decision in terms of utilizing density log outcomes. The graphical illustration (Figure 2.15) demonstrated below proves that core and density log porosity values are quite similar to each other with high degree of matching, as they almost lie on the same point in the graph (with few exceptions) dedicated to well X-1. Therefore, the same approach has been applied for all other cases even if there is no core data available for some wells since we believe in the reliability of density log, which was proven for wells with available core samples.

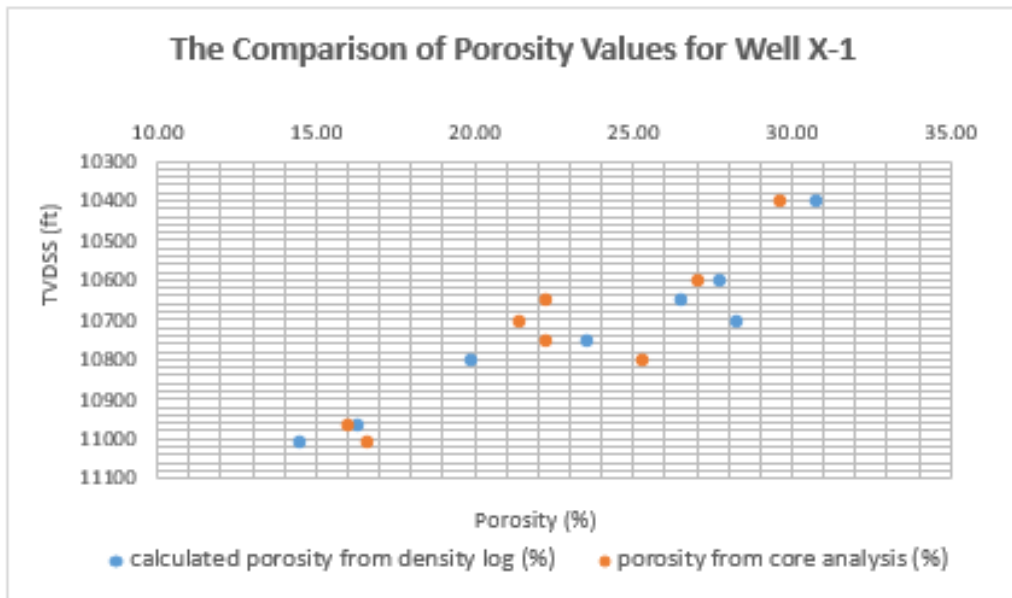


Figure 2.15. Comparison of core porosity and density log porosity values

For the sake of porosity calculation from density log, the well-known equation indicated beneath has been used which requires certain density values to be put into action.

$$\phi = \frac{\rho_{ma} - \rho_b}{\rho_{ma} - \rho_f}$$

Where,

- ρ_{ma} – is matrix density. Its value is taken as 2.65 g/cc corresponding to the sandstone density;
- ρ_f – is fluid density. Its value is taken as 0.99 g/cc corresponding to average crude oil density;
- ρ_b – is bulk density. Its value is taken from density log measurements;

For this calculation, oil bearing productive interval for each well is determined from log interpretation and then for specific depth values, corresponding density log measurement and the resultant porosity values have been computed. Subsequently, by using thickness weighted arithmetic average technique,

average porosity values have been ascertained for all wells [3]. As an example calculation, it is worthy to show the table belonging to well X-1:

Matrix density (g/cc)	2.65	
Fluid density (g/cc)	0.99	
TVDSS (ft)	bulk density g/cc (from logs)	calculated porosity from density log
10400	2.14	0.31
10550	2.2	0.27
10600	2.19	0.28
10650	2.21	0.27
10700	2.18	0.28
10750	2.26	0.23
10800	2.32	0.20
10960	2.38	0.16
11010	2.41	0.14
Average Porosity	0.22	

Table 2.3. Sample porosity calculation for Well X-1

The same procedure has been carried out sequentially for the rest of the wells and final outcomes of all calculations has been tabulated below for the ease of the result observation:

Wells	Productive Oil Zone (TVDSS, ft)	Average Porosity
X-1	10250-10831	0.22
X-2	10620-10860	0.24
X-3	10550-10855	0.24
X-4	10330-10840	0.28
X-5	10100-10680	0.23
X-6	10100-10550	0.22

Table 2.4. The results of porosity calculations

As a result of analysis of core sample measurements, it is valuable to illustrate the chart (Figure 2.16) which combines the average porosity values measured from core samples of certain depth points. The observation of the chart tells its readers that the majority of porosity readings for well X-1, X-4, and X-5 correspond to 20-27%, which is well close to the outcomes that we've obtained above.

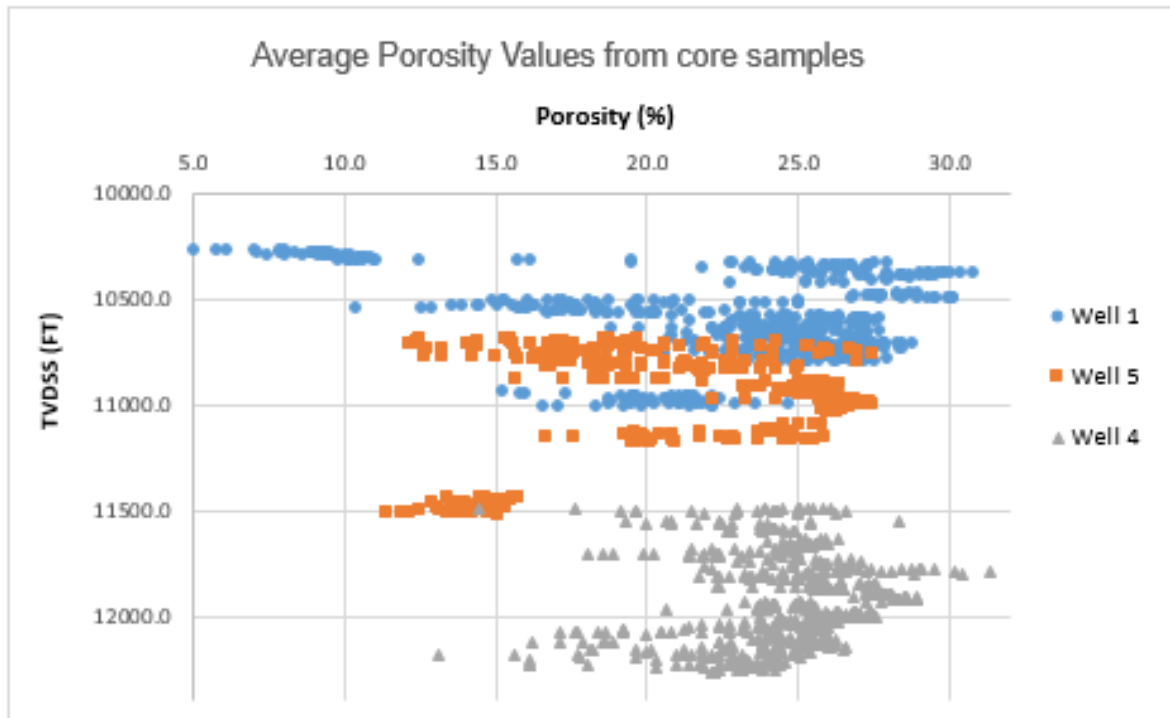


Figure 2.16. Average porosity values from core samples for three wells

Water saturation calculations. In order to figure out saturation values, the popular formula of “Archie’s equation” has been used. The equation itself and its explanation is given below:

$$S_w = \left(\frac{a R_w}{R_t \phi^m} \right)^{\frac{1}{n}}$$

Where,

- ϕ – is porosity at each depth;
- R_w – is water resistivity (Ohm*m);
- R_t – is true formation resistivity obtained from logs (Ohm*m);
- m – cementation factor;
- n – saturation exponent;
- a – constant;

Constants for each well separately have been provided to students in given data. Since the value of water resistivity has been indicated in the overview document provided, it is taken as 0.066 Ohm*m in our calculations. Additionally, in the case of well X-5, the resistivity log was interrupted due to some reasons and therefore, it did not show the resistivity values after the middle part of oil zone. The problem was solved by assuming that the water resistivity in the destroyed zone would be similar to the other

well nearby. The same averaging method has been applied to the saturation calculations as well as it was the case for porosity calculations. Sample calculation for saturation determination of well X-1 is given below in the tabulated form:

Rw (ohm*m)	0.066	
m	2	
n	2	
a	0.81	
TVDSS (ft)	Rt (ohm m)	Sw
10400	77.24	0.086
10550	61.81	0.108
10600	34.32	0.142
10650	28.42	0.164
10700	31.17	0.146
Average Saturation	0.13	

Table 2.5. Sample saturation calculation for Well X-1

Final outcomes of water saturation calculation is tabulated below. Finding oil saturation is an easy task since (1-Sw) gives oil saturation value.

Wells	Water Saturation	Oil Saturation
X-1	0.13	0.87
X-2	0.15	0.85
X-3	0.19	0.81
X-4	0.11	0.89
X-5	0.26	0.74
X-6	0.24	0.76

Table 2.6. The results of saturation calculations

In order to carry out average porosity and saturation calculations, thickness weighted arithmetic average technique is applied. For the ease of the process, the special Excel file was generated and all calculation steps were sequentially performed at it was given in the form of table previously. It is noteworthy to summarize equations used as a part of arithmetic averaging method:

$$\bar{\phi} = \frac{\sum_{i=1}^n \varphi_i h_i}{\sum_{i=1}^n h_i}$$

Where,

φ_i = point porosity (layer porosity)

h_i = interval, ft

$\bar{\phi}$ = weighted average porosity

$$\bar{S_w} = \frac{\sum_{i=1}^n S_{wi} \varphi_i h_i}{\sum_{i=1}^n \varphi_i h_i}$$

Where,

S_{wi} = point water saturation

φ_i = point porosity (layer porosity)

h_i = interval, ft

$\bar{S_w}$ = weighted average water saturation

2.12. Permeability Analysis

Permeability estimation can be performed by referring either well test data or lab core measurements. The application of these techniques is different and each one has its own positive and negative sides. However, since there is more core data available, permeability calculation is implemented on basis of this methodology. The graph below (Figure 2.17) illustrates correlation of horizontal permeability and helium porosity values from Well 1 core samples, which are then applied to evaluate log permeability by referring to log porosity. The power regression analysis demonstrates an acceptable correlation of 0.83 between core porosity and permeability [11]. Relevant graphs for wells 4 and 5 have been provided in the Appendix part.

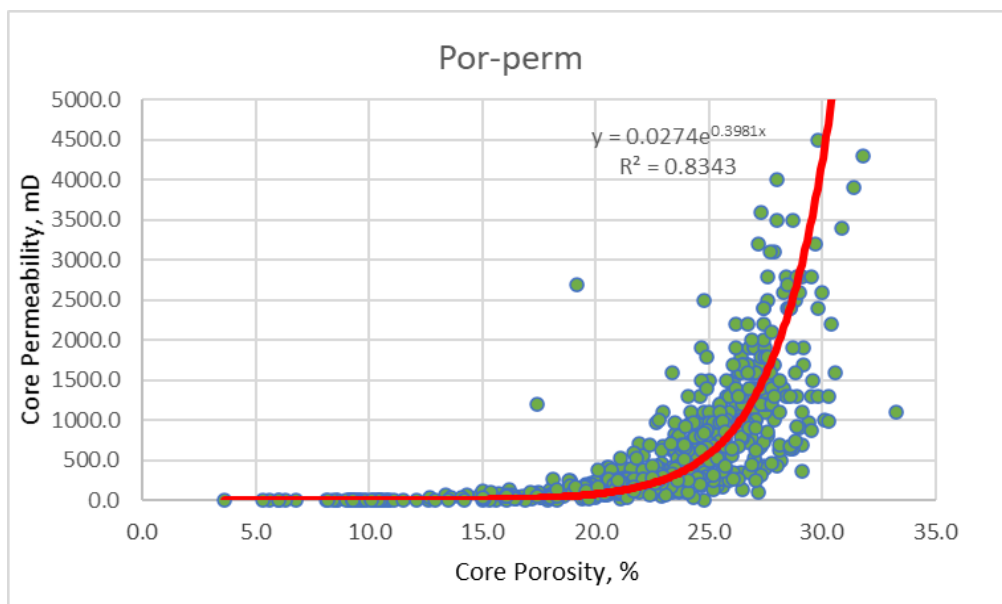


Figure 2.17. Porosity permeability correlation for well X-1

2.13. Reservoir Heterogeneity

The anisotropic characteristic of permeability can influence any procedure in which a density difference is observed between fluids such as gas cycling, water or gas coning and production below the bubble point and if anisotropy is severe, it also has an impact on injection and production rates. Moreover, anisotropy should also be taken into consideration when designing completion and workover strategies. Last but not least, it is very crucial input for dynamic reservoir modelling [17]. Therefore, it is worth to consider the anisotropic behavior of permeability. Horizontal and vertical permeability values from core samples of wells 1 (blue) and 5 (green) were utilized to construct relationship between TVD and the ratio of vertical and horizontal permeability in order to sketch permeability anisotropy graph. Isotropic behavior can be clearly seen from the graph as the majority of data values lie above 0.8.

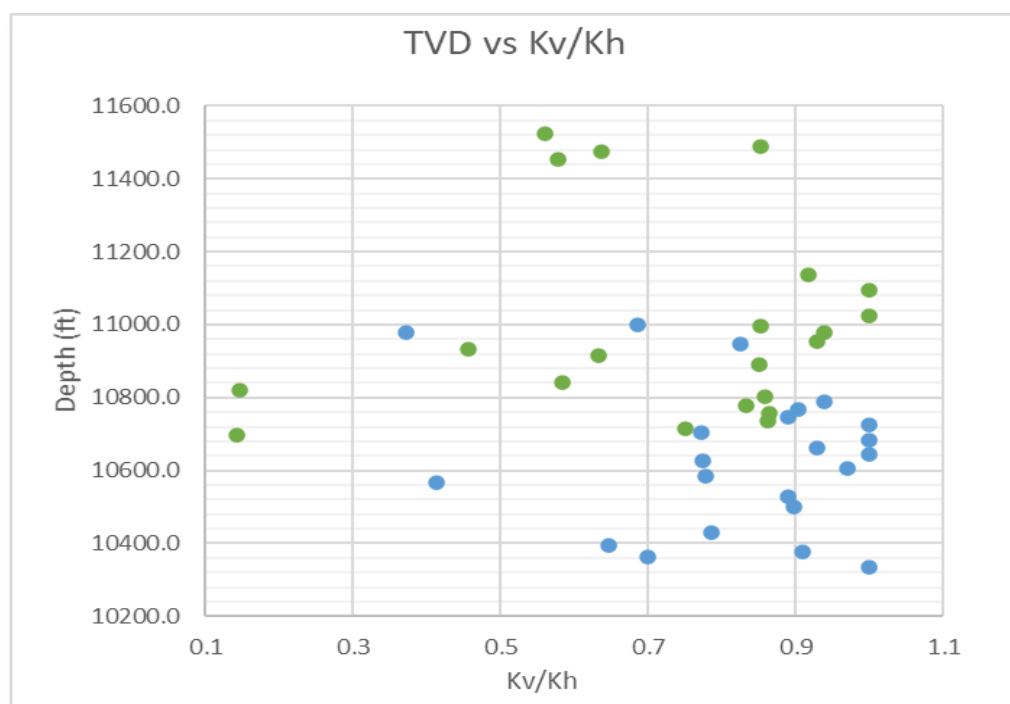


Figure 2.18. Permeability anisotropy

Reservoir heterogeneity is considered as a crucial factor affecting reservoir performance. Heterogeneity in the reservoir occurs as a result of different depositional and diagenetic processes. The degree of reservoir heterogeneity of three wells including X1, X4 and X5 has been effectively analyzed by constructing ordered and unordered Lorenz plots based on core data. The graph represents that the heterogeneity of reservoir changes from significant to fair. To construct the Lorenz plot, the product of reservoir permeability and thickness of reservoir for each interval was arranged in descending order. The same procedure is applied for porosity values. Following, the cumulative of the product (kh) was normalized between 0 and 1 which is known as fraction of total flow capacity. The same normalization

was realized on the cumulative of the (ϕh) values which represents the fraction of total storage capacity. Eventually, the fraction of total flow and storage capacity data was compared to sketch the Lorenz graph [15]. The diagonal line in the ordered Lorenz graph corresponds to perfectly homogeneous reservoir and deviation from this line indicates heterogeneity of the reservoir. The more deflection from the line, the higher degree of heterogeneity. It can be clearly seen that, well X4 is more likely homogeneous, whereas well X1 is determined as slightly heterogeneous and well X5 as highly heterogeneous. When it comes to modified Lorenz plot, for well 4, there is significant overlap between diagonal line and X4 curve, meaning approximately all pores are contributing to the flow and there is prospect of smooth hydrocarbon recovery. As regards the Well 1, there is slight difference between curves, meaning that some of the pores are not contributing to the flow. In terms of Well 5, the substantial difference between X5 curve and diagonal line shows that not all pores have equal contribution to the flow [16] [17].

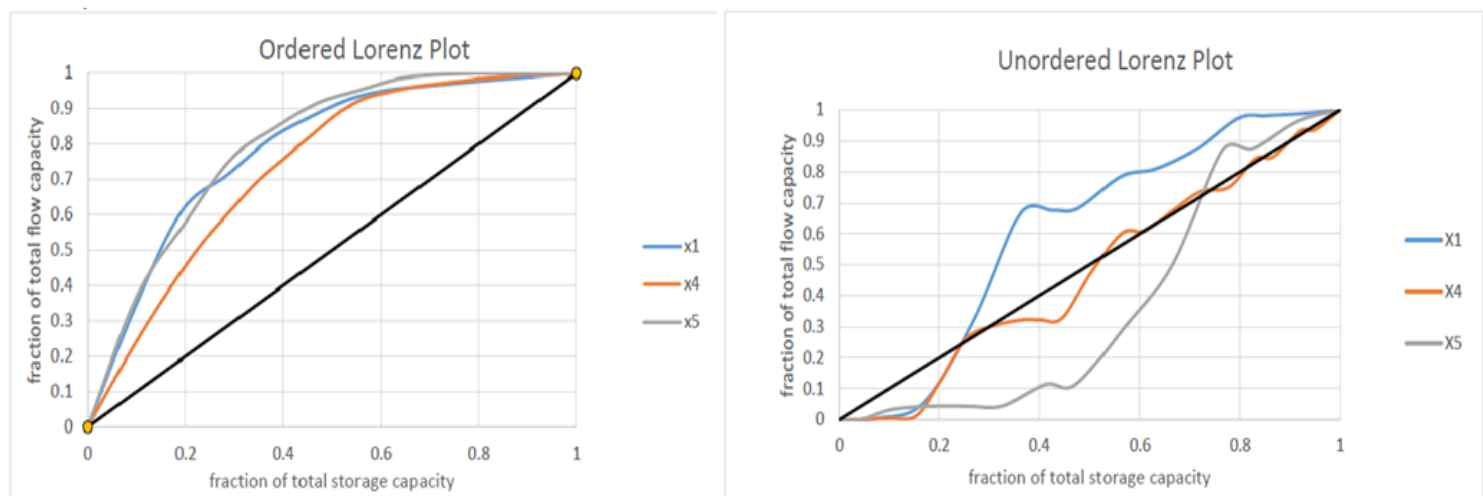


Figure 2.19. Ordered & Unordered Lorenz Plot

2.14. Shale Volume Calculation

Before calculation of shale volume, I_{GR} (gamma ray index) should be defined by using this equation:

$$I_{GR} = \frac{GR_{log} - GR_{min}}{GR_{max} - GR_{min}}$$

Where,

- GR_{log} -gamma ray reading, API
- GR_{min} -minimum gamma ray representing clean sand, API
- GR_{max} -maximum gamma ray representing clean sand, API

Following steps demonstrate calculation of shale volume:

Determination of productive zones using the well logs;

Defining of appropriate values of GR using the depth values;

Calculation of I_{GR} with equation that was shown above

After getting the value of I_{GR} , the shale volume can be calculated as shown below. Although different approaches exist for shale volume calculations, the team decided to use Larionov method suitable for old rocks. Considering the fact that X-field has been deposited during Jurassic period, the choice of equation is reasonable [\[26\]](#).

$$V_{shale} = 0.33 * (2^{2*I_{GR}} - 1)$$

The results have been used to construct cross plot graph between log porosity and shale volume.

2.15. Evaluation of Net Sand/Gross Interval

Before starting estimation, 2 terms should be clarified [\[22\]](#):

Gross interval is the interval where the reservoir locates (including non-productive ranges). For the current case, the range starts from the top of reservoir (appointed via well logs or structural maps) and ends at OWC (appointed via well log / RFT analysis).

Net pay are certain portions of the reservoir which encounter further standards for pay (such as permeability & hydrocarbon saturation). In order to identify this zone, cut-off criteria is mainly used. This criteria comprises application of the cut-offs values for parameters of the reservoir rock for avoiding uncommercial production. The determination process is carried out by means of both core & log data. Among them the log data analysis is considered as more precise method to make decisions regarding the reasonable cut-offs.

The cut-off criteria contains three cut-offs for defining thickness of the net pay zone: shale volume, porosity & water saturation. The shale cut-off removes the part of formation that covers relatively large portions of shale (non-productive zones) and provides cleaner sand intervals. The interval which satisfies the shale content is called **net interval (gross sand)**. The porosity cut-off delivers satisfactory

absolute permeability to acquire higher commercial production. **Net sand** zone (eliminates low porous areas) satisfies the shale & the porosity cut-offs. Productivity of satisfactory effective permeability is managed by the water saturation cut-off. Net pay zone satisfies all given types of cut-offs and comprises the movable hydrocarbons [23] [22].

In general, plenty of ways exist to identify reasonable cut-offs: Receivers Operating Characteristics (ROC) curve analysis, Discriminant Analysis (DA), Logistic Regression Analysis etc. Nevertheless, choosing the base figure for a cut-off type, such as resistivity, saturation or permeability (mostly used) is one of the most famous approach in petroleum industry. By knowing the certain base value for a parameter the equivalent quantity of the remaining rock properties is determined via graphical relationships (cross-plots). In this estimation, permeability and 1 mD of it are selected as base conditions for further evaluation [21]. This figure is considered a lower permeability limit (higher limit: 5 mD) for a productive oil reservoir. Following conditions are required for cut-off values of net pay zone:

$$\phi \geq 0.15$$

$$S_w \leq 0.45$$

$$0.15 < V_{sh} < 0.45$$

In the following part, all steps in the determination of cut-off values for well X-1 have been illustrated. The procedure will be repeated for the rest of the well to find respective cut-off values and net-to-gross ratios.

Cut-off for Porosity. Graph of cross-plot relationship between core porosity & permeability (Figure 2.20) is generated in order to clarify cut-off for porosity:

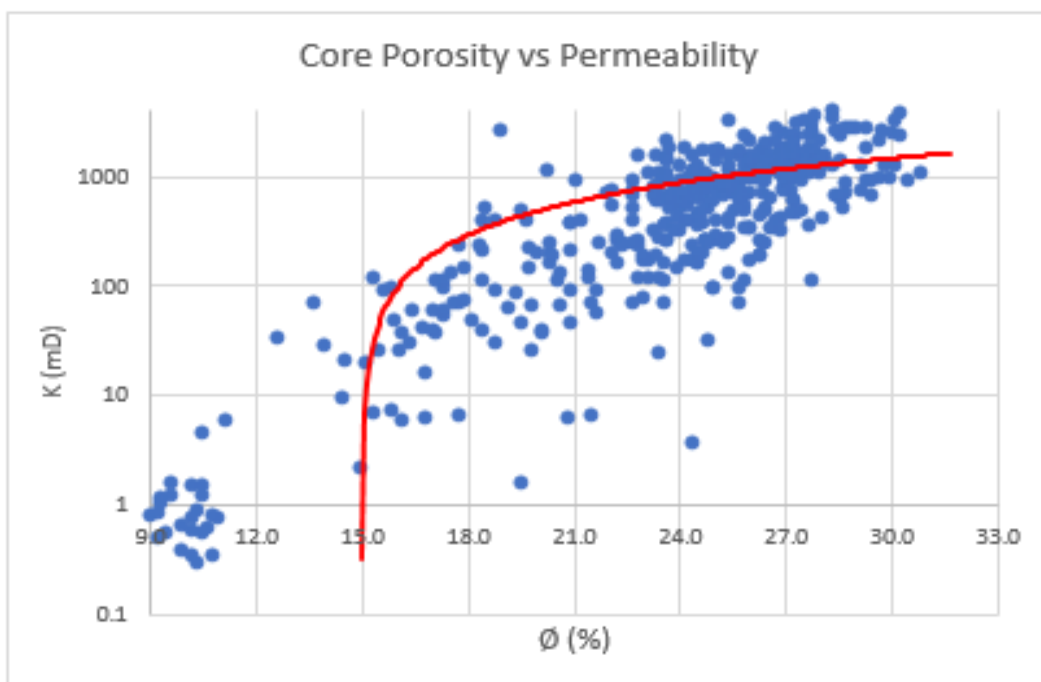


Figure 2.20. Cross-plot relationship between core porosity & permeability

As it is seen from the figure, cut-off for porosity at the base point (1 mD permeability) is about 15%.

Note: Starting from here this number (15% porosity) will be used as base condition during determination of cut-offs (for remaining wells as well).

Cut-off for Saturation. Graph of cross-plot relationship between log porosity & water saturation (Figure 2.21) is generated in order to clarify cut-off for saturation:

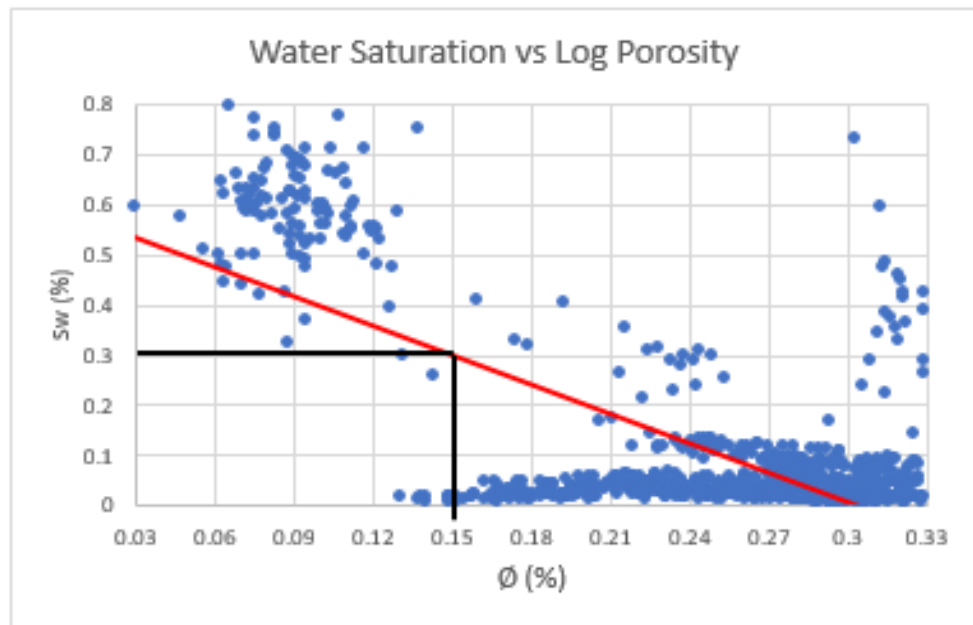


Figure 2.21. Cross-plot relationship between water saturation & log porosity

Cut-off for saturation is about 0.3 (in accordance with the equivalent porosity – 15%).

Cut-off for Shale Volume. Graph of cross-plot relationship between log porosity & shale volume (Figure 2.22) is generated in order to clarify cut-off for shale volume:

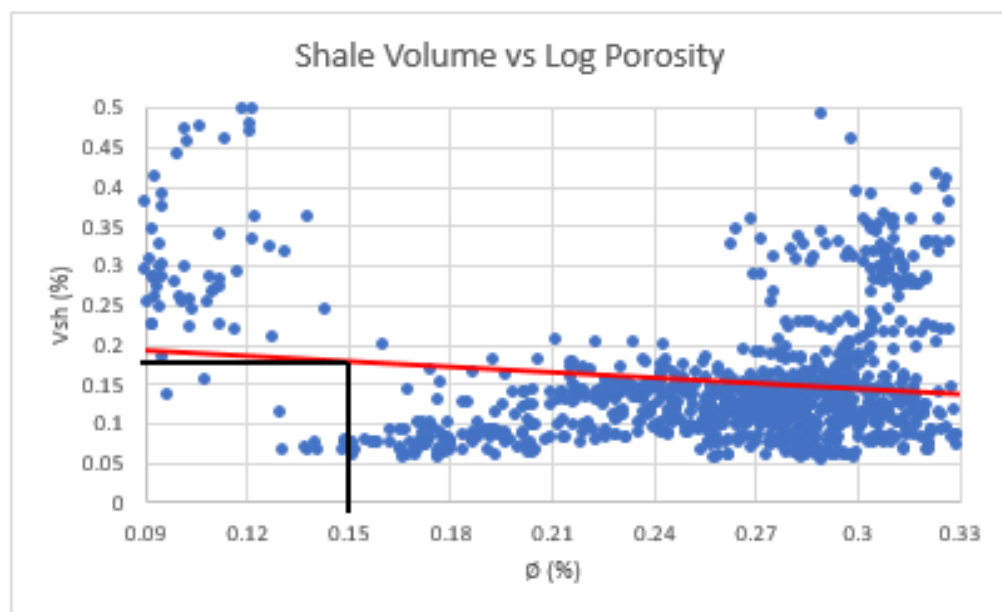


Figure 2.22. Cross-plot relationship between shale volume & log porosity

Cut-off for shale volume is about 0.18 (in accordance with the equivalent porosity – 15%).

As a result, cut-off values for provided parameters (Well X-1):

Porosity – 15%

Water saturation – 30%

Shale volume – 18%

When it comes to determination of required zones, core calibration method (Figure 2.23) has been applied. This method highlights clarifying gross sand, net sand & net pay zones with the help of log scale. In order to carry out this process, shale volume, porosity and water saturation values obtained from log data are plotted separately [24]. The cut-off values (which play limiting role in given data) define each necessary zone one by one. Going into more detailed information,

- V_{sh} values that are lower than cut-off for shale volume identify gross sand interval (eliminating shale zones);
- ϕ values that are more than cut-off for porosity identify net sand interval (eliminating nonporous zones);
- S_w values that are lower than cut-off for water saturation identify net pay interval (eliminating water zones);

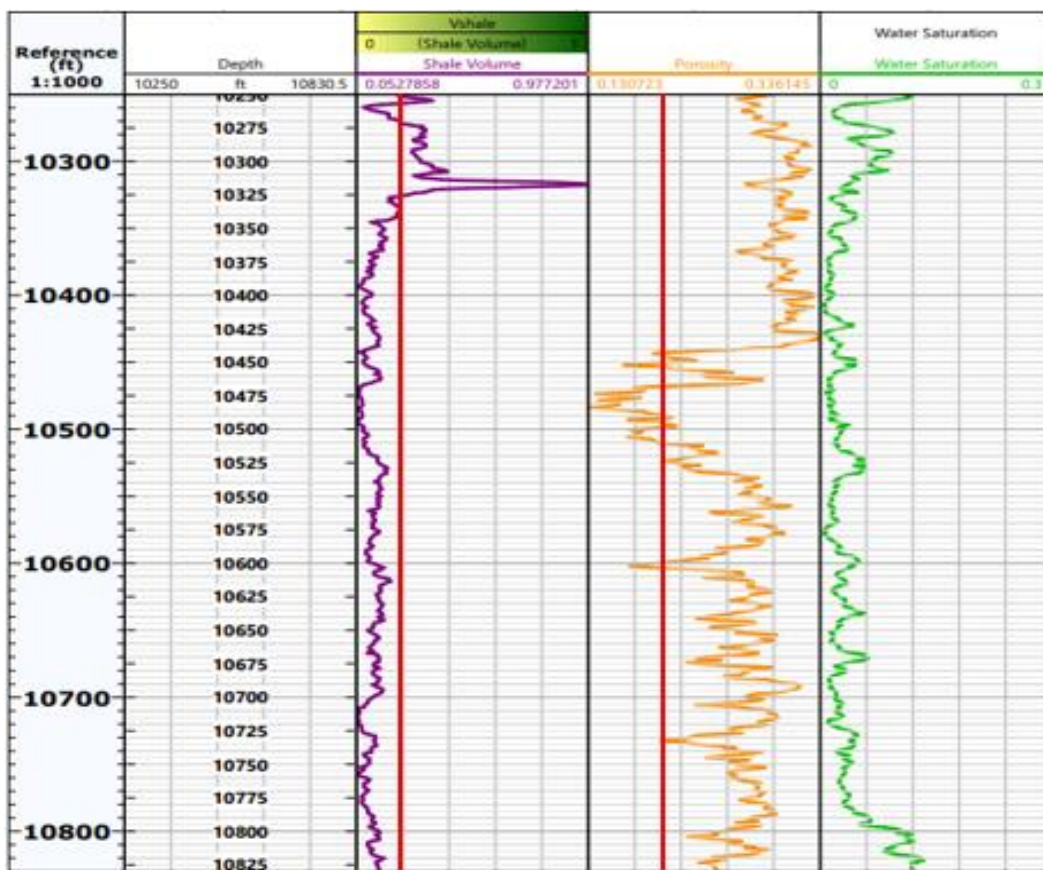


Figure 2.23. Core Calibration Method

- Gross interval: 10830 ft – 10250 ft = 580 ft;
- Gross Sand (applying cut-off for shale volume): 10830 ft – 10320 ft = 510 ft;
- Net Sand (applying cut-offs for shale volume & porosity): (10450 ft – 10320 ft) + (10830 ft – 10510 ft) = 450 ft;
- Net pay (applying cut-offs for shale volume, porosity & water saturation): (10450 ft – 10320 ft) + (10830 ft – 10510 ft) = 450 ft.

Once the net pay zone is declared, then it is time to determine Net to Gross ratio (N/G) which will be necessary in STOIIP calculations during “Reservoir Engineering” section. N/G is the ratio of the figures of net pay zone to gross interval.

$$N/G = \frac{450 \text{ ft}}{580 \text{ ft}} = 0.77$$

The same method has been applied to the rest of wells (Appendix A3). The outcomes acquired from all wells are tabulated beneath:

Well	Productive Oil Zone “ft” (TVDSS)	Gross Interval “ft”	Gross Sand “ft” (V_{sh} cut-off)	Net Sand “ft” (V_{sh} & \emptyset cut-offs)	Net Pay “ft” (V_{sh} , \emptyset & S_w cut-offs)	N/G
X-1	10350-10830	480	420	370	370	0.77
X-2	10620-10860	240	140	135	135	0.56
X-3	10550-10855	305	240	240	230	0.75
X-4	10330-10840	510	480	480	450	0.88
X-5	10100-10680	580	510	360	360	0.62
X-6	10100-10550	450	430	430	410	0.91

Table 2.7. Results of Net to Gross ratio calculations

3. RESERVOIR ENGINEERING

3.1. Gross Rock Volume (GRV) Calculation

To begin with, the preliminary assignment is associated with the determination of Stock Tank Oil Initially in Place (STOIP). Before starting STOIP calculation, it is required to make sure that all necessary parameters for STOIP estimation are ready to put into equation and subsequently, compute STOIP value. In geology part, some key parameters, including porosity, saturation, and net to gross ratio have been identified except from gross rock volume. As these parameters will be inputs for STOIP equation, all of them should be calculated beforehand. In this case, the only remaining one is GRV so that GRV calculation steps will be introduced first.

To perform GRV calculation, the top structure map for the X field will be utilized in order to determine area values between contour lines. In our case, counting square method will be applied to figure out areas and then triangular shape will be assumed while finding volume from depth versus area graph. This methodology is called “Depth-Area-Thickness” (DAT) and provides better accuracy & flexibility in GRV calculation [5]. As it was shown previously, the X-field has been compartmentalized caused by the presence of faults. This can also be proven by having different OWCs for wells X-1,2,3,4 and wells X-5,6. Therefore, GRV and resultant STOIP calculations will be carried out separately for each compartmentalization. Southern compartment being larger one, includes wells X-1,2,3,4 while relatively smaller compartment – Northern compartment covers well X-5,6. As an example of DAT methodology and counting square technique, area bounded by contour depth of 10300ft has been illustrated below (Figure 3.1) where pink and red shadings correspond to the north and south compartment respectively.

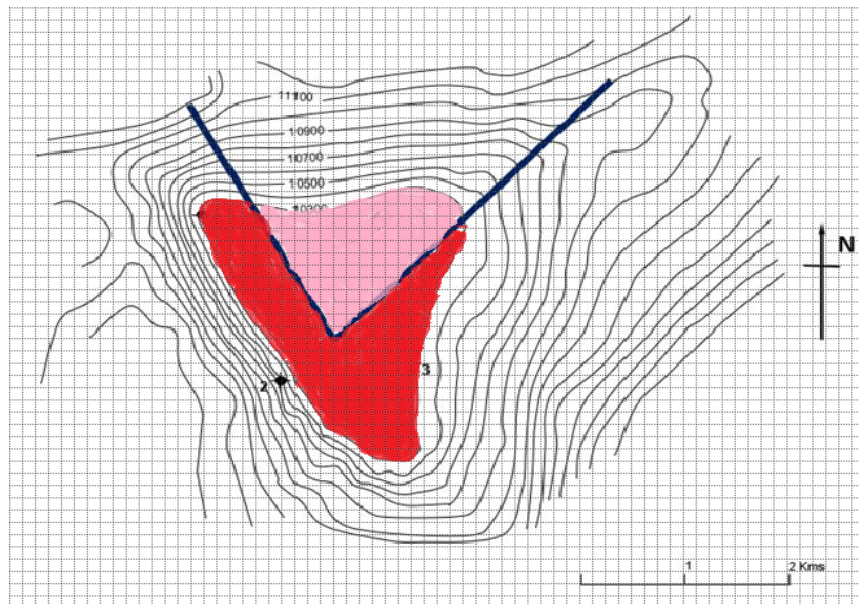


Figure 3.1. Square counting method for 10300ft

This procedure has been repeated for the depth intervals of 9776-10860ft and 9776-10600ft for South and North compartments respectively. The value of 9776ft estimates the top of the reservoir and it has been found via the extrapolation. The end value of these intervals has been selected based on the OWCs of the wells grouped together. After determining area values for separate depths, the graph expressing the relationship between depth (ft) and area (ft²) has been constructed for both compartments (Figure 3.2 and 3.3):

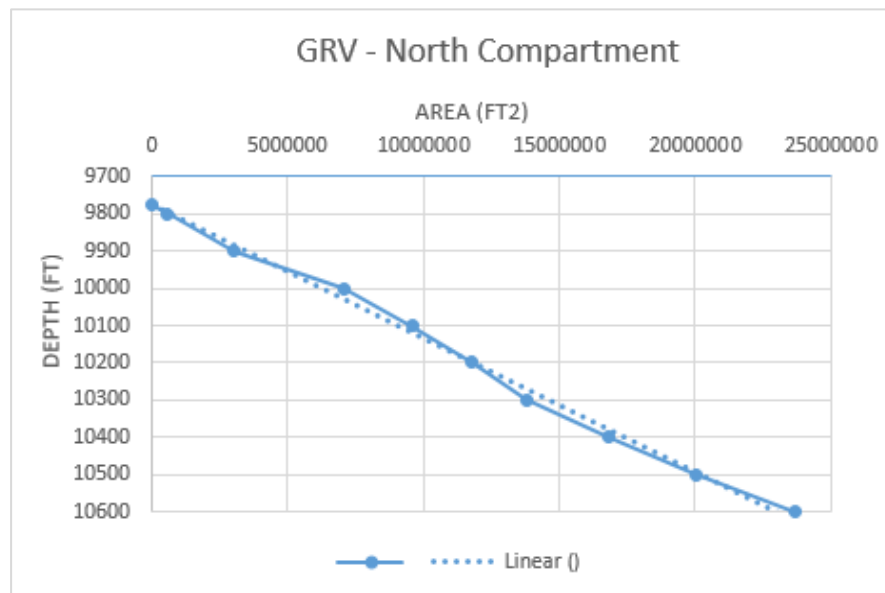


Figure 3.2. GRV calculation via triangular method (North Compartment)

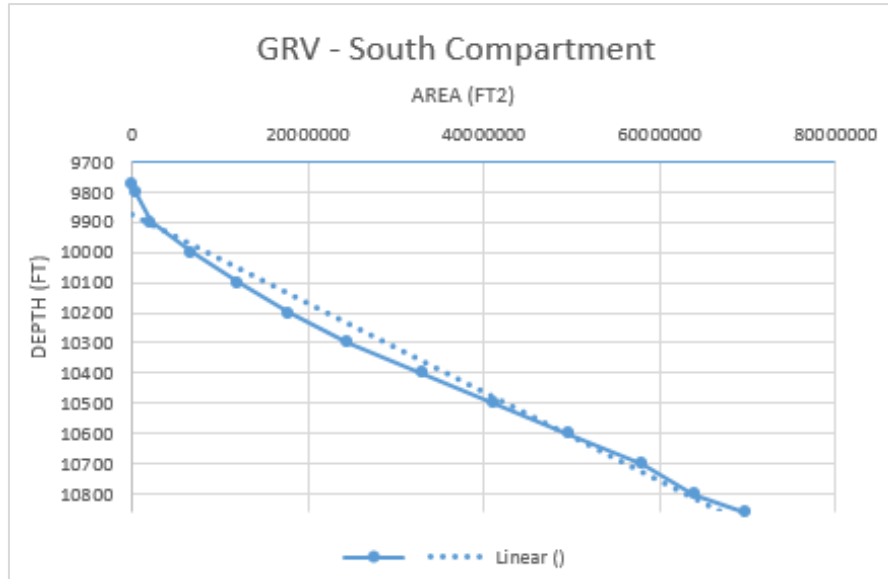


Figure 3.3. GRV calculation via triangular method (South Compartment)

At the end of calculations, GRV for both compartments have been figured out and the results have been tabulated beneath (Table 3.1):

Compartments	GRV (acre-ft)
South	777127.11
North	224294.46

Table 3.1. GRV values

3.2. STOIIP Calculation

STOIIP calculation and following reserve estimation are highly essential aspects of the field development project. With the aim of estimating the reserves, first, it is required to calculate STOIIP, which will be done through two different approaches: deterministic and probabilistic. In the end, the final results will be compared to each other to assess the reliability of calculations.

3.2.1. Deterministic STOIIP Calculation

In this technique, previously obtained parameters (net to gross, porosity, saturation, and GRV) will be used as an input to the following well-known equation:

$$STOIIP = \frac{7758 * GRV * \varphi * (1 - S_w) * N/G}{B_o}$$

In the equation above,

- GRV – gross rock volume (acre-ft);
- φ – porosity (in fraction);
- S_w – water saturation;
- N/G – net to gross ratio;
- B_o – oil formation volume factor (rb/stb);
- 7758 – conversion factor from acre-ft to bbl;

With the help of equation given above, three STOIIP calculations can be done to find out minimum, maximum, and most likely values. Detailed calculation steps have been provided in Appendix part. Briefly describing, maximum, minimum, and average values of porosity & saturation should be determined for all wells which then need to be averaged again in order to obtain single porosity & saturation value for each compartment. As regards formation volume factor, it has been taken as constant value of 1.323 (from overview document) throughout the calculations. The table 3.2 below summarizes all outcomes of STOIIP calculations:

Compartments	Minimum STOIPP (MMSTB)	Most Likely STOIPP (MMSTB)	Maximum STOIPP (MMSTB)
South	412	683	903
North	103	171	219
TOTAL STOIPP (MMSTB)	515	854	1122

Table 3.2. The results of deterministic STOIP calculation

3.2.2. Probabilistic STOIP Calculation

Probabilistic method of STOIP is determined by applying Monte Carlo simulation which is implemented via Oracle Crystall Ball software. Minimum, maximum and average values of porosity and saturation along with constant parameters such as GRV, N/G and Bo were inserted into the program to identify probabilistic STOIP. It can be clearly seen from Figures 1 and 2, triangular method was applied by running 5000 iterations which gave P10, P50 and P90 values of STOIP. After summing STOIP figures of North and South compartments, the results were represented in the Table 1. The most likely value of STOIP was determined as 839 MM STB which can be considered close to the deterministic value of STOIP (854 MM STB). The slight deviation of 1.76 % proves preciseness of our computations.

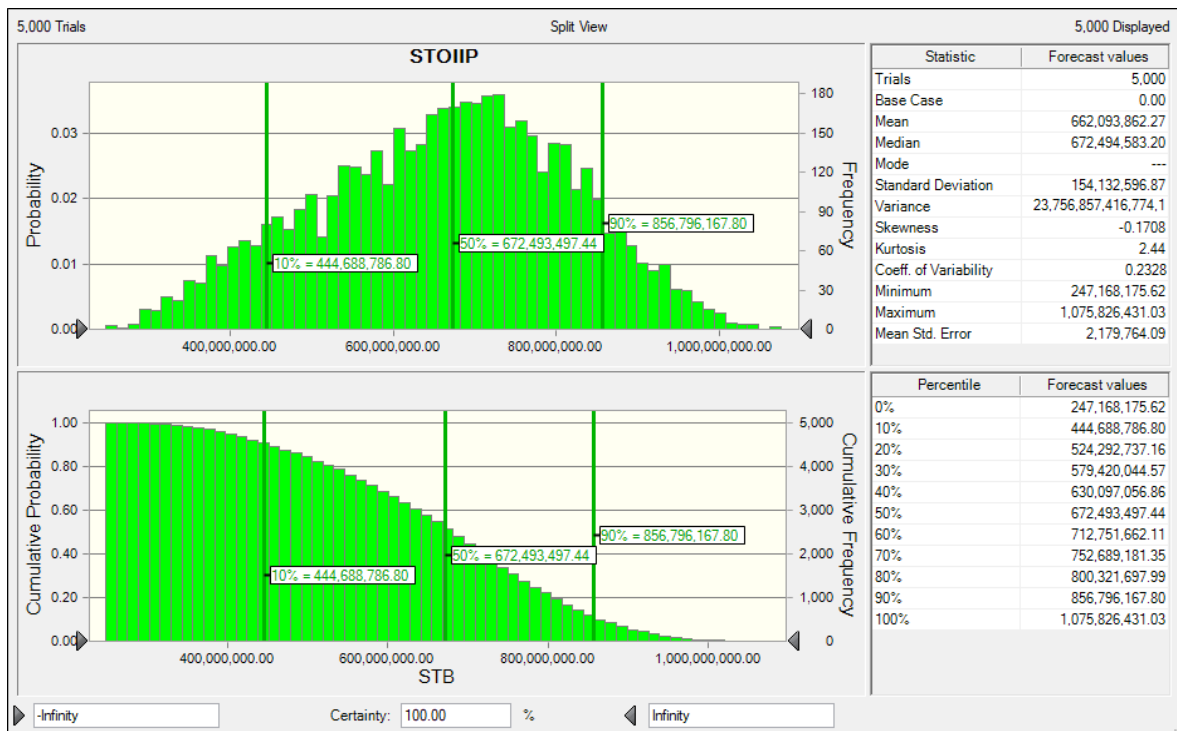


Figure 3.4. Probabilistic STOIP estimation for North compartment

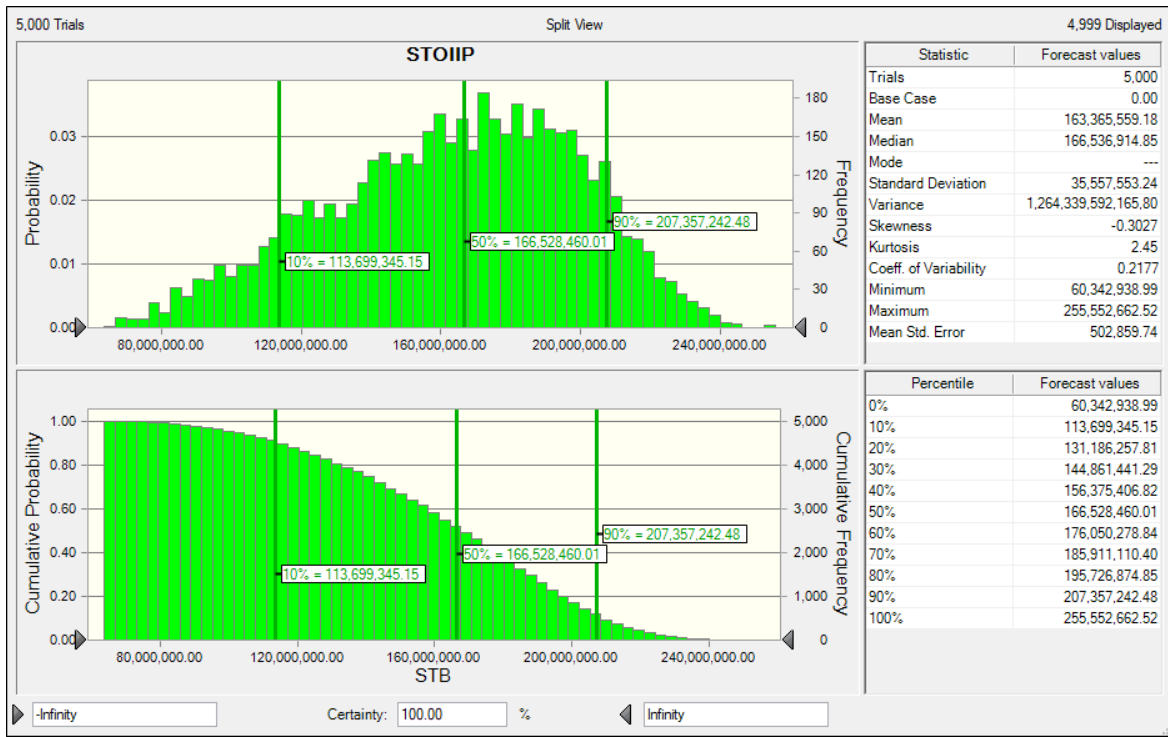


Figure 3.5. Probabilistic STOIP estimation for South compartment

Probability	STOIP (STB)	STOIP (MM STB)
90%	558,388,131	558
50%	839,021,957	839
10%	1,064,153,409	1064

Table 3.3. The results of probabilistic STOIP calculation

3.3. STOIP Sensitivity Analysis

This analysis is principally aimed to identify how different reservoir parameters affect STOIP evaluation and changes in these properties influence on STOIP value. STOIP estimation depends on four parameters (gross rock volume, porosity, net to gross ratio & water saturation) that may have deviation from their initially calculated values due to various reasons. For instance, inappropriate fault locations and fluid contacts can contribute to error in GRV value. Besides it, undesirable quality of the logs where the values of porosity & water saturation have been defined can also result in deviation. Human factor (not taking precise figures from log data) plays an important role in this part. Lastly, inexactness in the values of N/G is not exceptional as well. In the sensitivity analysis, the figure of each property is deviated between -20% and +20% once, while other parameters remain stable. Contribution of these alteration to STOIP value have been provided on Figure 3.6 in which it is obvious that GRV, N/G & porosity are linearly proportional to STOIP (by taking its

formula into account). Given deviation interval of aforementioned parameters can cause STOIIP to change between 683 MMSTB and 1025 MM STB. The least affecting reservoir property is water saturation whose 20% rise will descend STOIIP by only 32 MM STB from 854 MM STB to about 822 MM STB. Table 3.4 in given below highlights the STOIIP values in each deviation of input parameters.

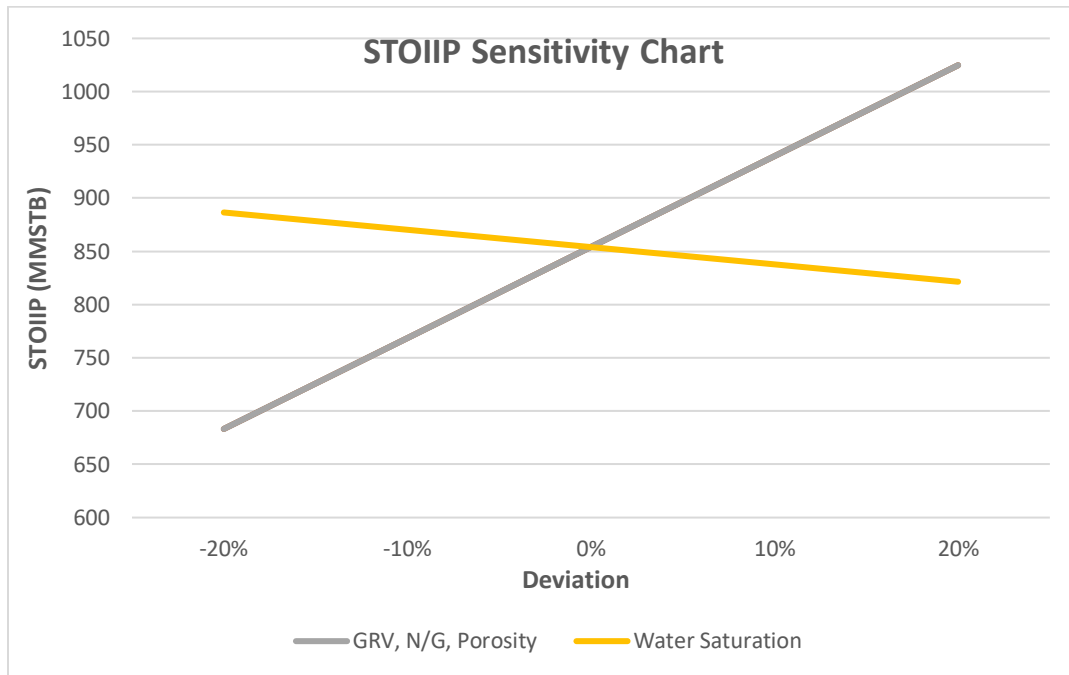


Figure 3.6. STOIIP value change by means of given parameters

Parameters \ Deviations	-20%	-10%	0%	+10%	+20%
Gross Rock Volume	683.2	768.6	854	939.4	1024.8
Porosity	683.2	768.6	854	939.4	1024.8
Net to Gross	683.2	768.6	854	939.4	1024.8
Water Saturation	886.5	870.3	854	837.7	821.5

Table 3.4. Sensitivity analysis

3.4. Drive mechanism and Reserves Estimation

3.4.1. Drive Mechanism

In order to calculate field reserves, first, it is necessary to ascertain the drive mechanism as it influences the recover factor. Examination of the field overview document suggests that initially, reservoir pressure is higher than bubble point pressure, which proves the presence of undersaturated reservoir. Moreover, the log analysis also proves that no any gas region has been encountered in the reservoir. Consequently, neither gas cap nor solution gas is active drive mechanism for the X-field. Gravity drive mechanism is not the option, as its effects seem to be negligible. On the other hand, injectivity test results for some wells prove that aquifer support is weak caused by low permeability and tight aquifer sand as after one years production, reservoir pressure declined by 1000 psi. This means eventually, to sustain the oil production, water injection scenario will be considered in the future. Finally, it can be stated that the main driving force for the reservoir in question comes from expansion drive mechanism.

3.4.2. Recovery Factor (RF) Estimation

In order to estimate the recoverable amount of hydrocarbons, we need to find out recovery factor value and then by using the well-known equation below, reserves can be predicted. Recovery factor is a function of various parameters, including drive mechanism, rock & fluid properties, and reservoir heterogeneity. However, to have initial estimation of reserves, it is necessary to assume reasonable recovery factor value for utilizing in the calculations. This has been achieved by examining nearby analogous fields, such as Fulmar, Nelson, and Forties. In the mentioned field, recovery factors change between 40%-60% depending on the previously stated factors [5]. However, it is expected to have relatively high recovery factor in X-field due to combined effects of the large length of reservoir perforated, excellent reservoir quality, sweep efficiency by water injection, and further strong pressure support [5]. In the future section of the report, a kind of sensitivity analysis for reserve estimation (where the impact of recovery factor on reserves will be evaluated) will be performed by using the equation below:

$$\text{Reserves} = \text{Hydrocarbons in Place} * \text{Recovery Factor}$$

Recovery factors depends on fluid properties, petrophysical properties and differences due to architecture and reservoir heterogeneities. However, different drive mechanisms can cause various recovery factors as well. Since the X field is one-phase oil reservoir type, its natural recovery factor will be less than 10% because of drive energy coming from fluid-rock system expansion. Gravity drainage can improve the recovery as well (dip angle less than 20°). Moreover, supplementary drive mechanism is required due to the poor aquifer support. Overall, recovery factor tends to rise up to 60%.

In terms of secondary recovery, the core idea is to hold reservoir pressure as high as possible and to obtain large displacing amounts of hydrocarbons. To do so, two main conventional techniques are applied: water injection and immiscible hydrocarbon gas flooding. In fact, immiscible hydrocarbon gas flooding cannot be applied because reservoir pressure is above bubble point. On the other hand, injection of water is more practical solution in the North Sea fields [9]. Actually, if oil is light (X field crude oil has API 39°), water injection is very advantageous. Finally, if we consider reservoir fluid properties, reservoir conditions and availability for water injection, it has been chosen as a secondary recovery mechanism.

3.4.3. Reserve Estimation & Its Sensitivity Analysis

After considering all factors, total field reserves have been calculated by using the recovery interval of 40-60% justified previously. It is worthy to note that final results of reserve calculation for both deterministic and probabilistic methods have been tabulated below:

Total Reserves (MMSTB)	RF=40%	RF=50%	RF=60%
MIN Reserves	206	257	309
Most Likely Reserves	342	427	513
MAX Reserves	449	561	673

Table 3.5. Total reserves of X-field when using **deterministic** STOIIP

Total Reserves (MMSTB)	RF=40%	RF=50%	RF=60%
P90 Reserves	218	273	327
P50 Reserves	333	417	500
P10 Reserves	426	533	640

Table 3.6. Total reserves of X-field when using **probabilistic** STOIIP

3.5. Special Core Analysis

The fundamental aim of this analysis is to identify characteristics of capillary pressure & relative oil permeability by carrying out several investigations on the core samples obtained from the reservoir section of the appraisal wells. Generally, in reservoir engineering the role of capillary pressure phenomena is remarkable since it helps to clarify different reservoir properties. For instance, graphical relationship between capillary pressure and saturation determines transition zone range of OWC which is a crucial parameter within identification of suitable zones for water injection wells. Special core

analysis has been done on the core plugs taken from various depths of X-1 & X-5 wells. The process is called Mercury Injection. Certain amount of mercury is injected to the sample under pressure until its void spaces are fulfilled with that liquid. The figures of pressure and occupied volume are accurately recorded in each stage.

Analysis of 13 core samples taken from X-5 well distinguishing by different porosity & permeability values has been conducted via mercury injection method. The following figure showing pressure – saturation graph contains the data acquired from each plug.

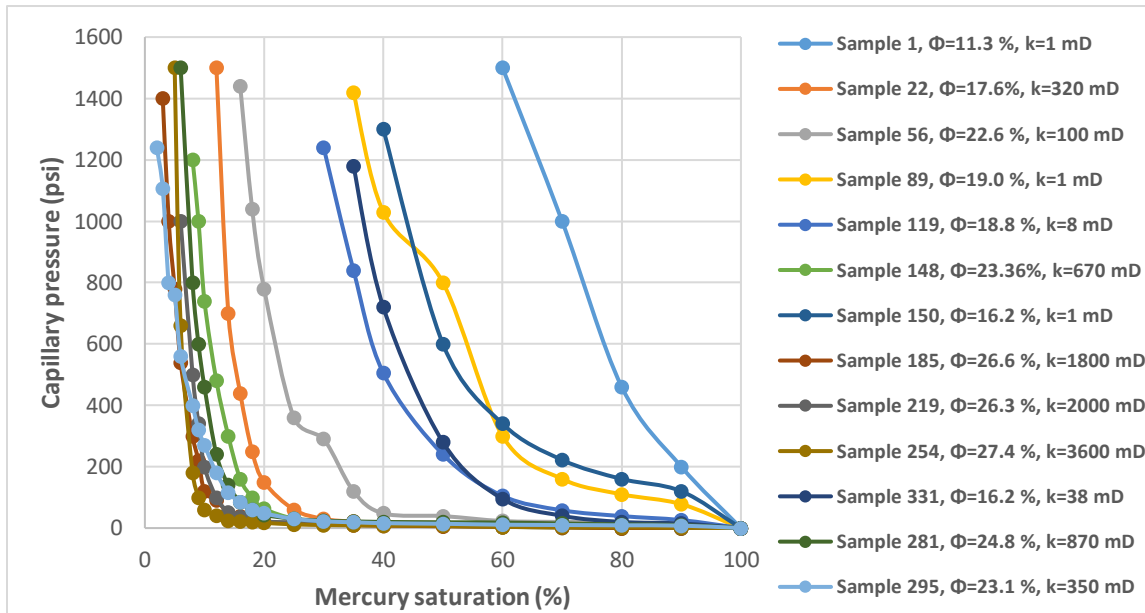


Figure 3.7. Pressure-saturation relationship for core analysis

However, the above investigation is not relevant for reservoir condition. In order to reach this condition the air-mercury system must be converted to oil-water system. The formula beneath indicates how to do this operation:

$$\frac{(P_c)_{oil-water}}{(P_c)_{air-Hg}} = \frac{(2\sigma\cos\theta)_{oil-water}}{(2\sigma\cos\theta)_{air-Hg}}$$

In which, σ & θ are interfacial tension and contact angle between fluids, respectively.

$$\sigma_{oil-water} = 16 \text{ dynes/cm}; \quad \sigma_{air-Hg} = 486 \text{ dynes/cm}$$

$$\theta_{oil-water} = 0 \text{ degrees}; \quad \theta_{air-Hg} = 130 \text{ degrees}$$

$$\text{Conversion Factor} = \frac{(\sigma\cos\theta)_{oil-water}}{(\sigma\cos\theta)_{air-Hg}} = \frac{16 * 1}{486 * 0.642} = 0.051$$

The data on Figure 3.7 can be converted into the reservoir condition now:

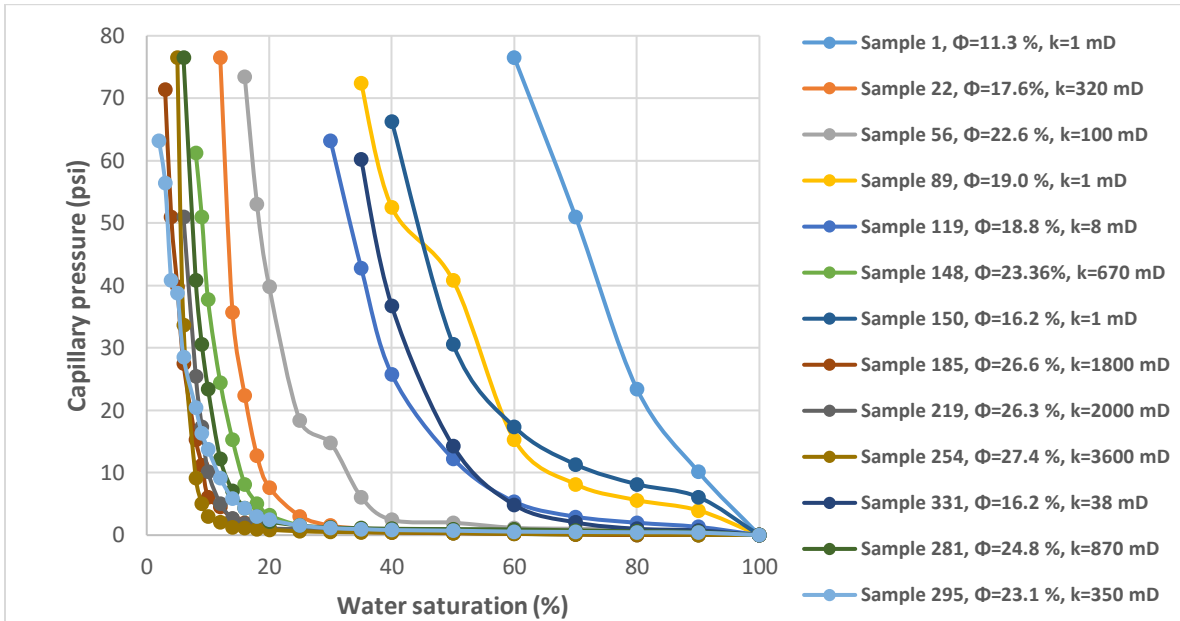


Figure 3.8. Capillary pressure and water saturation relationship for core analysis

Figure 3.8 displays relationship between capillary pressure and water saturation for each sample in which it is evident that longer transition zone is caused by lower porosity and permeability. Going into more details, despite the fact that samples № 1, № 89 & № 150 display undesirable transition zone for having low porosity and permeability properties (low interaction between pores and small radius of pore throat), samples № 185, № 254 & № 295 have shorter transition zone due to high porosity and permeability values.

Turning to relative permeability analysis, it has been carried out for two different cases having the same OWC depth (10840 ft TVDSS) and various ranges of porosities & air permeabilities. These cases are differentiated for their compartments. One (relative permeability curves of $\phi > 27\%$ & $k_{air} > 1000 \text{ mD}$ on Figure 3.9) has small compartment whereas the other one (relative permeability curves of $\phi < 20\%$ & $k_{air} < 10 \text{ mD}$ on Figure 3.9) experiences large compartment. Graphical representation of the aforementioned two regimes have been provided below. It should be noted that the given data belong to the core samples taken from X-6 well.

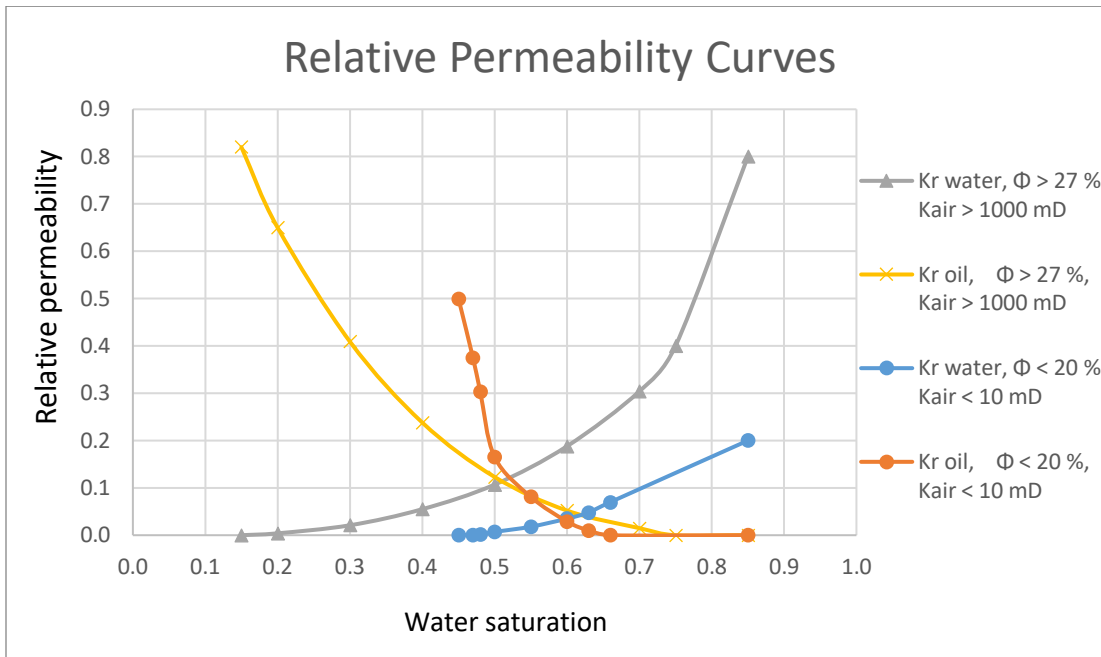


Figure 3.9. Relative permeability to oil and water

As it is shown in Figure 3.9 primarily connate or irreducible water saturation exists for small compartment. Later, when water saturation rises, the relative permeability to oil reduces. For the time being, with augmentation in water saturation relative permeability to water increases. For minor compartment, critical saturation of water where the relative permeability to water begins to ascend is between 10% and 20%, while this figure for major compartment is around 40-50%. The principal reason is diverse wettability & permeability aspects of two various compartments. Last but not least, residual oil saturation is also present at final points of the relative permeability to water curve for minor compartment. [6]

3.6. Fractional Flow Evaluation

3.6.1. Water Injection Analysis

As it was discussed earlier in the drive mechanism section, X-field requires to perform water injection with the aim of maintaining reservoir pressure above the bubble point pressure as pressure support coming from aquifer is not strong enough. The key reason behind this issue is sourced from the fact that the aquifer rock is consisted of low permeable and tight sand as proved by the injectivity tests conducted in the aquifer. The primary objective of water injection will be to procrastinate the occurrence of reservoir pressure drop below the bubble point pressure. Water injection wells should be drilled and designed carefully by considering geological and engineering matters in order to meet the injection requirements and avoid the early water breakthrough. Being one of the most effective types of secondary recovery techniques, water flooding targets to increase the oil recovery by “voidage replacement” which means increasing the reservoir pressure to its preliminary level and keeping it near that pressure value during

the well life. In addition to reservoir pressure support, injected water sweeps or displaces oil from the reservoir by pushing it towards wellbore. However, the efficiency of such displacement process depends on certain factors, such as mobility ratio and rock properties.

The source of injected water may change based on some factors, including availability and location of the field. Sometimes, produced water itself is utilized as an injection fluid after treatment processes as it can reduce the possibility of formation damage caused by incompatibility of fluids. However, the amount of produced water is not sufficient for effective injection process therefore; supplementary water usually from sea is the most convenient option considering offshore operations [1].

On the other hand, water injection brings some associated technical challenges as well. In the process of water injection, eventually, the water production will be inevitable. Additionally, if one wants to use produced water as an injection fluid, it is necessary to follow some treatment steps, which requires employing a set of surface equipment being able to handle produced water. Another problem related to water production is associated with environmental matters as sometimes, the disposal of contaminated water is challenging. Moreover, the presence of incompatibility, tubular corrosion and bacteria issues can be problematic.

The zone of interest for water injection is also essential in order to achieve the key objectives mentioned above. If water is being injected into the aquifer zone, this will not be efficient due to low permeable and tight aquifer rock. In order to get enough pressure support from water injection, it is much more recommendable to inject water to just below the OWC or transition zone. Improved sweep efficiency will lead to the increased recovery factor.

3.6.2. Fractional Flow Analysis

The fractional flow analysis was done to sketch the fractional flow curve illustrating the relationship between fractional flow and saturation. Fractional flow means the ratio of water flow to the total fluid flow at any point in the reservoir or core plug. The basic fractional flow equation (f_w) has been demonstrated below (equation 1); however, after making some assumptions, the derivation procedure helps us to obtain simpler equation to use throughout the calculations (equation 2) [2]:

$$f_w = \frac{q_w}{q_w + q_o} \quad (1) \quad f_w = \frac{M}{M+1} \quad (2)$$

Where,

- M is mobility ratio: $M = \left(\frac{k_{rw}}{\mu_w} \right) / \left(\frac{k_{ro}}{\mu_o} \right)$;
- k_{rw} and k_{ro} – relative permeability to water and oil respectively;

- μ_w and μ_o – water and oil viscosity respectively;

Before obtaining the simple fractional flow equation (2), assumptions listed below need to be considered [9]:

- Displacement is incompressible;
- Diffuse flow (saturations at any point are uniformly distributed over the thickness);
- Both oil and water are incompressible and immiscible;
- Impacts of dip angle and capillary pressure are neglected;

In order to calculate fractional flow, it is required to make certain calculations in terms of relative permeability concept. Relative permeability data is highly essential to model the relevant displacement type that is dominant in the reservoir. To initiate calculations, firstly, we need to decide which empirical correlations will be used to find out relative permeability values. Different approaches exist for relative permeability computations, such as “Modified Brooks and Corey”, “Corey’s model”, “Pirson’s model”, and “Kam & Rossen model”. After making detailed research, the team decided to take advantage of the famous model in the petroleum industry – **“Modified Brooks and Corey (MBC)”**. The equations suggested by MBC method have been listed below [3]:

$$k_{rw} = k_{rw}^* \left(\frac{S_w - S_{wc}}{1 - S_{wc} - S_{or}} \right)^{n_w} \quad (3) \quad k_{ro} = k_{ro}^* \left(\frac{1 - S_w - S_{or}}{1 - S_{wc} - S_{or}} \right)^{n_o} \quad (4)$$

Where,

- k_{rw}^* and k_{ro}^* – end-point relative permeabilities for water and oil respectively;
- S_{wc} and S_{or} – connate water and residual oil saturations respectively;
- n_w and n_o – exponents derived from experimental data (for water oil system both are equal to 3) are measure of degree of heterogeneity;

The outcomes of all calculations by using the equations above have been tabulated in Table 3.8. It is worthy to highlight some input parameters for these equations, such as end-point relative permeabilities, connate water and residual oil saturations. By using the relative permeability curve for porosity corresponding to 22-25% (Figure 3.10), it is possible to identify the previously mentioned parameters easily. All input parameters have been given in Table 3.7:

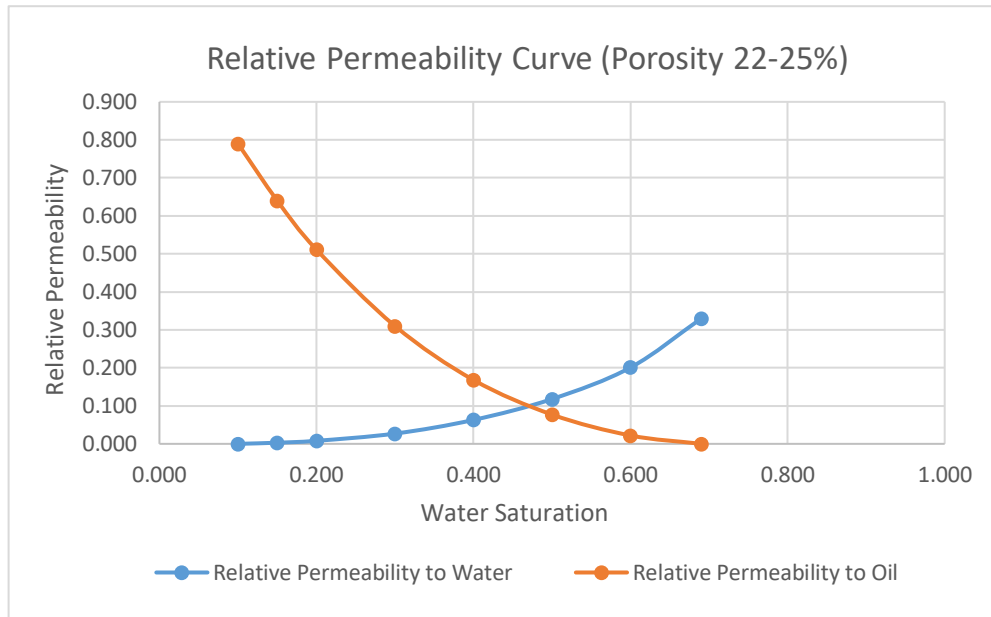


Figure 3.10. Relative Permeability Curve

K_{ro}^*	K_{rw}^*	S_{or}	S_{wc}	n_o	n_w	μ_o	μ_w
0.79	0.33	0.31	0.1	3	3	0.49	0.23

Table 3.7. Input parameters for fractional flow equation

S_w	K_{rw}	K_{ro}	M	f_w
0.10	0.0000	0.7900	0.0000	0.0000
0.15	0.0002	0.6057	0.0007	0.0007
0.20	0.0016	0.4525	0.0076	0.0075
0.25	0.0054	0.3277	0.0353	0.0341
0.30	0.0129	0.2282	0.1200	0.1072
0.35	0.0251	0.1512	0.3538	0.2613
0.40	0.0434	0.0938	0.9852	0.4963
0.45	0.0689	0.0532	2.7601	0.7340
0.50	0.1028	0.0264	8.3037	0.8925
0.55	0.1464	0.0106	29.55	0.9673
0.60	0.2008	0.0028	152.59	0.9935
0.65	0.2673	0.0002	2313.47	0.9996

Table 3.8. Results of fractional flow equation

Now, by using the figures in Table 3.6, the plot of fractional flow versus water saturation has been generated as shown in Figure 3.11. Following this, water saturation at the front can be determined by drawing a tangent line to the fractional flow passing from initial water saturation. This technique is called "Welge Tangent Method" [4]. It is obvious from the graph that at the tangent point, water saturation at the front is $S_{wf}=0.5$ whereas fractional flow of water corresponds to $f_{wf}=0.89$. Moreover, if the tangent line is extrapolated to $f_w = 1$, the value of water saturation ($\bar{S}_w = 0.54$) will be equivalent to average water saturation.

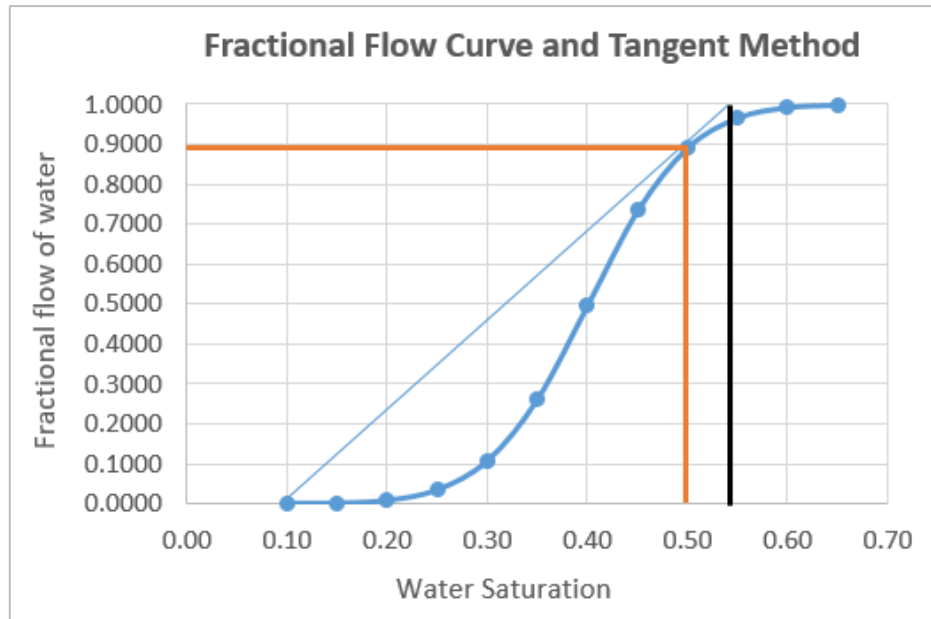


Figure 3.11. Fractional Flow Curve

3.7. PVT Analysis

PVT (Pressure, Volume and Temperature) analysis is utilized to determine various significant properties of reservoir fluid, obtain data for reservoir calculations and surface facility design. Density, viscosity, compressibility, formation volume factor, gas oil ratio, bubble point pressure, mole or mass percent composition and so on should be included in this list. In order to conduct PVT analysis, representative fluid samples are required. They can be taken from bottom hole, wellhead and separator with certain methods and via the help of sophisticated technology. PVT analysis is of pretty much significance for the following production process over the field. As it is mentioned above, while surface equipment is designed, PVT analysis is also required. For instance, the number of stages of separation process and optimum pressure and temperature for separators can be selected with separator test of PVT analysis [9].

Over the field, from the X-1 and X-2 wells, several subsurface samples were taken, while only a few of them (samples from 8 different depth intervals of both wells) is taken into account as uncontaminated. One (sample from 10362 ft) of two samples which were collected from X-1 well was analysed and

analysis process over the other sample is not gone on as the oil content of this sample was not sufficient to perform PVT analysis. Eight valid wellhead and separator samples were also taken from Well X-2, X-3, X-5 and X-6 with DST (drill stem testing), while only surface samples from X-3 were analysed. At the end, results of Well X-3 samples were compared with those of subsurface samples. Certain results and interpretations were ensured at the following section.

Averaged results of PVT analysis for Well X-1, X-2 and X-3 were provided in the following table (**at overview**).

PVT Parameters	Initial conditions	Bubble point
Pressure (psia)	5722 @ 10500 ft	1800
Temperature (°F)	250	250
Bo (RB/STB)	1.323	1.395
Rs (SCF/STB)	505	505
Viscosity (cP)	0.49	0.41
Compressibility Co (10^{-6} Psi$^{-1}$)	10.4	18

Table 3.9. Averaged Results of PVT Analysis

There is huge amount of data for samples of Well X-1 and Well X-2 in excel file of 2020-2021 folder. They were tabulated and certain portion of this data was explained below and graphs were also plotted.

For Well 2

Note: Liquid above bubble point is oil with dissolved gas

From the next figure (**Figure 3.12**), bubble point pressure for Well 2 can be determined. Flash vaporization test is carried out at 250 F in order to obtain the data to plot this graph. Certain amount of reservoir oil (under reservoir temperature and pressure) is filled into PVT cell and pressure in the cell is decreased with movement of piston. While pressure falls, gas gets started to separate at the bubble point. Relative volume is simultaneously noted at the various pressures. It is ratio of **total volume of fluid** (total volume is volume of oil above bubble point, while it is sum of gas and oil volumes below bubble point) to the **oil volume** at the bubble point pressure and temperature (250 F) in the cell. Therefore, value of relative volume should be identical to 1 at the bubble point. Bubble point pressure from x axis can be determined as 1813 psia with this value (1) of y axis.

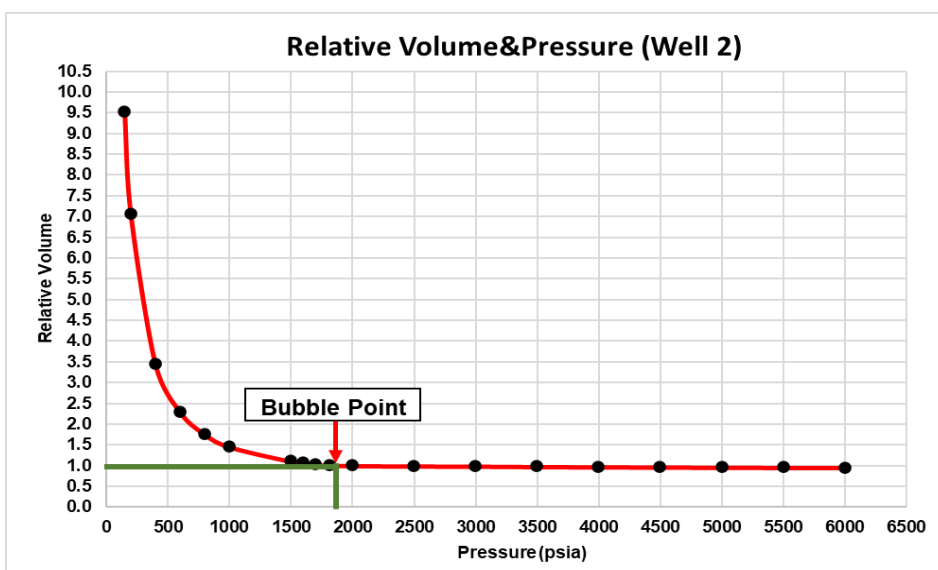


Figure 3.12. Determination of Bubble Point Pressure

Bubble point pressure (1813 psia) which was obtained from the above graph can be proved with Total Fluid Density & Pressure plot (**Figure 3.13**). It can be easily seen from the graph that **total fluid density** reduces gradually from 6000 psia to 1813 psia and then this decrease accelerates between 150 and 1813 psia. Because fluid in the PVT cell is firstly in liquid phase (**oil with dissolved gas**) and until decrease to 1813 psia, the liquid phase expands, without existence of separated gas. After that pressure point, gas begins to separate from liquid (**oil with dissolved gas**), generating higher reduction over the total fluid density.

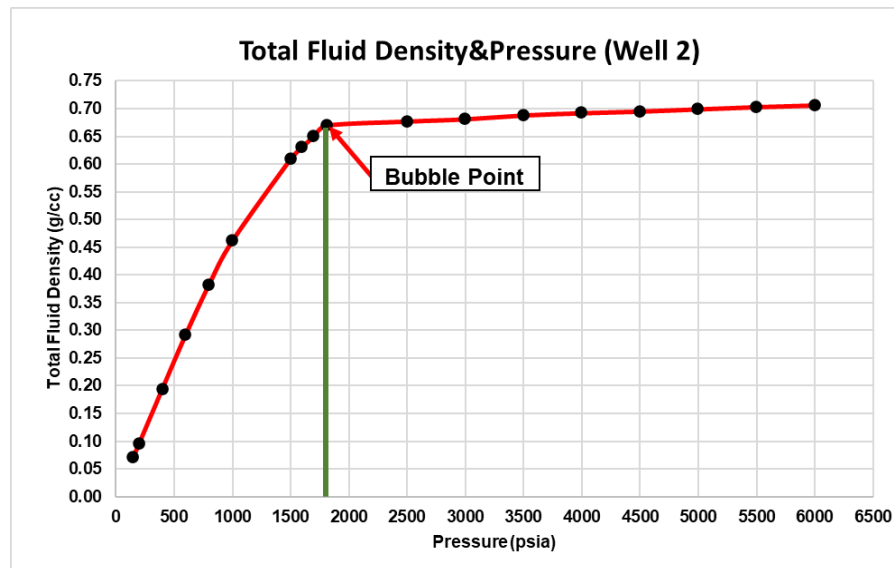


Figure 3.13. Total Fluid Density & Pressure Relationship

Bubble point can be even determined or confirmed with the Oil Density & Pressure plot below (**Figure 3.14**). Minimum point of plot is suitable for bubble point. As it is mentioned above, fluid in the PVT cell is initially liquid (**oil with dissolved gas**). Pressure reduction between 6000 psia and bubble point pressure (1813 psia) causes expansion of liquid (oil with dissolved gas) and decrease of viscosity. However, while the same process is continued on pressure below bubble point, gas liberates and due to that, viscosity of remaining liquid (oil with dissolved gas) increases. **Viscosity of dead oil at 100 F and atmospheric pressure (14.7 psia) is 3.17 cP.**

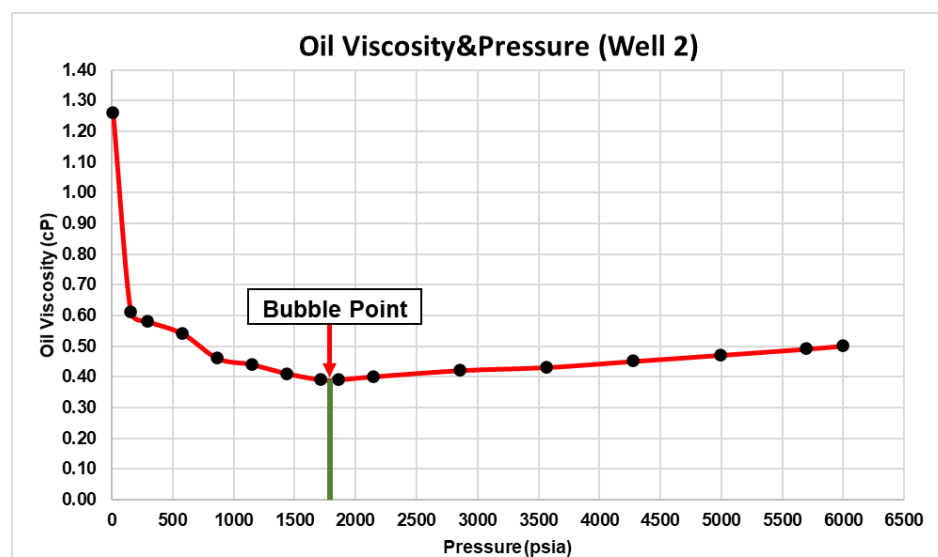


Figure 3.14. Oil Viscosity & Pressure Relationship

In order to plot Oil Formation Factor (above bubble point and at 250 F) & Pressure plot (**Figure 3.15**), certain calculation is done and suitable data is prepared with the following equation.

$$Bo = Bob * \text{Relative Volume} \quad (1)$$

Where,

- Bo is oil formation volume factor at 250 F and above bubble point pressure
- Bob is oil formation volume factor at 250 F and bubble point pressure.

Relative Volume is ratio of liquid volume above bubble point pressure to oil volume at 250 F and bubble point pressure.

Bob is taken as 1.411 RB/STB and it was obtained from separator test. It can be easily seen that as pressure is decreased, Bo at 250 F and above bubble point pressure increases up to bubble point.

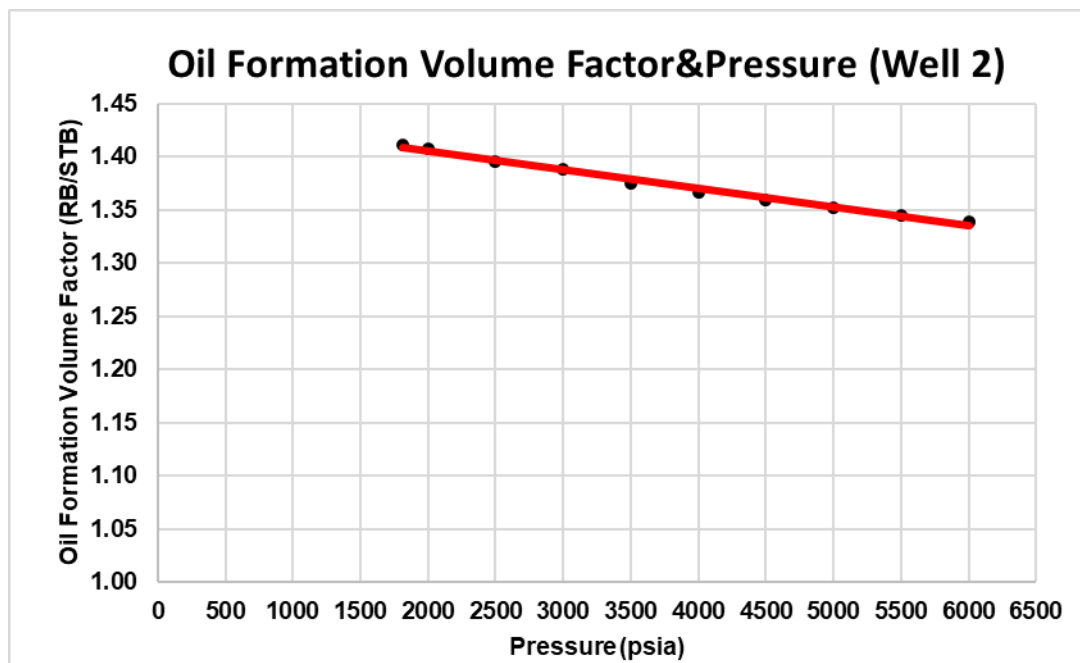


Figure 3.15. Oil Formation Volume Factor & Pressure Relationship

Utilizing above equation (1), Total Formation Volume Factor & Pressure graph (**Figure 3.16**) can be also plotted. However, **Relative Volume** demonstrates both of cases (below and above bubble point). Therefore, Oil Formation Factor & Pressure plot is a part of Total Formation Volume Factor & Pressure graph.

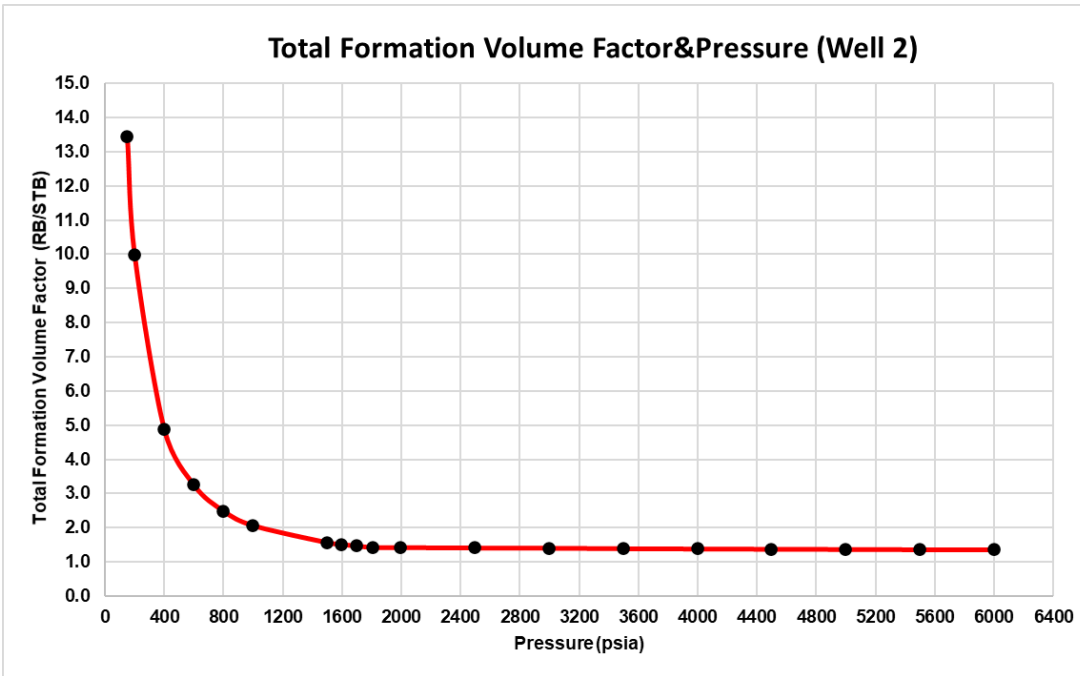


Figure 3.16. Total Formation Volume Factor & Pressure Relationship

For Well 1

It should be noted that Relative volume & Pressure plot are mostly utilised to determine bubble point. However, there is not any data to create this plot for well 1. Therefore, Oil Density and Viscosity & Pressure plots (**Figure 3.17 and 3.18**) are used for this purpose. Minimum points of plots (1895 psia) are suitable for bubble point. Pressure reduction above bubble point causes decrease of liquid (oil with dissolved gas) viscosity and density, while reverse case occurs for pressure decrease at the below bubble point. Temperature of reservoir fluid at reservoir conditions is **245 F**.

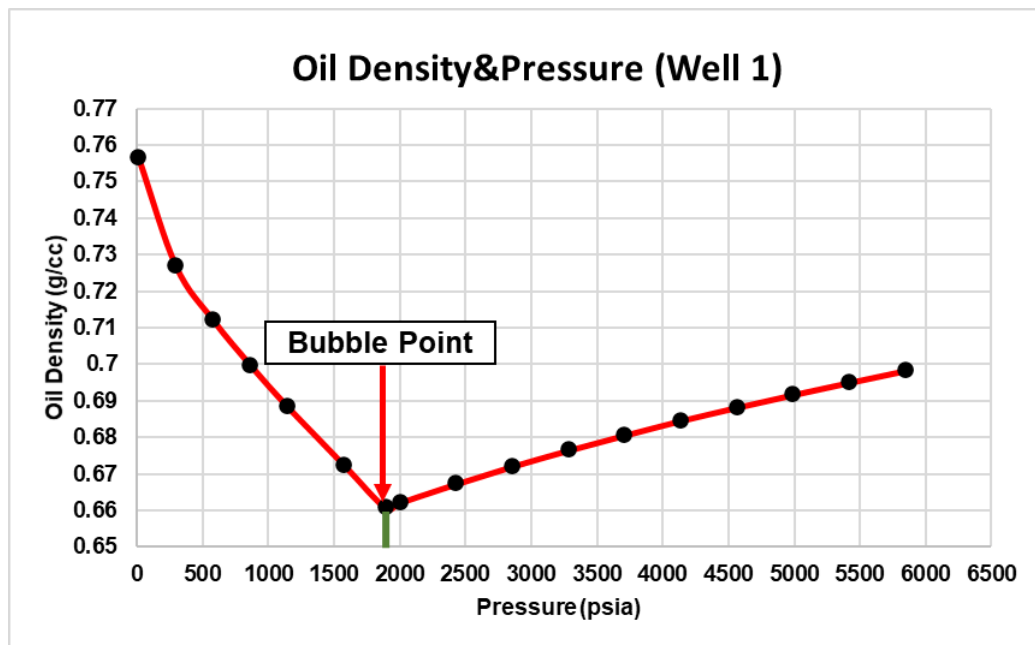


Figure 3.17. Oil density & Pressure Relationship for well X-1

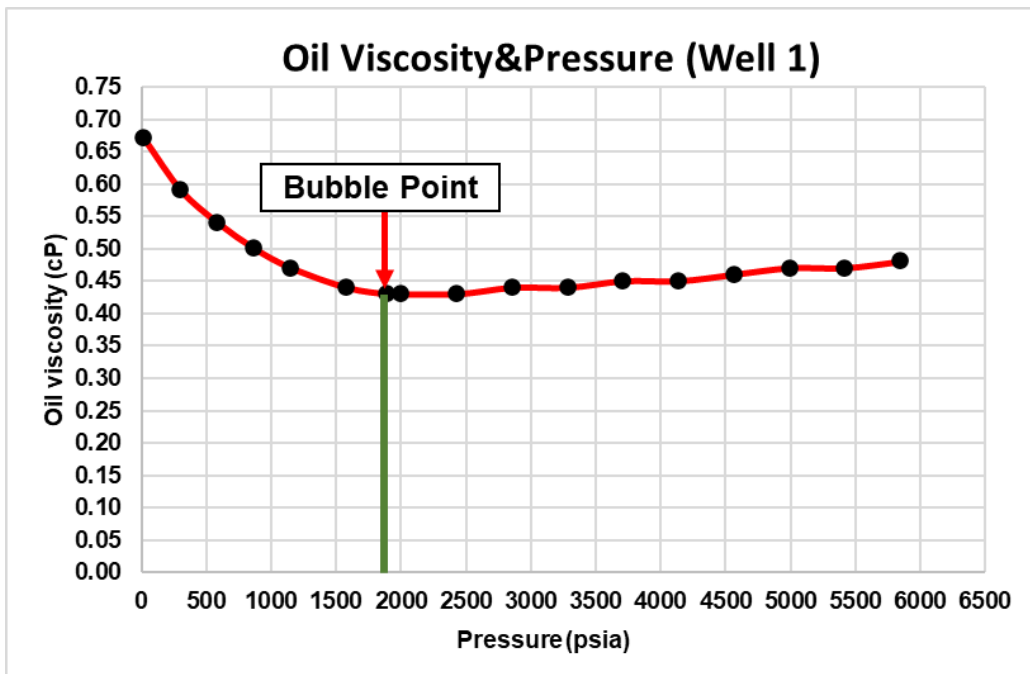


Figure 3.18. Oil viscosity & Pressure Relationship for well X-1

Above graphs (**Figure 3.17 and 3.18**) were generated for density and viscosity of reservoir fluid (oil with dissolved gas) at the reservoir temperature and decreased pressure range. However, density and viscosity values of **tank oil** for separator and /or tank conditions are higher than those values and they are displayed at the following table (**Table 3.10**).

Temperature F	Density of Tank Oil g/cc	Viscosity (1)	
		centistokes	centipoise
77	0.8158	4.62	3.77
95	0.8090	3.63	3.94
113	0.8022	2.63	2.11

Table 3.10. Density and Viscosity Data at SP and/or Tank Conditions

Note: Reservoir Temperature and Bubble Point Pressure for both of the wells (Well 1 and Well 2) are not the same.

Pressure	Relative Gas Volume at P and T	Relative Gas Volume under SC	Cumulative Relative Gas Volume under SC	Gas Expansion Factor	Gas Formation Factor
P psia	VG	VGG	F	E	Bg
	-	-	-	SCF/RB	RB/SCF
1895	-	-	-	-	-
1729	0.06180	6.163	6.163	99.72	0.010028
1444	0.12600	10.34	16.503	82.06	0.012186
1160	0.15210	9.893	26.396	65.04	0.015375
875	0.20360	9.853	36.249	48.39	0.020664
591	0.31640	10.16	46.409	32.11	0.031142
306	0.72270	11.81	58.219	16.34	0.061194
170	0.79550	7.191	65.410	9.04	0.110624
110	0.81380	4.818	70.228	5.92	0.168908

Results of differential liberation test are demonstrated at the following tables. Some of them were obtained directly from the differential liberation test, while the other properties were calculated later with equations below the tables.

Pressure	Gas Deviation Factor	Gas Density	Relative Oil Volume at P and T	Relative Total Volume at Pand T	Oil Density at P and T	Y Value
P	Z	(g/litre)	VO	VT		
psia	-	-	-	-	(g/cc)	-
1895	-	-	1	1	0.6607	-
1729	0.870	1.042	0.9812	1.043	0.6668	2.2
1444	0.883	1.051	0.9497	1.151	0.6775	2.1
1160	0.895	1.069	0.9196	1.325	0.6880	1.9
875	0.907	1.108	0.8893	1.638	0.6994	1.8
591	0.923	1.187	0.8569	2.302	0.7117	1.7
306	0.939	1.396	0.8170	4.380	0.7263	1.5
170	0.943	1.671	0.7867	8.023	0.7371	1.4
110	0.932	1.928	0.7688	12.631	0.7446	1.4

Table 3.11. Differential Liberation Test Data (Two Tables Together)

$$2) E = \frac{VG}{VG} \quad 3) Z = \frac{1}{14.70 * E * \frac{1}{459.7+T}}$$

$$4) VT = VO + \frac{F}{E} \quad 5) Y = \frac{Pb-P}{P*(VT-1)} \quad 6) Bg = \frac{1}{E}$$

Complete names of properties in the equations are shown in the above tables respectively. Another name of deviation factor is compressibility factor. All the volumes in the tables are volumes which are relative to oil volume at bubble point pressure and reservoir temperature.

Utilizing corresponding data from the above tables, two following plots (**Figure 3.19 and 3.20**) are generated.

It can be easily seen from **Figure 3.19** that Gas Formation Volume Factor is inversely proportional to Pressure. While pressure decreases, deviation factor increases for **Figure 3.20**. However, At the left end of line in the graph, there is sudden decrease. It should not normally occur.

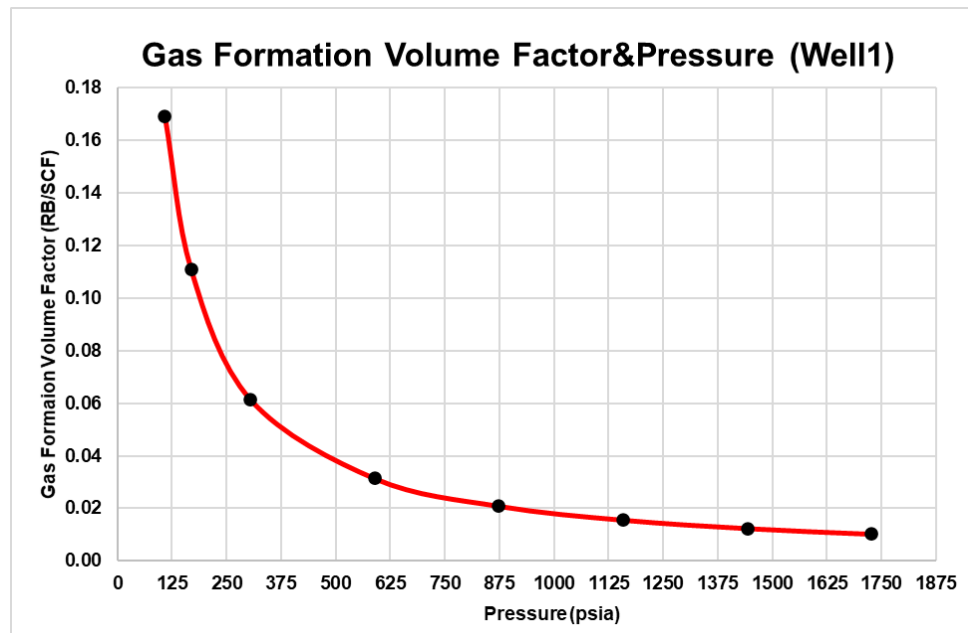


Figure 3.19. Gas Formation Volume factor & Pressure for well X-1

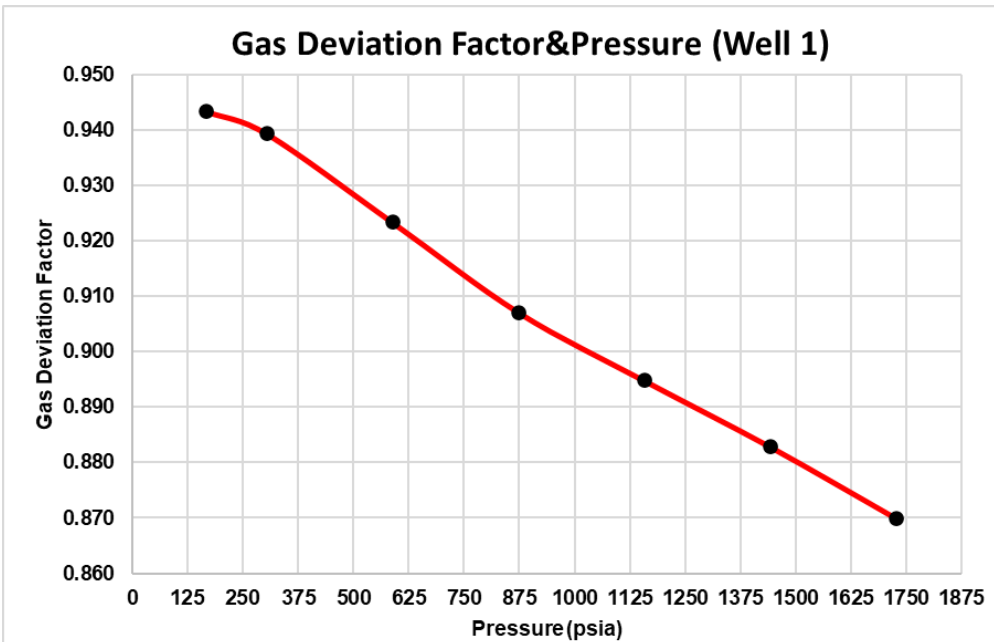


Figure 3.20. Gas Deviation Factor & Pressure for well X-1

Oil Formation Volume Factor (below bubble point and 245 F) & Pressure graph (**Figure 3.21**) is plotted with utilizing suitable data and following equation.

$$Bo = Bob * VO \quad (7)$$

Complete names of parameters were mentioned before and Bob is taken as 1.3803 RB/STB from separator test data. It can be seen from the next graph that as pressure decreases below the bubble point, Oil Formation Volume Factor also reduces.

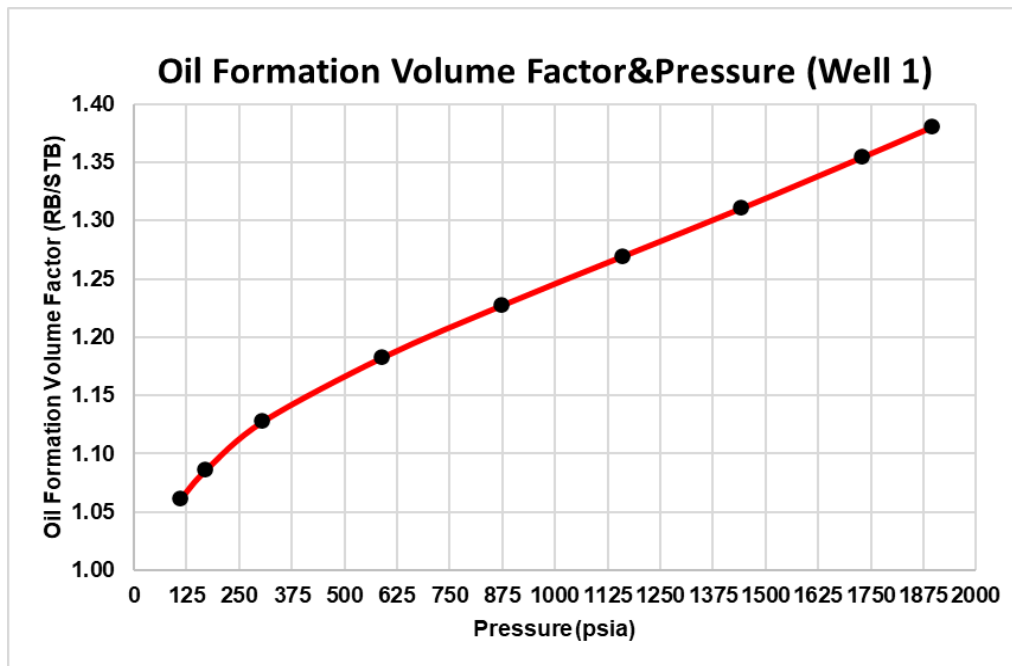


Figure 3.21. Oil Formation Volume Factor & Pressure for well X-1

At the last step, Solution Gas Oil Ratio & Pressure graph (**Figure 3.22**) is plotted with the suitable data. Also following equation is utilized

$$Rs = Rsi - F * Bob \quad (8)$$

Where,

Rsi is initial Gas Oil Ratio (gas solubility) at bubble point and above it under temperature of 245 F and its value for well 1 is around 539 SCF/STB.

Rs is Gas Oil Ratio (gas solubility) below bubble point under temperature of 245 F. Complete names of other parameters are given before at the PVT report. As it is mentioned before, Bob for well 1 is taken as 1.3803 RB/STB. Analysis of Figure 3.22 shows that above bubble point GOR is constant, while it decreases below bubble point.

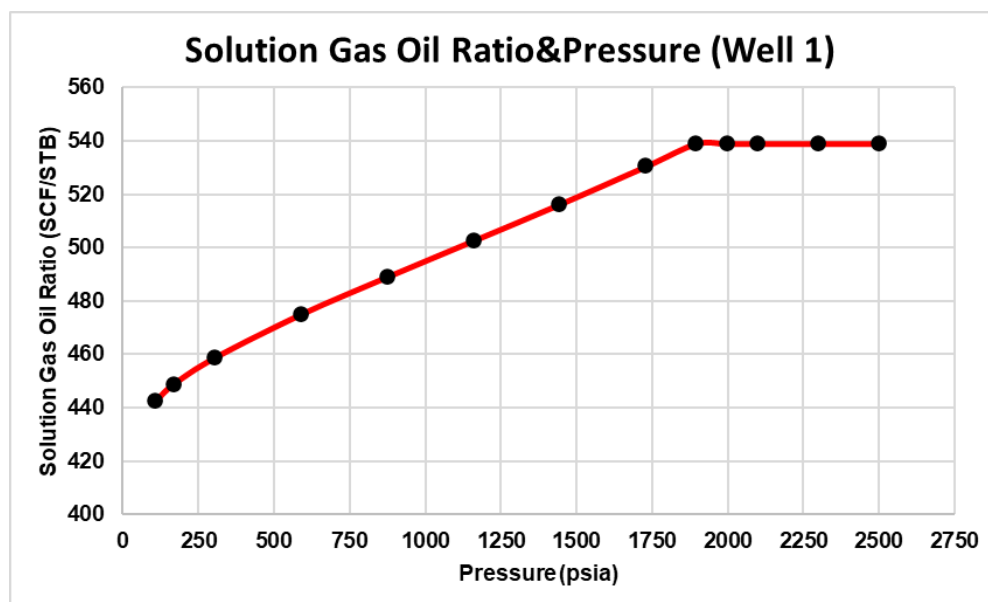


Figure 3.22. Solution Gas Oil Ratio & Pressure for well X-1

3.8. Reservoir Property Distribution Maps

In order to estimate the number of production and injection wells and determine their locations, first, it is required to generate a set of reservoir properties distribution maps. In our case, mainly, four reservoir properties have been taken into account as the basis while locating the wells: porosity, oil saturation, net pay thickness and permeability. To produce such maps, we used the kriging method in Python, which can be considered a kind of interpolation & extrapolation technique. The key principle in this geostatistical estimation includes the determination of various property values in the laterally undefined zones by using the values that are given for the specific zones. The table 3.12 below summarizes all the input parameters used for python script followed by illustration of created distribution maps:

Wells	Porosity	Oil Saturation	Net Pay Thickness (ft)	Permeability (mD)
X-1	0.22	0.87	370	174
X-2	0.24	0.85	135	247
X-3	0.24	0.81	230	2163
X-4	0.28	0.89	450	1069
X-5	0.23	0.74	360	719
X-6	0.22	0.76	410	998

Table 3.12. Reservoir properties and their values

Figure 3.23. Porosity Map

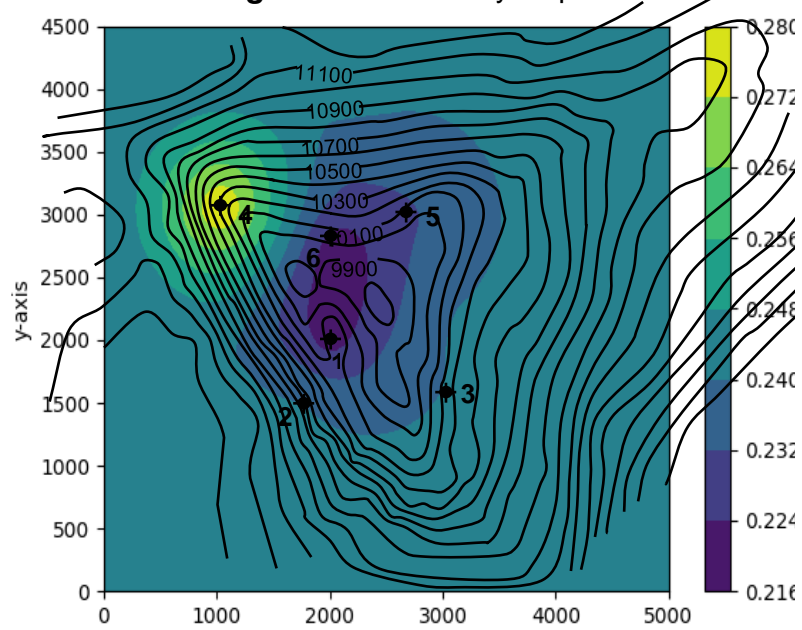


Figure 3.24. Oil Saturation Map

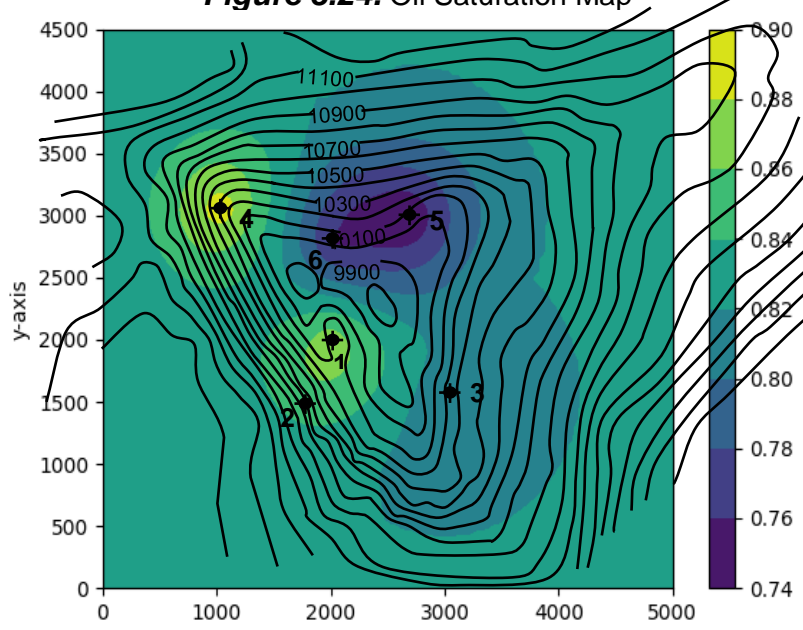


Figure 3.25. Net Pay Thickness Map

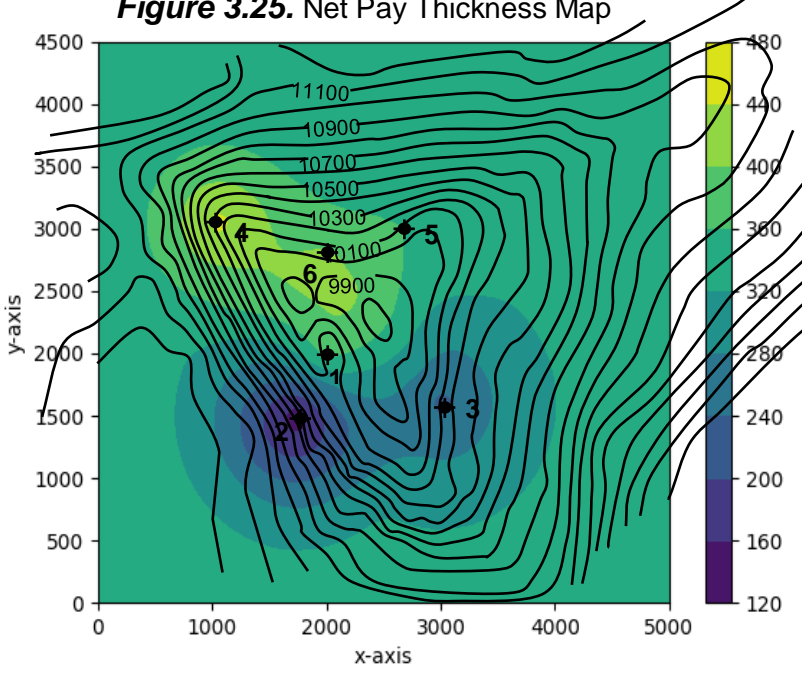
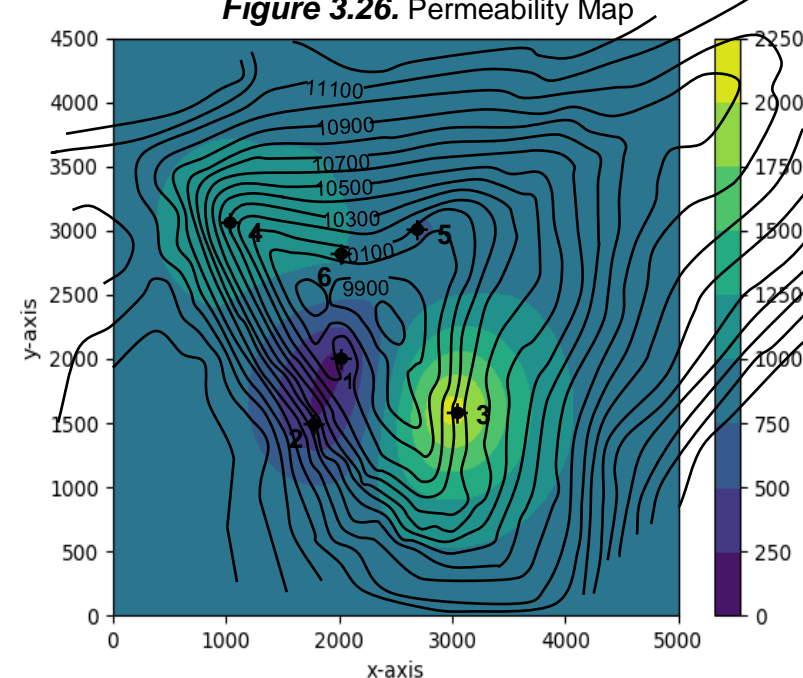


Figure 3.26. Permeability Map



3.9. Number & Location of Production and Injection Wells

The usage of the special simulation software is highly recommended in order to determine the number of production and injection wells more accurately. However, it is planned to take the advantage of simulation software package in the 2nd semester. For making initial estimation in the number of wells, certain assumptions were made and rough estimations were done with the certain equations to find the number of wells.

3.9.1. Number of Production Wells

The following equation is utilized in order to find the number of production wells [7]:

$$\text{The Number of Production Wells} = \frac{\text{Plateau Production Rate} (\frac{\text{STB}}{\text{d}})}{\text{Assumed Well Initial Production Rate} (\frac{\text{STB}}{\text{d}})}$$

Plateau production rate is usually placed between 2 and 5 % of reserves per year [7]. Therefore, volume of reserves (most likely at the RF=50%) is firstly selected as 427 MMSTB. At the next step, 4 % is taken from the interval of 2-5 % of reserves per year. While this percentage is selected, it is also taken into account that there are a number of faults in the reservoir and they can cause problems at the reservoir management. At the end, reserve volume is multiplied by 4% and divided by 1 year, before plateau production rate is obtained.

$$\text{Plateau Production Rate} = 427 \text{ MMSTB} * \frac{4\%}{1 \text{ year}} \approx 47000 \frac{\text{STB}}{\text{d}}$$

Certain analysis is conducted in order to find assumed well initial production rate. From the Drill Stem Test (DST), it is determined that only one well demonstrated sand production of 4lbs/1000bbl of liquid at the 4500bbl/d of oil production rate, while sand production was not detected at the other wells at the higher flow rates (20000-25000bbl/d). However, it was mentioned that well clean-up was conducted before the production. Due to that, these wells may not show sand production. Therefore, sand production can suddenly start during oil production at such higher production rates and it can cause sand plug in the wells. Furthermore, well integrity can be weakened due to higher level of corrosion at the higher flow rates. Form analysis above, lower flow rate can be a good choice and 4500bbl/d can be taken as well initial production rate. Sand production is less than allowable sand production limit (30 lbs/1000bbl of liquid for the flow rates below 5000bbl/d) at this flow rate. To summarize, well initial oil production rate is assumed to be 4500 STB/d.

After determination of plateau production rate and assumption of well initial production rate, the number of producers can be calculated with suitable equation.

$$\text{The Number of Production Wells} = \frac{47000 \left(\frac{\text{STB}}{d} \right)}{4500 \left(\frac{\text{STB}}{d} \right)} \approx 10$$

3.9.2. Number of Water Injection Wells

In the aquifer, permeability is very low, being around 14mD. Due to that, injection rate into aquifer is lower and it was determined as 3600bbl/d at the surface pressure of 8000 psi during the injection test of the well №2. It demonstrates that many injector wells should be drilled into aquifer to support reservoir pressure. Furthermore, there are a number of faults in the reservoir, which affect the number of injection wells. By taking into account the reasons above, number of injector wells may be equal to that of producer wells. On the other side, if the number of injector and producer wells is taken equal to each other, volumes of produced (for 4500bbl/d) and injected fluid (for 3600bbl/d) will be closer. It will cause gradual decrease at the reservoir pressure.

3.9.3. Location of Injector and Producer Wells

At the following map, the locations of injectors (green point) and producers (red point) are demonstrated. In order to determine the well locations, distribution (saturation, porosity, permeability and net pay thickness) maps were utilized

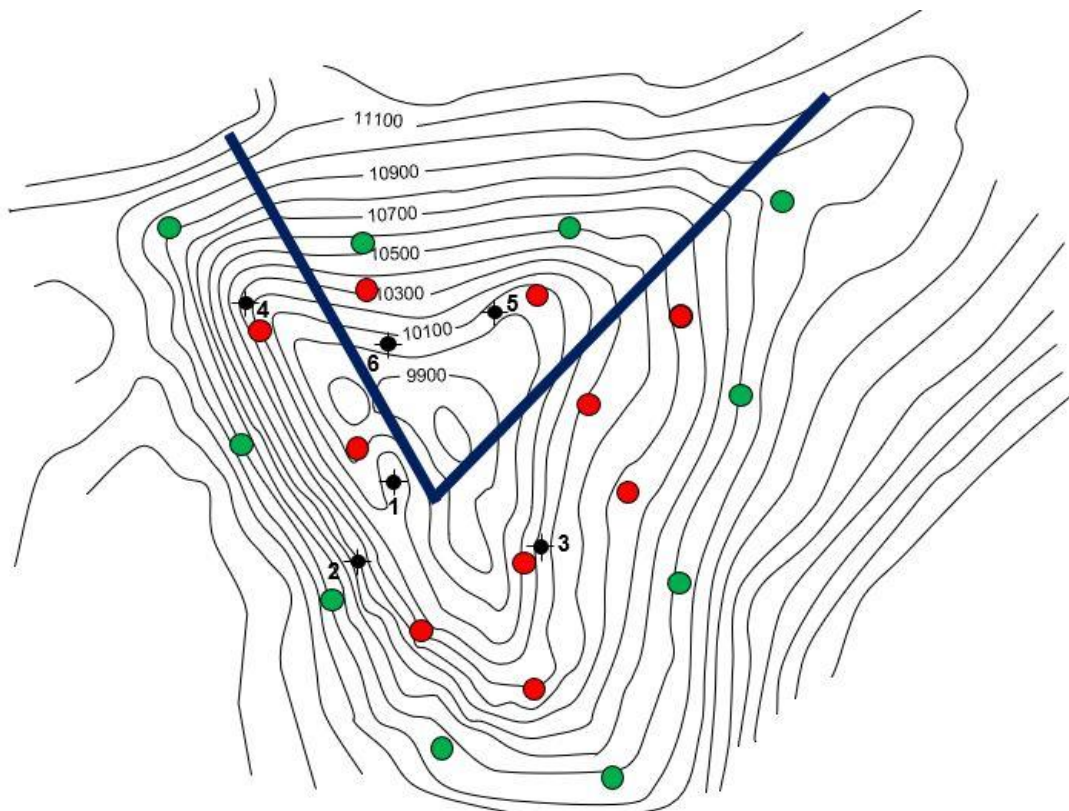


Figure 1. Location of producer and injector wells

4. DRILLING ENGINEERING

4.1. Drilling Rig Selection & Location

Selection of the type of drilling rig is important and has dependence on several parameters:

- economical sides (in particular cost);
- depth of target area & formation pressure anticipation;
- typical weather conditions in the operation area;
- water depth in given zone (81 m / 266 ft in this case);
- safety issues

By investigating neighboring oil fields (Fulmar & Nelson fields) and considering all the factors above it has been decided to choose a single fixed-type steel jacket platform for development of X-field. Small area of the field, shallow water depth, number of the wells planned to be drilled (at least 10 production/injection wells), severeness of weather conditions in North Sea, interval of target zone depth (between 10000 ft and 15000 ft) claim how correct the decision is. Besides it, platform rig will be able to work under quite high pressure & temperature and allow long time development of the field. Utilization of semi-submersible drilling rig is also another option since the water depth is shallow. Moreover, this rig enables to start the production much earlier and gives more detailed information regarding the region in terms of accurate selection of the platform location. However, this offshore drilling rig is not suitable for its non-cost effectiveness which has a pivotal effect on making design considerations [\[23\]](#) [\[25\]](#).

On the other hand, some possible risks of fixed platform installation exist as well. The top one is the platform loss if the X-field is not developed further. Nevertheless, as the presence of hydrocarbon (oil) has been approved via some certain analysis during exploration stage, this undesirable situation is minimized.

When it comes to the selection of drilling rig model, Euro Rig 350 t from Bentec (one of the top drilling rig manufacturers) has been considered appropriate for this field. Technical data of this rig model is given beneath [\[21\]](#) [\[22\]](#):

MAST

Manufacturer:	Bentec
System:	Vertical lift
Mast free height:	142.00 ft (43.80 m)
Mast base:	28.54 ft x 18.54 ft (8.70 m x 5.65 m)
Hook load capacity @ 10 lines:	772,000 lbs (350 t)
Racking capacity:	Approx. 19,700 ft (6,000 m)

TOP DRIVE

Manufacturer:	Bentec
Type:	TD-500-HT
Load capacity:	500 ton / 454 t
Electric motor:	1,030 hp (758 kW)
Output torque:	46,500 ft-lbs (63,000 Nm)

POWER GENERATION

Manufacturer:	Bentec
Engine type:	4 x CAT 3512B (or equivalent)
Generator type:	4 x CAT SR4 (or equivalent)
Emergency generator set:	1 x CAT 3456 (or equivalent)

POWER CONTROL ROOM

Manufacturer:	Bentec
Type:	Variable frequency drive 690 V, 50 Hz or 600 V, 50/60 Hz

SUBSTRUCTURE

Manufacturer:	Bentec
System:	Box-on-box substructure
Height of drill floor:	29.53 ft (9.00 m)
Height underneath rotary table:	24.28 ft (7.40 m)
Rotary capacity max.:	772,000 lbs (350 t)
Setback load max.:	450,000 lbs (204 t)

DRAWWORKS

Manufacturer:	Bentec
Type:	DW-E-1500-AC
Power rating:	1,500 hp (1,150 kW)
Drill line diameter:	1 3/8" (35 mm)
Max. line pull:	87,100 lbs (39,5 t)

MUD PUMPS

Manufacturer:	Bentec
Type:	3 x MP-T-1600-AC
Electric motor:	1,600 hp (1,200 kW) AC
Max. pressure:	5,000 PSI (350 bar) 7,500 PSI (500 bar) on request

Figure 4.1. Euro Rig 350 t Technical Data

Another pivotal factor is to choose correct place of the platform that influences drilling cost and well trajectories. In order to decrease the drilling cost measured well (deviated) depths should be feasibly low. It contributes to development of X-field as much as possible (achieving farthest reservoir goals). Additionally, there is a fault in north part of the field which can be reason for several drilling barriers: potential cause of a kick, fluid loss, formation fracture and consequently, well control loss [24]. Furthermore, dogleg severity (change in well direction) can be minimized by the correct placement of the fixed platform. Last but not least, for being able to reach all available points in X-field, the platform should be constructed near to the center point. One platform will be enough to attain the targets of all wells in anticline structure within this area [26]. The structural map with platform icon has been provided in Figure 4.2.

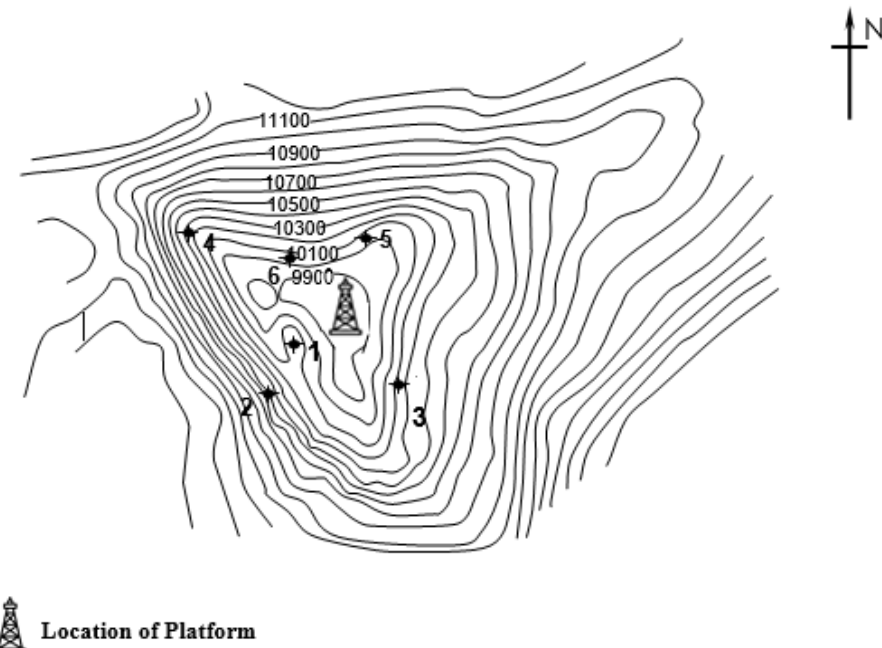


Figure 4.2. Platform location

4.2. Pressure Profile

Pressure profile is extremely important for determining drilling mud program, casing setting depths and the number of casings required. During drilling operations, if the pressure exerted by mud is lower than the pressure of formation, there can be kick which is the cause of blowout. On the other hand, if the mud pressure exceeds formation fracture pressure, losses can be observed. Therefore, it is crucial to estimate pressure profile of X field by referring to nearby fields [15]. The main reason of using pressure profile of nearby fields was unavailability of log data from 0ft to 10200ft. After searching on the internet, pressure profile for the Central Graben was identified and provided below (Figure 4.3). This graph was used for pore pressure estimation. For the reservoir section, relevant RFT data was employed. The pressure and its respective depth values were taken from the plot by applying online web plot digitizer software. In terms of normal and overburden pressures, they were assumed as 0.465 psi/ft and roughly 1 psi/ft respectively after investigating nearby fields.

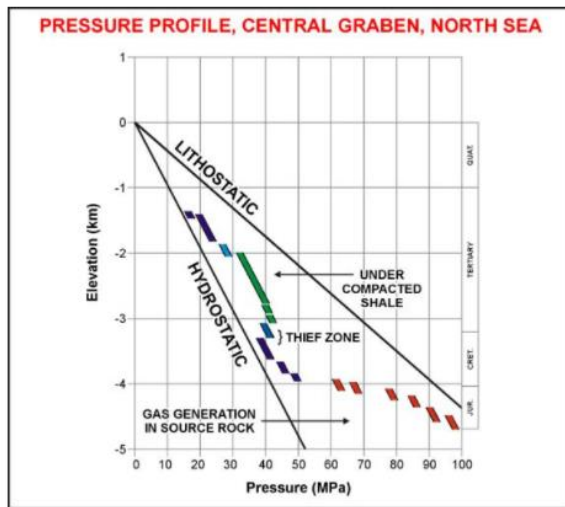


Figure 4.3. Pressure Profile of Central Graben

After getting pore pressure values, fracture pressure was calculated by using Ben Eaton method. This method takes into consideration changes in rock matrix stresses which gives more accurate results compared to other equations [16] [17]. For estimation of fracture pressure, the lithology of formations are required, however, due to lack of data in X field, lithology of nearby formations were considered. This explains reasons of errors as poisson's ratio values were taken by referring to lithology of Fulmar field. The lithology of formation mainly consists of claystone, siltstone, marlstone and Kimmeridge clay. Poisson's ratios of these formations have been provided in appendix part. After calculation of fracture pressure values, pressure profile (Figure 4.4) and PPFG (Figure 4.5) plots of X field were sketched. For safe drilling operations, 0.3 safety factor was taken into account when constructing PPFG plot. All calculations and tables are given in the appendix part.

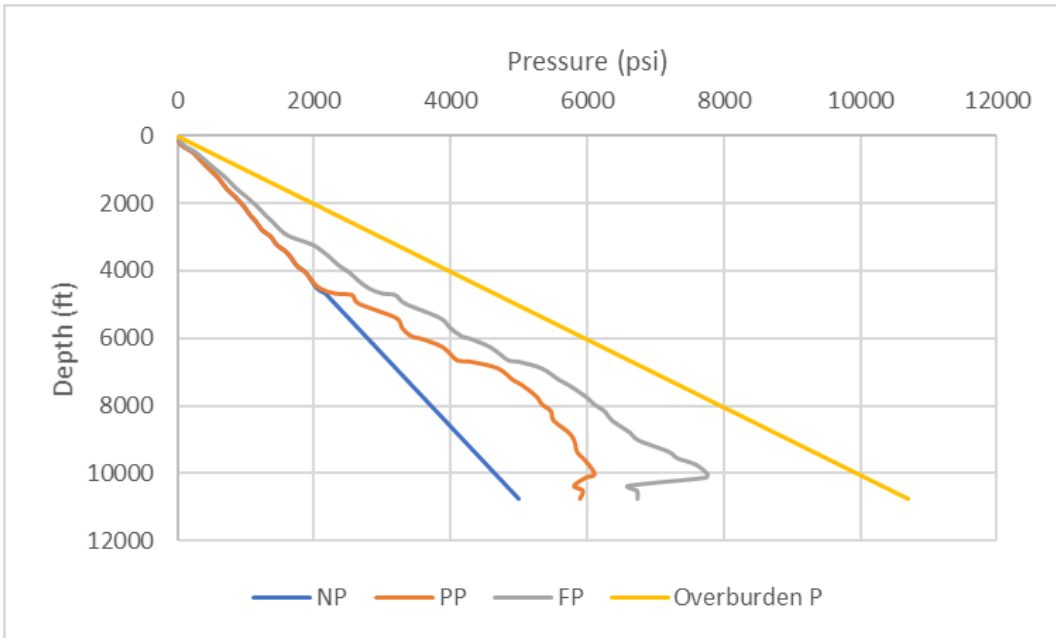


Figure 4.4. Pressure Profile of X field

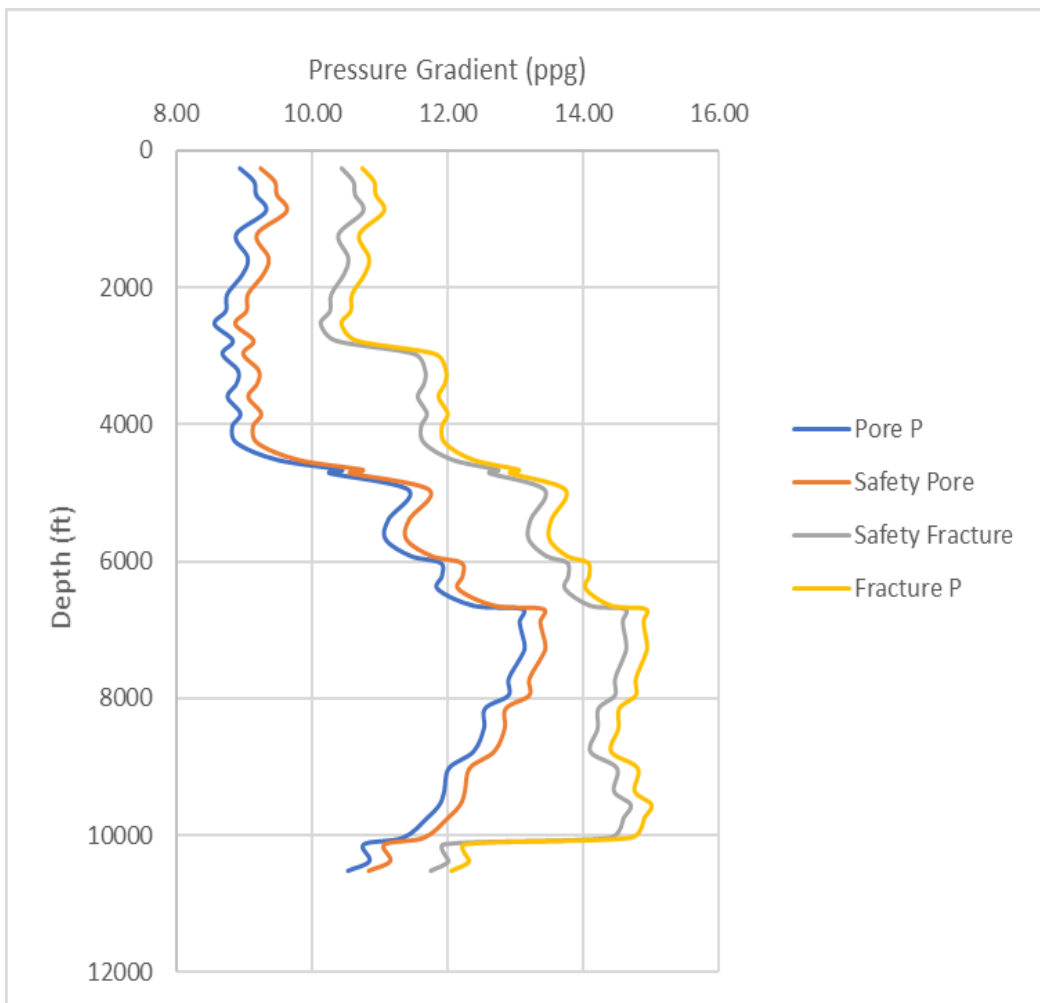


Figure 4.5. PPFG plot of X field

4.3. Casing Design

Casing design is the fundamental part of well planning and construction. Each casing string has its own purpose in well planning and they will be discussed separately further in this section. Casing strings are also the major contribution to the total cost of wells; therefore, selecting proper casing numbers & sizes, setting depth and grade & weight plays a crucial role in terms of engineering and project economics consideration. It is decided to divide casing design process into two stages: **preliminary** and **detailed casing design**. The whole process typically followed in casing design stage is given below [1]:

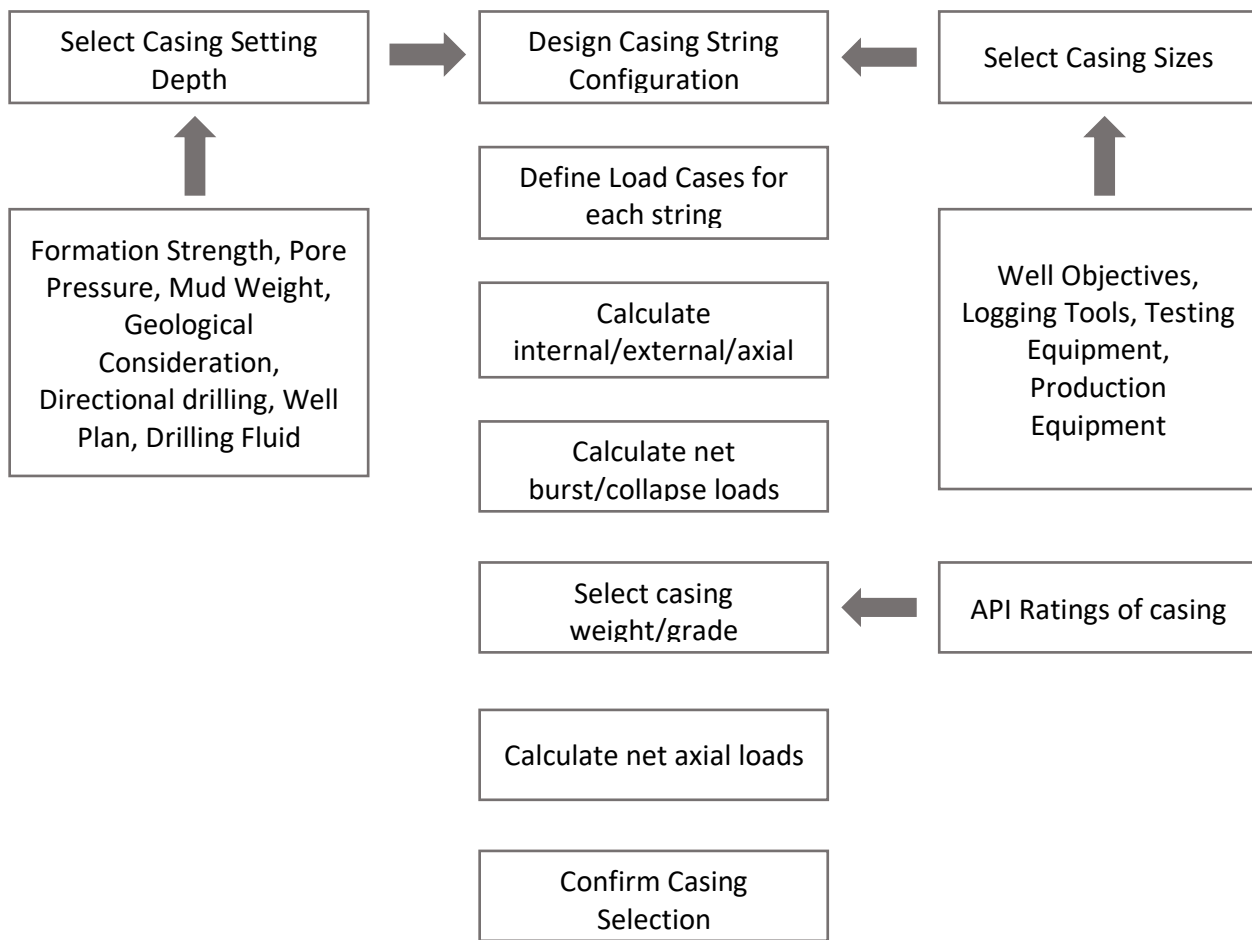


Figure 4.6. Casing Design Process

4.3.1. Preliminary Casing Design

Preliminary casing design is the stage where we can achieve the largest cost savings and improve the overall project economy. The key purposes of this stage for the X-field have been listed below:

- Determining the number of casing strings;
- Setting depths of each casing string;

- Sizes of casing strings and corresponding drill bits;
- Drilling fluid – mud densities for each depth interval;

PPFG plot generated in the previous section is used in order to determine casing setting points and prepare mud program. Consideration of a safety factor of 0.3 ppg for both pore and fracture pressure allows carrying out much safer drilling operations. The final hole or casing diameter mainly depends on the production requirements, such as size of tubing, presence downhole valves & other devices and type of completion [2]. In the case of X-field, the analysis of the overview file shows that the production tubing size is 4.5 in. Moreover, drilling costs section in the overview presents all casing strings used in the wells of X-field. This casing design is typical to the other nearby fields located in the North Sea – Central Graben. The figure 4.7 below illustrates the determination of casing setting points on the PPFG plot and visual illustration of casing strings & sizes.

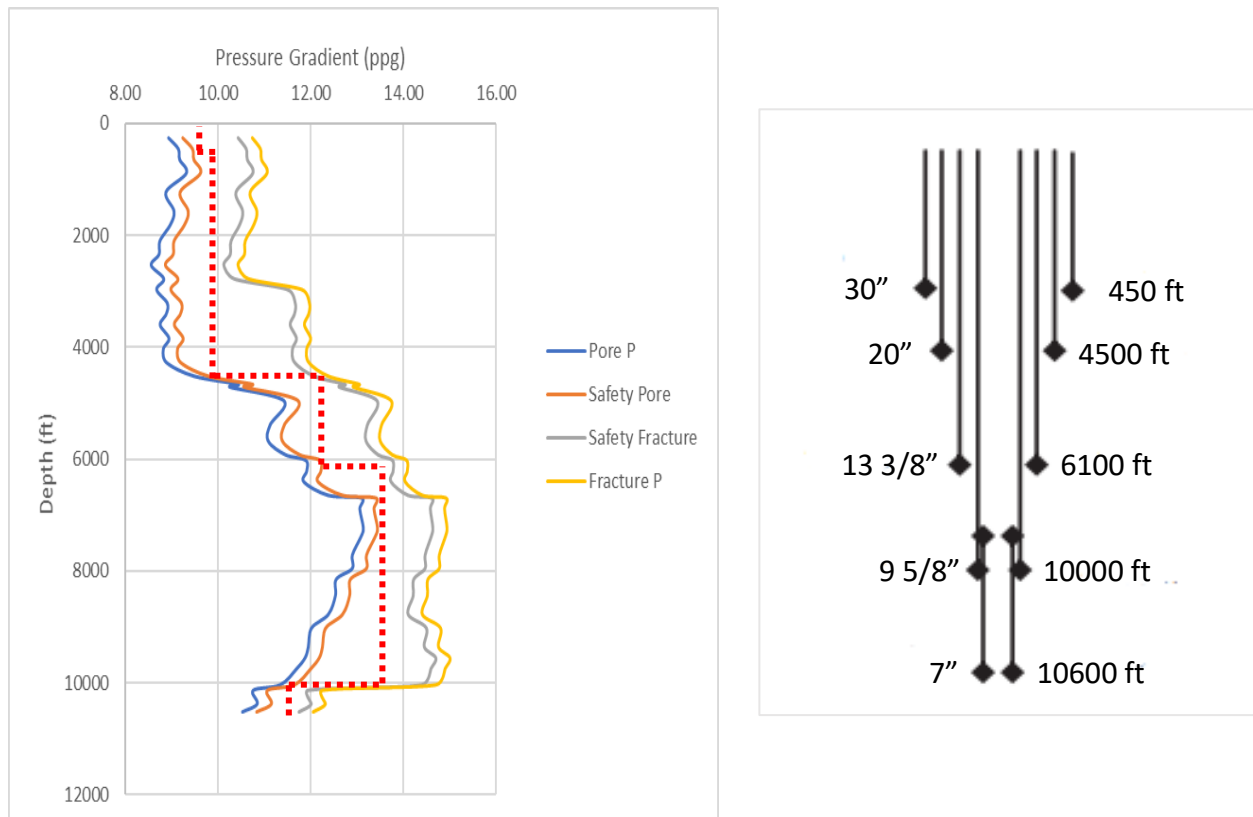


Figure 4.7. Preliminary casing design

- **30" Conductor Casing** – it is the first casing string set to the depth of 450 ft in order to isolate soft unconsolidated formations (claystone & siltstone) to prevent collapsing and protect against shallow formation gas. Since the formation at shallower depth is soft, conductor casing can be installed by hammering instead of drilling and cementing a hole. This would reduce the drilling & cementing costs as well.

- **20" Surface Casing** - after setting the conductor, surface casing is the next one installed to the depth of 4500 ft. It provides blowout protection by accommodating blowout preventer (BOP), isolation from water sands and support for the weight of BOP and subsequent casing strings.
- **13 3/8" Intermediate Casing** – this is the first intermediate casing string run after the surface casing. Its seating depth corresponds to 6100 ft according to PPFG graph. It is mainly installed to the transition zone from normal to abnormal pressure so that low-pressure formations (where lost circulation could happen) and unstable hole sections are isolated. Sometimes, multiple intermediate casing strings can be run into wellbore, as it is the case for X-field.
- **9 5/8" Intermediate Casing** – the second intermediate casing is set to the depth of 10000 ft with the aim of sealing abnormally high-pressured zones.
- **7" Liner** – it is installed to the depth of 10600 ft with the purpose of isolating the productive zones when the target hydrocarbon formation is reached. While drilling the production zone, extra care should be taken in order not to cause any damage to the formation. Liner is hung from the previous casing string instead of extending back to the wellhead. Utilization of liner as the production casing brings many benefits, such as considerable cost reduction and improved hydraulic performance while drilling.

4.3.2. Detailed Casing Design

With the aim of selecting appropriate casing weight, grade and connections, detailed casing design has been made, which mainly includes different load calculations for each casing string separately. The key loads to be considered in this casing design stage are listed beneath:

- Burst loads;
- Collapse loads;
- Tensile loads;

The design procedure of the surface casing will be presented as an example and the same procedure will be followed for the rest of casing strings. Outcomes of the design and all relevant figures have been provided in Appendix part.

For both burst and collapse loads, the worst case scenarios are taken into consideration during calculations. The collapse loads are determined in the condition of full evacuation owing to the lost circulation and only pore pressure is acting outside the casing. In terms of burst loads, maximum pressure is encountered when well is shut in due to gas kick reaching the surface. The assumptions for production liner include the evacuation of tubing due to gas-lift operations and the leak of tubing just below tubing hanger in the case of collapse and burst load calculation respectively [2]. Firstly, the calculation step itself has been shown and then its outcomes are tabulated below:

Surface Casing	
Casing size (in)	20
Setting depth (ft)	4500
Min. Pore Pressure above 4500ft (ppg)	4.58
Max. Pore Pressure above 4500ft (ppg)	9.2
Depth of next 17 1/2 hole (ft)	6100
Max. Pore Pressure at bottom of next hole	11.94
Frac. Pressure Gradient at shoe (ppg)	11.66
Expected gas gradient (psi/ft)	0.1
Design Factor for Burst	1.1
Design Factor for Collapse	1

Table 4.1. Input parameters for burst & collapse load calculation of surface casing

BURST DESIGN:

1. *Pore pressure at bottom of 17 1/2" hole = $6100 * 0.052 * 11.94 = 3787 \text{ psi}$*
2. *Internal pressure at surface = $3787 - 0.1 * 6100 = 3177 \text{ psi}$*
3. *External pressure at 20" casing shoe = $3787 - 0.1 * (6100 - 4500) = 3627 \text{ psi}$*
4. *LOT pressure at 20" casing shoe = $11.66 * 0.052 * 4500 = 2728 \text{ psi}$*

At casing shoe, formation fracture occurs when the well is shut in after gas has reached surface.

Therefore, possible maximum pressure inside casing is 2728 psi.

5. *Possible maximum internal pressure at surface = $2728 - 0.1 * 4500 = 2278 \text{ psi}$*
6. *External pressure at surface = 0 psi*
7. *External pore pressure at casing shoe = $4.58 * 4500 * 0.052 = 1071 \text{ psi}$*

COLLAPSE DESIGN:

1. *Internal pressure at surface = 0 psi*
2. *Internal pressure at casing shoe = 0 psi*
3. *External pressure at casing shoe = $0.052 * 11.94 * 4500 = 2153 \text{ psi}$*
4. *External pressure at surface = 0 psi*

BURST	TVDS (ft)	External Load (psi)	Internal Load (psi)	Net Load (psi)	Design Load (psi)
	Surface	0	2278.44	2278.4	2506.284
	Casing Shoe (4500ft)	1071.72	2728.44	1656.7	1822.392
<hr/>					
COLLAPSE	DEPTH (ft)	External Load	Internal Load	Net Load	Design Load

	Surface	0	0	0	0
	Casing Shoe (4500ft)	2152.8	0	2152.8	2152.8

Table 4.2. Burst & Collapse Load Calculation Results for Surface Casing

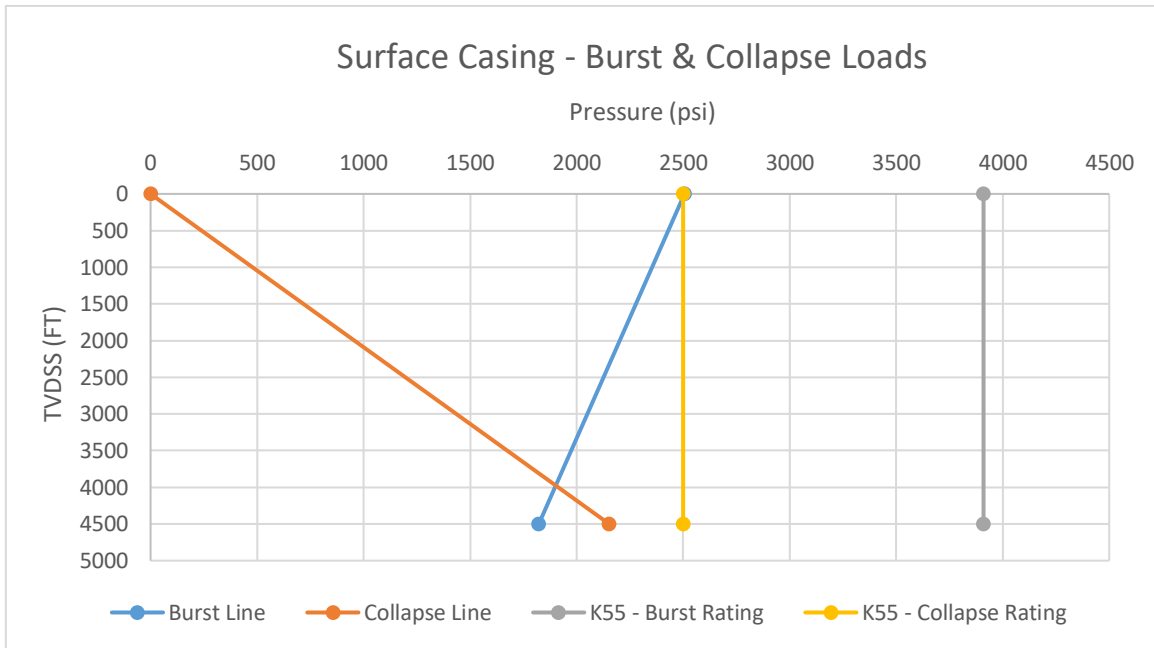


Figure 4.8. Surface Casing Design with Burst & Collapse Ratings

"K-55" 20" surface casing with 18.376" ID and 169 lb/ft weight has been selected based on the calculated burst & collapse loads [5]. It is obvious from the figure above that the rating of the selected casing string prevents any casing damage due to burst & collapse loads. After analyzing burst & collapse loads, tension load is also calculated in order to ensure the reliability of the selected casing material. To do so, dry weight, buoyant weight, and static load to which casing string will be subjected, have been calculated at both surface and bottom of the well [3] [4]. These calculation steps have been listed below in sequential form. Moreover, the illustration (Figure 4.9) below summarizes tension loads mentioned and confirms the reliability of selection as yield strength of the chosen casing is higher than any type of tensile load.

$$\text{Dry weight (lb) @ surface} = \text{weight } \left(\frac{\text{lb}}{\text{ft}} \right) * \text{setting depth (ft)} = 169 * 4500 = 760500 \text{ lb}$$

$$2) \text{ Dry weight (lb) @ 4500ft} = 1\text{ft} * \text{weight } \left(\frac{\text{lb}}{\text{ft}} \right) = 169 \text{ lb}$$

$$3) \text{ Buoyancy factor} = \frac{65.5 - \text{mud density}}{65.5} = \frac{65.5 - 9.9}{65.5} = 0.8489$$

$$4) \text{ Buoyant weight (lb)@ surface} = \text{buoyancy factor} * \text{dry weight} = 0.8489 * 760500 = 645554 \text{ lb}$$

$$5) \text{ Buoyant weight (lb)@4500ft} = \text{buoyancy factor} * \text{dry weight} = 0.8489 * 169 = 143 \text{ lb}$$

$$6) \text{ Bending Force} = 63 * \text{Build up Rate} * \text{Casing OD} * \frac{\text{Weight}}{\text{ft}} = 638820 \text{ lb}$$

$$7) \text{ Static load @ surface} = \text{Bending force} + \text{Buoyant Weight}@surface = 1284374 \text{ lb}$$

$$8) \text{ Static load @ 4500ft} = \text{Bending force} + \text{Buoyant weight}@4500ft = 638963 \text{ lb}$$

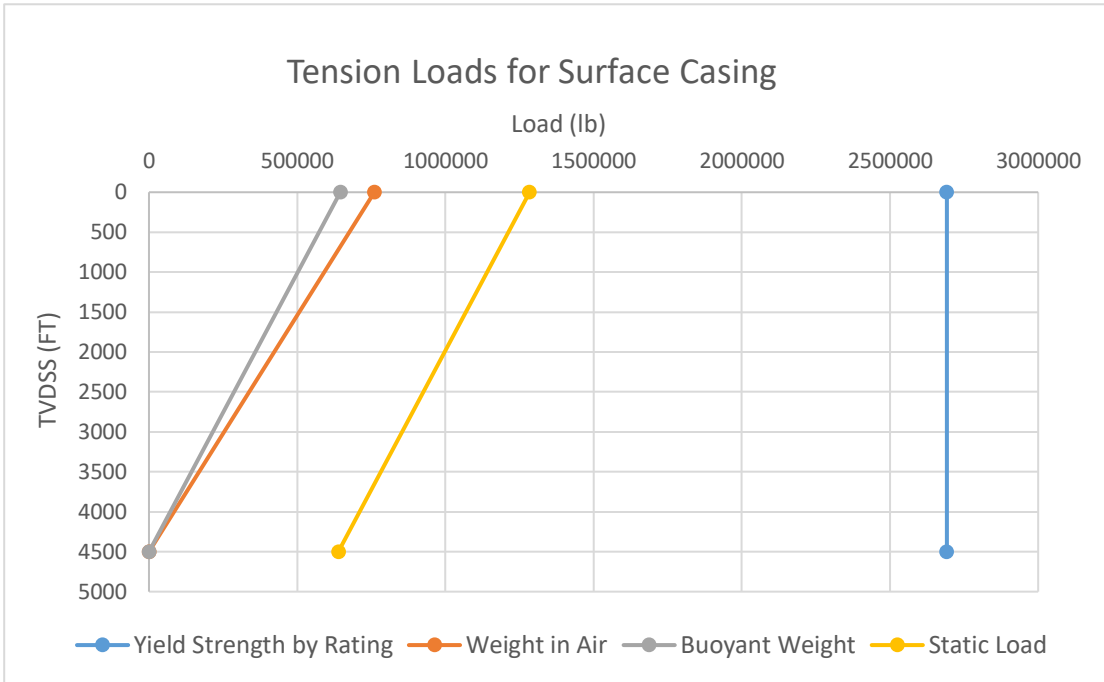


Figure 4.9. Tensile load demonstration for 20" Surface Casing

With the aim of making proper casing design, “Tenaris Casing Catalogue” has been used which gives an opportunity to view and compare the performance data for the chosen pipe [6]. A piece of table showing pipe body data and type of connection for 20" surface casing has been extracted and illustrated below:

Pipe Body Data			
Geometry			
Nominal OD	20.000 in.	Wall Thickness	0.812 in.
Nominal Weight	169 lb/ft	Plain End Weight	166.56 lb/ft
Drift	18.188 in.	OD Tolerance	API
Nominal ID	18.376 in.		
Performance			
Body Yield Strength	2692 x1000 lb		
Min. Internal Yield Pressure	3910 psi		
SMYS	55,000 psi		
Collapse Pressure	2500 psi		



**Blue® Quick Seal
Dopeless®**

Figure 4.10. Pipe body performance for 20" Surface Casing

Casing Strings	Size (OD,inch)	Hole or Bit Size (inch)	Setting Depth (ft)	Grade	Weight (lbs/ft)	ID (inch)	Connection	Burst Design/Rating (psi)	Collapse Design/Rating (psi)
Surface	20"	26"	4500	K-55	169	18.376	Blue Quick Seal	2506/3910	2153/2500
1st Intermediate	13 3/8"	17 1/2"	6100	Q125-IC	77	12.275	Wedge 623	4067/9250	3787/3920
2nd Intermediate	9 5/8"	12 1/4"	10000	P110-IC	47	8.681	TXP-BTC	5522/9710	6240/7100
Production Liner	7"	8 1/2"	10600	C110	26	6.276	Wedge 563	2100/9960	6080/6230

Table 4.3. Casing Design Summary

4.4. Cementing Design

30" Conductor Casing --- This casing is normally hammered in the shallow water depth instead of drilling and cementing in order to decrease total expenditure of project. The water depth is approximately 81 m at the location of the selected platform, which means wells that are going to be drilled are shallow-water oil wells.

20" Surface Casing --- Back of surface casing is cemented completely in order to support weight of blowout preventer and wellhead which are hanged from this casing. Single stage cementing procedure is utilized for the casing. During the cementing of the surface casing, maximum pressure in borehole is normally less than fracture strength of the weakest formation in the cementing interval. Portland cement is chosen for cementing of surface casing. This cement is very lightweight and durable cement. It is cheaper than other cement types.

13 3/8" and 9 5/8" Intermediate Casings --- These casings are not cemented completely in order to decrease the total expenditure of cementing operation. Top of Cement (TOC) is considered to be 400 ft (normal range between 300 ft and 500 ft) above than shoe of previous casing in order to prevent any formation fluid influx into the annulus of previous casing. For cementing of casings, two stage cementing operation is utilized to prevent formation fracture during cement injection into annulus at the back of casings. Class G cement is chosen for its good retarding properties at the deeper section of wells and it is also applicable for wide ranges of pressure and temperature.

7" Liner – Liner are completely cemented and it should be noted that top of liner is 400 ft above than shoe of previous intermediate casing. Content of cement for liner cementing is approximately similar to that of intermediate casings.

At all the cementing operations above, spacer is utilized to prevent contamination of cement with mud.

During the calculations, 15 ft of rat hole and 65 ft of shoe track should also be taken into account. Due to deviations at the size of borehole, 20 % excess of cement volume is utilized for cementing.

Cementing the deviated well is much more difficult in contrast to the vertical well. Because deviated well lies on low side of borehole due to gravity and it causes mud channels while cementing. In order to achieve, good cement job, centralizers are used.

The results of the cementing calculations are provided at the following table (Table 4.4).

Casing Size (in)	Casing Setting Depth (ft)	Previous Casing Shoe (ft)	TOC (ft)	Number of Sacks	Mixwater (bbl)	Displacement Volume (bbl)
20	4500	0	0	4619	570	1455
13 3/8	6100	4500	4100	1594	188	959
9 5/8	10000	6100	5700	2059	244	871
7	10600	10000	9600	190	22	490

Table 4.4. Cementing Calculation Results

4.5. Drilling Fluid Design

Drilling fluid design plays a crucial role in the well planning since it is the only element that keeps the contact with wellbore and formation during the entire drilling operations. In the case of X-field, the key aims for mud system design include the proper mud weight estimation based on the previously obtained PPFG graph and reasonable mud type selection for each interval. Our primary purpose is to select the correct mud density values, which are neither below the formation pore pressure nor above the fracture pressure. Being within the borders of mud weight window will ensure safe drilling operations. Moreover, 0.3 ppg safety factor was also considered for both pore and fracture pressure while constructing the PPFG graph. Then, compatible drilling fluid type for each depth interval has been selected by taking formation type and potential drilling problems into account.

26" hole (surface casing) covering 450-4500ft depth interval was drilled by using water-based mud – *WBM with low-solids non-dispersed (LSND) viscous polymer system* and mud weight of 9.9 ppg. Drilling this surface interval with seawater-based mud containing few commercial additives is sensible and cost-effective since soft claystone & siltstone formations are not troublesome in terms of drilling operations. LSND polymer system consists of long-chain polymers providing effective fluid loss control and viscosity. In turn, usage of viscous WBM system allows preventing pipe-sticking issues, which are possible to encounter in weak consolidated formations [8].

17 1/2" hole (1st intermediate casing) covering 4500-6100ft depth interval was drilled by using WBM with *KCl* viscous polymer mud system and initial mud weight of 12 ppg. Since well conditions do not require to change the mud type (almost the same formation type to be drilled), WBM has been applied

for this section too. Availability of seawater, environmental factors, and lower costs associated with WBM also supports the decision made. However, as deeper hole sections are being drilled, having WBM with *KCl* concentration provides much safer drilling process and prevents the potential shale inhibition phenomenon (Tertiary Hordaland group shales). Drilling fluid practices and experience for Central North Sea Tertiary shales demonstrate that a steady increase in mud weight while drilling through Tertiary shales are necessary to minimize excessive shale swelling tendency [7]. Initial mud density of 12 ppg has been increased to 12.5 ppg by applying 0.833 ppg increment per 300ft drilled formation. The successful implementation of the similar practice has also been observed in nearby Forties field.

12 1/4" hole (2nd intermediate casing) covering 6100-10000ft depth interval was drilled by using oil-based mud – OBM with highly saline water phase and initial mud weight of 13.5 ppg. This hole section includes formations, such as chalk, Kimmeridge clay and shale; therefore, using WBM would be inefficient since potential chalk solubility in WBM and shale inhibition issues may occur. Dissolution of soft chalk deposits has been reported as the critical problem in nearby Vallhall field, which proves important measures should be taken in terms of drilling fluid selection [9]. This time, initial mud weight of 13.5 ppg has been increased to 14 ppg by applying 0.04 ppg increment per 300ft drilled formation in order to perform safe drilling operations in high pressurized thief zone.

8 1/2" hole (production liner) covering 10000-10600ft depth interval was drilled by using OBM drill-in fluid (DIF) system with saline *CaCl₂* brine and mud weight of 11.6 ppg. It is highly essential to use such a drilling fluid that does not damage the pay zone in addition to being compatible with native reservoir fluids. The selected DIF will cause less or no damage to natural reservoir permeability by forming a thin & impermeable filter cake on the face of formation and provide better hole cleaning. Additionally, the lowest possible mud density should be used whilst drilling the pay zone with the purpose of avoiding drilling problems related to differential sticking.

Hole Size (inch)	Section Depth (ft)	Mud Weight (ppg)	Mud Type
26" Hole	450-4500	9.9	WBM with low-solids non-dispersed (LSND) viscous polymer system
17 1/2" Hole	4500-6100	12-12.5	WBM with KCl, viscous polymer mud system
12" Hole	6100-10000	13.5-14	OBM with KCl polymer system
8 1/2" Hole	10000-10600	11.6	DIF (OBM) system with saline CaCl ₂ brine

Table 4.5. Drilling Fluid Design Summary

4.6. Drill Bit Design

Proper drill bit selection plays a critical role in petroleum engineering since it affects drilling operations, the total cost and rig time. The key factor influencing the drill bit design is the type of formations to be drilled. In the case of X-field, the lithology data of nearby and analogous Fulmar field will be considered for bit selection except from the reservoir section as well logs give sufficient information about the lithology of the reservoir interval. However, no lithological data above the reservoir section has been provided for the X-field; therefore, using data from another nearby Central Graben field is a reasonable approach.

26" hole section (450ft – 4500ft) – this interval consists of soft Glauconitic Calcareous claystones & siltstones. To drill this section, mill tooth roller cone bit with long, thin and widely spaced teeth, low journal angle (33°), large cone & oversize angle, and high offset is selected. Widely spaced & long steel teeth will prevent bit balling. Since the formation to be drilled is soft, the strength of bit components may be lower. The size of the bit in this section corresponds to 26".

17 ½" hole section (4500ft – 6100ft) – this interval also consists of previously mentioned soft claystone & siltstone formations; therefore, it is pointless to change the bit type in this section. However, as the depth is increasing, the formations tend to be less softer compared to the layers encountered in the previous hole size. That is why, it is recommended to have relatively decreased tooth height and increased width. The size of the bit in this section corresponds to 17 ½".

12" hole section (6100ft – 10000ft) – this section contains comparatively harder formations, such as chalk, Kimmeridge clay, and shale. As mill tooth bits tend to be subjected to rapid wear in harder and deeper formations, the better choice is to employ tungsten carbide insert (TCI) bit – being another type of roller cone bits. TCI bits are much more preferable to drill in medium to harder formations due to its durability. Tungsten carbide teeth are selected to be shorter and closely spaced to achieve better ROP. The size of the bit in this section corresponds to 12".

8 ½" hole section (10000ft – 10600ft) – the reservoir section contains medium to fine well sorted and consolidated sandstone formation. Polycrystalline Diamond Compact (PDC) bit with higher number of blades, matrix body, and disc-shaped cutters is the optimal selection for this section. The productive interval was drilled with oil-based mud and PDC bit is much compatible with non-hydrating formations. Moreover, PDC bits are frequently applied in offshore fields to drill longer sections where tripping time is an essential factor. The size of the bit in this section corresponds to 8 ½".

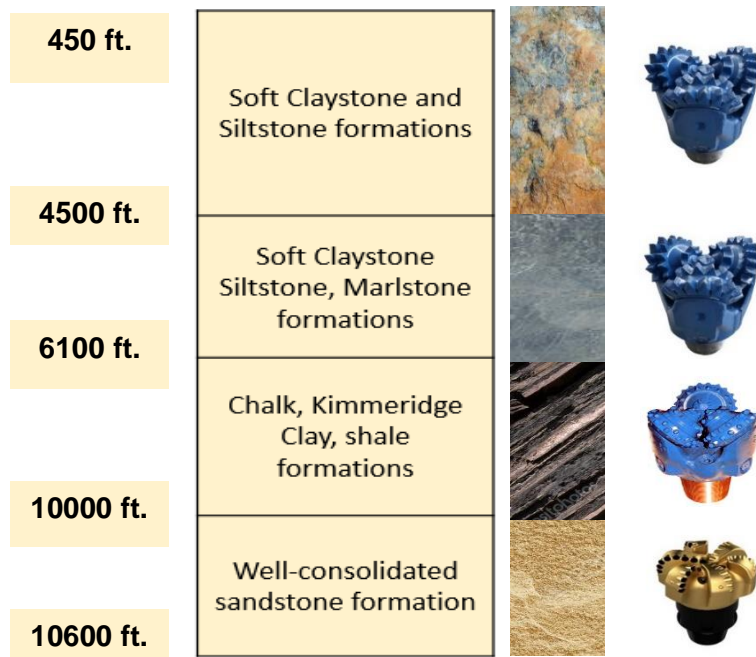


Figure 4.11. Drill Bit Design Summary

4.7. Directional Drilling

After modelling process was conducted to determine positions of wells in the reservoir, one of production wells was placed at distance of 4400 ft from the platform, while its True Vertical Depth (TVD) was selected as 10600 ft. At the following steps, Kick-off Point (KOP) and Build-up Rate were decided as 4950 ft and $2.7^{\circ}/100\text{ ft}$. It should be noted that position of KOP is recommended at the shallower depths, while build-up should be in the interval of 1° and 3° per 100 ft. The shallowest KOP can decrease Build-up Rate to reach the well position and on the other hand, it is easy to kick off a well at the shallow formations (shallow formations are more likely to be softer). In term of the Build-up Rate, lower values of this parameter can reduce severity of dog leg which can cause the drilling problems in the well.

Other parameters for directional drilling of well were calculated with the help of the above values and their tabulation was demonstrated in the following table (Table 4.6), while the calculation process was added to Appendix part.

Parameter	Value	Unit
Build-up Rate (γ°)	2.7	$^{\circ}/100\text{ ft}$
Kick-off Point (KOP)	4950	ft
Tangent Angle (α)	48.5	$^{\circ}$
Along Hole Depth (AHD)	12874	ft
Horizontal Departure (d)	4400	ft
True Vertical Depth (TVD)	10600	ft
Build-up Radius (R)	2122	ft

Table 4.6. Directional Drilling Data

After calculation of the parameters, the profile of the well trajectory was prepared in the following form (Figure 4.12).

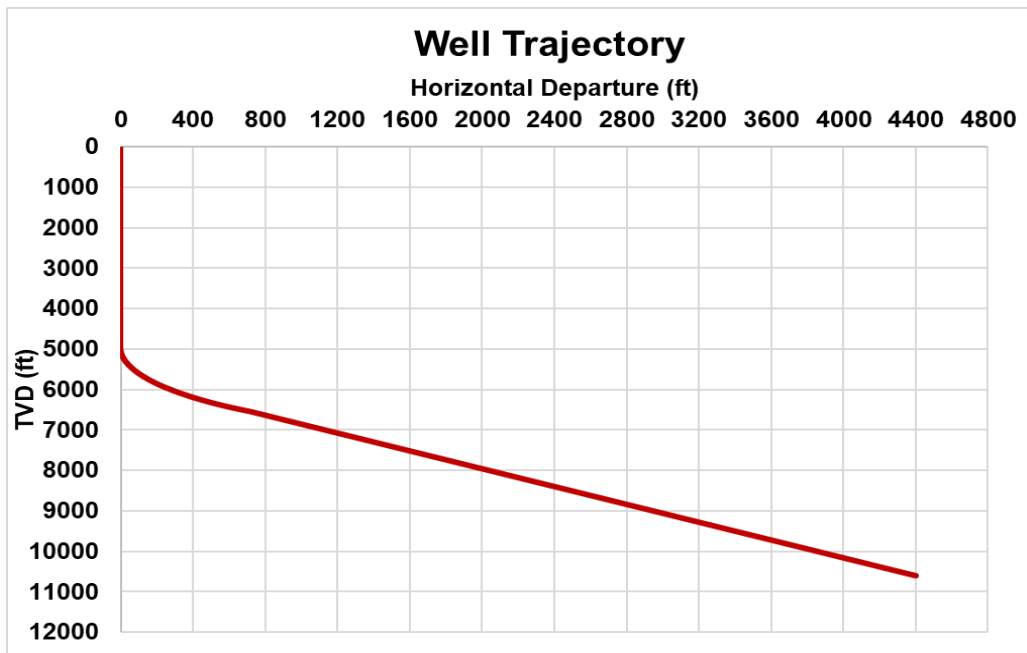


Figure 4.12. Well Trajectory Profile

4.8. BHA Design

The bottom-hole assembly is a part of drill string, which influences trajectory of the bit and as a result, of the wellbore. BHA design will be conducted on the base of length of the drilled section, type of formation, appropriate wellbore shape etc. As it was previously mentioned, nearby fields (particularly Fulmar field) have been examined for being aware of geological description.

26" hole section – conventional BHA is used for drilling. Since the section covers soft formations, basically uniform siltstone & claystone layers, simple assembly is enough for it. The assembly contains: HWDP for reducing stiffness ratio; anti-wall stick drill collar to thwart pipe sticking, drilling jar for striking stuck drilling string up/down to identify whether pipe is stuck or not, stabilizer to centralize the drill bit and MWD/LWD for drilling program consisting of detailed lithological acquired from nearby fields. Additionally, for having high rpm, mud motor that helps to drill faster is used.

17 ½" hole section – directional drilling starts from here. Rotary Steerable System (RSS) BHA is applied in this section because of its benefits, such as no trip out necessities for changing the BHA. Moreover, it delivers simple trajectory and can be considered relatively cheaper option. RSS mode provides less drilling time and decreases formation damage due to excessive balance allowed in the reservoir. This system can rotate the whole drill string that diminishes friction, rises ROP and helps to carry out better hole cleaning. Additionally, KOP of the well is observed in the harder formations, thus,

desired parameters may be efficiently achieved via RSS BHA [26] [27]. Taking M/LWD survey should not be also forgotten to obtain clear data of trajectory & parameters. Besides it, stabilizers are used for centralization of the drill bit avoiding undesirable dogleg severities. They tend to protect expensive MWD tools as well. In order to visualize RSS BHA design of this section the following table have been constructed:

Component of BHA	Role in process
Drill pipe	Drilling fluid is pumped through it
HWDP	Transition between drill pipe and DC
DC	Supply of WOB for stable drilling
Drilling jar	Freeing stuck pipe
DC	Supply of WOB for stable drilling
Stabilizer (string)	To centralize & protect MWD
MWD	Controlling deviation at KOP
Steerable mud motor	To drill KOP
Stabilizer (near-bit)	To centralize & protect drill bit
17 1/2" roller cone bit	To drill

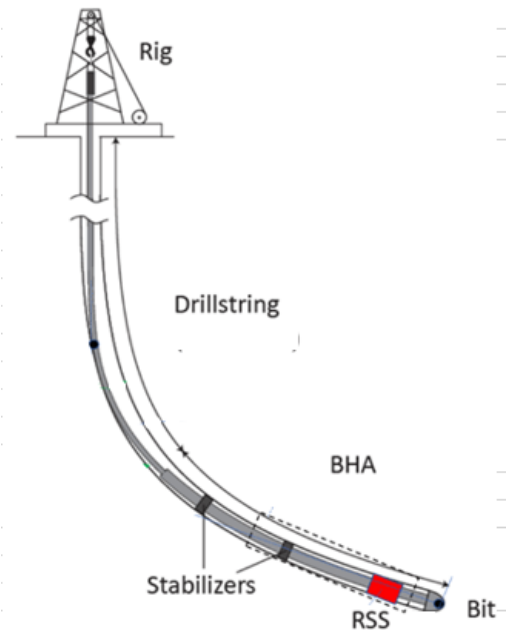


Table 4.7. BHA Design for directional drilling

12 1/4" hole section – tangent part of well trajectory including consolidated formations. Hence, shock subs should be added to BHA for absorbing too much vibrations and loads of bit shock in DC strings. BHA includes DC, stabilizers like in above sections. By using RSS feeds the intervals below this section are also scheduled to be neglected for minimizing doglegs & wells. Data obtained from LWD are pivotal for clarifying finish of anticipated Kimmeridge Clay development and top of sand zone. It is beneficial in casing design to identify setting depth of 9 5/8" casing. To declare top of sand before penetration, opening drilling pilot holes is considered. Flat hole may be drilled with RSS as a reservoir zone surrounding sands that will most likely be consolidated.

8 1/2" hole section – sophisticated BHA can be applied. Along with usage of shock subs in solid reservoir sandstone, under reamer is utilized to increase radius of the hole section for easy cement slurry flow.

4.9. BOP Design

During drilling operation, one of the most crucial functions of drilling mud is to counteract the pressure of the formation. Nevertheless, due to the number of reasons, well may take a kick and if left uncontrolled, formation fluids may flow to the surface in an uncontrolled manner, which is called a blowout. Blowout preventers have been designed specifically to seal the annular section between the hole and the pipe through which drilling fluid comes back to the surface. Closing off this space allows the mud and the formation fluids to be moved through an adjustable choke by which drillers can control the pressure in the borehole. BOPs can be classified into 2 types: annular or ram types. The annular preventer contains circular rubber packing unit that can close off around any size of pipe. Ram type preventers either seal off around a specific size of pipe with pipe rams, close off the wellbore completely with blind rams when there is no pipe or cut through drillpipe with shear rams in emergency cases. The following factors should be taken into account when designing BOP stack [\[17\]](#) [\[19\]](#):

- Pressure rating should be higher than the predicted surface pressure when the well control problem is encountered.
- The placement of rams should allow the optimum operational flexibility.
- The BOP stack should not only shut the well in but also allow stripping operation.
- The excessive use of rams may lead to additional cost and maintenance problems.

The API offers a variety of recommended stack configurations depending on the pressure ratings [\[18\]](#). In our case, since the maximum possible pore pressure is expected as 6100 psi, the following configuration is used which have a pressure limit of at least 10000 psi. This stack contains annular preventer, three ram type preventers (2 sets of pipe rams plus shear/blind rams) as shown in Figure 4.13.

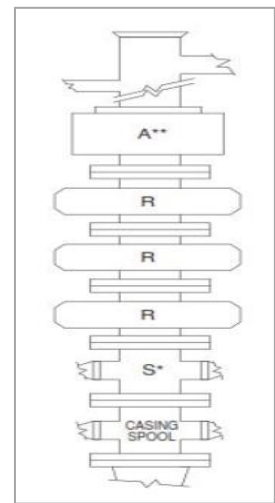


Figure 4.13. BOP Design Summary

4.10. Drilling Risks

Drilling operation can be linked with multiple factors which consequently contribute to major / minor drilling issues that might subject the crew to risks & danger. While different causes of drilling problems exist, typically they are associated with the drilling fluid characteristics and optimization of which may be advantageous to avoid or mitigate several problems. Some of the problems connected with this uncertainty have been listed below [\[28\]](#) [\[29\]](#):

Pipe sticking – one of the most widespread problems experienced while drilling which results in a lot of nonproductive time (NPT). Pipe becomes stuck if it may not be dragged out of hole and freed without causing damage to the pipe itself or exceeding the maximally allowable hook load. Several protections can be conducted during drilling process for decreasing the feasibility of sticking: retaining lowest continuous fluid loss, removing all solids as applicable as possible, utilizing lowest differential pressure.

Loss of circulation – the portion or whole mud flow into the formation that can subsequently induces formation damage & wellbore instability. Mitigations to eliminate this problem may be maintenance of proper mud weight, minimization of pressure losses and sufficient cleaning of hole.

Drill pipe failure – another severe problem which commonly occur during drilling. Improper storing, installing or transporting may have impact on development of this issue. It cannot be completely prevented but to minimize probability of this problem occurrence these stages may be strictly carried out: by selecting proper components of drill string, safety checks before usage and fatigue failures should be reduced as well.

Gas kick – shallow gas cap within abnormal pressure zone (thief zone) & reservoir section itself may contribute to gas kick into wellbore and blowout. It also can further lead to well and human losses. Therefore, both drill pipe and annular pressures should be regularly monitored for diminishing risks.

Besides the aforementioned mitigation techniques, additives can be used to tackle the problems related to drilling fluid. Various types of mud additives have considerable effect on this stage, namely viscosifiers, densifiers, filtration, lost circulation and rheology control materials.

In cementing design, numerous inevitable risks are also present. Some of them are as follows [30]:

Hole-cleaning & displacement mechanics – somehow complicated in deviated wells since fluids can stratify, and drilled solid cuttings stick in the narrow part of the casing. The settling is linked with a balance between viscous drag from the fluid viscosity and buoyant settling and yield stress. Hence, in this type of wells, a higher yield stress is profitable in order to take the cuttings away during the displacement. Both these issues can be handled by rotation & reciprocation.

Design of cement slurry – in addition to having a possibly high yield stress for dragging the cuttings, other parameters have to be taken into account. For instance, if free water exists in a cement slurry utilized in a deviated well, a water channel may form within the cemented interval, causing communication of reservoir / fracturing fluids. Several certain additives in concrete doses should be used to decrease risks of this uncertainty.

Subsequent to the given solution methods of the problems, pipe centralizers must be applied in this stage. Because pipe centralization is pivotal for desirable performance of cement-job, design reflections,

and usage. The fundamental aim of centralizers is to thwart channeling while displacing the drilling-fluid process by putting the pipe centered in the hole. Moreover, centralizers may be beneficial in avoiding sticking in formations having highly permeability and in descending casing wear.

For the current project, there are some additional specific problems such as absence of PPFG data and deficiency in lithology. They unavoidably influence casing & mud programs and bit design. These risks can give a path to development of fracture and abnormal pressurized zones, kick and blowout. When it comes to solutions, appraisal wells should be drilled for investigating hydrocarbon potential and LWD/MWD tools installed for clarifying the lithology. With the help of tools targeted path can be monitored as well if there is any deviation in it or not. At the same time, directional survey must be conducted for determination of the exact location of bottom-hole for monitoring reservoir performance

Last but not least, weather forecasting should be done routinely in order to be aware of severe weather conditions.

4.11. Drilling Schedule

For the clarification of the time needed to drill a well, duration of each process within the drilling operation should be identified. Generally, drilling the well is full of time-consuming processes: offshore transportation, fishing, cementing, casing running, logging, directional survey, drilling, rig maintenance and so on. Therefore, a reasonable data set is needed to declare the amount of time for these aspects. There are also some factors affecting the precise time such as well depth, weather and efficiency of the staff.

Overall, the drilling program has been estimated with the assumptions of: ROP commences with 100 ft/hr and decreases by means of depth (because of consolidation of deeper rocks); & speed of travel is taken up to 1,000 ft/hr. It is not secret that drilling in the North Sea is complex. Hence, the time dedicated to each well is roughly 60 days considering the maximum time spent in the field development with a correlation of depths and the duration of drilling. By taking all aforementioned factors into account drilling schedule for current case have been indicated in the following table. The time period given below is not precise and occurrence of pipe sticking, severe weather conditions is not exceptional [\[31\]](#) [\[32\]](#).

Process	TVD (ft)	Duration (days)
30" Casing (Conductor) Hammering	0 – 450	5
26" Hole Section Drilling	450 – 4500	10
20" Casing (Surface) Cementing	4500	3
17 ½" Hole Section Drilling	4500 – 6100	14

13 3/8" Casing (1st Intermediate) Cementing	6100	3
12 1/2" Hole Section Drilling	6100-10000	17
9 5/8" Casing (2nd Intermediate) Cementing	10000	3
8 1/2" Hole Section Drilling	10000-10600	7
7" Production Liner Cementing	10600	3
Total		65

Table 4.8. Drilling Schedule

4.12. Lower Completion Design

After placing the last casing string - production liner into the wellbore, we started to investigate on possible options for lower completion. Several methods exist for the reservoir completion, such as liner or screen completion, cemented & perforated liner or casing and cased hole gravel pack being the most common ones (Figure 4.14). At the end of the careful examination of their benefits and drawbacks, the team decided to select "cemented & perforated liner" completion design for the wells of X-field. There are several driving forces behind this decision, which have been discussed below:

- ❖ It is stated in the overview document that the reservoir sand is relatively well consolidated as proven by the analysis of core samples. This would trigger the idea of implementing openhole completion method; however, small interval was identified to be slightly friable. Another indicator was from the sonic log measurements as sonic travel time dictated the reservoir sand to be friable to moderately hard. Therefore, opting for barefoot completion design would be a bit risky. Moreover, the lack of selectivity over production zones and stimulation eliminated this option.

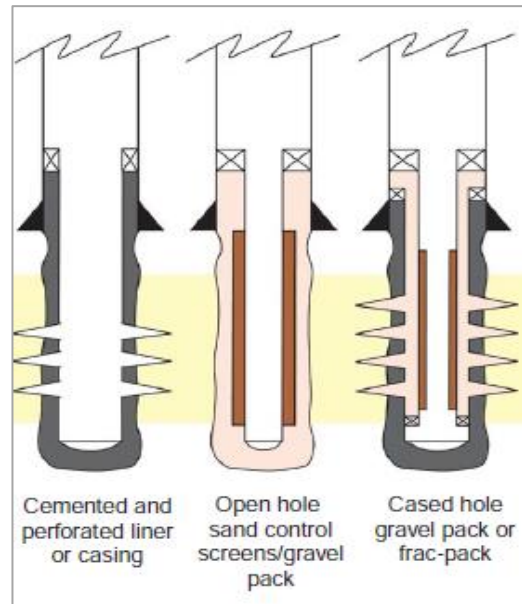


Figure 4.14. Lower Completion Methods

- ❖ Referring to the overview file once again, six drill stem tests (DST) have been performed in four wells; only one of them showed a little sand production of 4lbs/1000bbl at production rate of 4500bbl/day. This amount of sand was well below the allowed limit of 30lbs/1000bbl. Furthermore, the tests in the other wells of much higher production rates even did not demonstrate any sand producing to the surface. These facts prove that sand production issue is not typical for the wells of X-field and there is no need for taking sand control measures, such as installing screens or pumping gravel.
- ❖ The examination of the field properties and corresponding well test results lead to the selection of cased & perforated completion design. Firstly, it provides zonal isolation and selectivity for production or injection zones. Since water injection will be applied to maintain the reservoir pressure, the water breakthrough issue is not the exception in our case and this is the point where the preferred completion type comes as a possible solution by enabling the isolation of water producing zones and re-perforation of new zones. Our investigation on the lower completion method of the fields in the UK sector of the North Sea also showed that cased & perforated lower completion is the most extensively applied one. Although this method brings additional costs due to cementing and perforating operations, considerable cost reduction is expected due to the installation of liner rather than full-length casing.

4.11. Perforation Design

Successful perforation design plays a key role in terms of creating a connection between the desired reservoir zone and the wellbore by bypassing near wellbore formation damage. The key criteria leading to the success of the perforation design include the charge type, explosive type, size of the gun, shot density, phasing, and gun conveyance method. All these factors have been discussed below in order to achieve optimum perforation design.

The analysis of the case study about the perforation design procedure in nearby North Sea fields, such as Fulmar and Forties proved the success of dynamic underbalanced perforation (DUP), which improved the completion efficiency and reduced the formation damage [10]. It has been decided to follow the same perforation design strategy for the producers and injectors of the X-field as well; however, it is necessary to take reservoir fluid type and the mechanical properties of the formation into account before making a decision. As discussed before in the report, Fulmar field has a high level of analogy with the X-field, therefore the application of this technique being proved in several wells of the North Sea is a reasonable approach. DUP method was implemented in one producer and one injector well with the aim of enhancing the well productivity and avoiding back flowing the well respectively. Characterizing the formation damage is also an important point to consider, as we need to know what are being dealt with. Two main types of damage mechanisms anticipated as a result of drilling activities

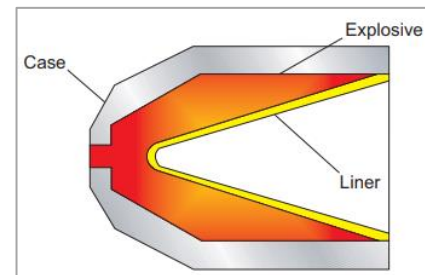
include filtrate & solid invasion caused by drilling mud and rock deformation around the wellbore provoked by drilling operation itself. Therefore, ensuring a deep enough charge penetration depth is essential. This can be estimated by using simulation tools provided by service companies; however, sometimes, such software packages may underestimate the real dimension of the damage zone. The tests performed to ascertain the level of remaining formation damage and deliverability or injectivity of the wells showed that DUP was highly effective to clean perforation path from debris and achieve the desired production or injection rates. The permeability impairment was avoided since even negative skin for the producer was recorded. The results after the DUP have tabulated below:

WELL PARAMETERS /	PRODUCER
Proposed DUB	2600 psi
Applied DUB	3400 psi
Original skin	> 11
Post-perforating skin	- 2.3
Remarks	For the producer the DUB was at the high permeability zones. High skin for most of the 6 layers

Table 4.9. Post-perforation results for Fulmar Field producer well

This successfully applied perforation design is selected as the reference to our design for the X-field. The key design features have been listed beneath [\[11\]](#):

- ❖ **Shaped charge design** – metallic conical liner has been selected as it increases the penetration depth by creating lined cavity effect. This design concentrates the explosive force into the target over a limited area. Moreover, as gravel-packing operations are not considered in our case, a low angle apex cone will be employed to provide long but small diameter perforation tunnel [\[13\]](#).
- ❖ **Gun conveyance method** – tubing conveyed perforation (TCP) is the preferred one for the X-field. Firstly, historical cases in the North Sea fields proved the success of TCP operation. Secondly, it provides several benefits over the other conveyance methods: high power charges, possibility to perforate long intervals in one run and allowance for running in highly deviated or even in horizontal wells.
- ❖ **Explosive type** – the main decisive factor in terms of explosive type is the reservoir temperature. The temperature in the case of X-field is given as 250°F or 121°C in the overview file. By using



the allowable temperature values for TCP method given in the Table C5.1 (Appendix), type of the explosive is chosen to be HMX.

- ❖ **Phasing** – the phasing angle is determined as 45° in order to achieve radial flow and avoid tortuous flow to perforation path. By doing so, skin will be reduced sourced by the flow distortion and higher well productivity will be obtained. Moreover, our analysis showed that 45° phasing is the most commonly used one in cased & cemented completion to achieve almost radial flow [\[12\]](#).
- ❖ **Shot density** – it is possible to select shot density up to 12 shots/ft. One of the main influencing factors in this case is k_v/k_h ratio. It can be stated that for the wells of X-field, this ratio is relatively higher - approximately 0.8-0.9. Based on the chart given in the appendix (Figure C5.2) [\[11\]](#), increasing the shot density for higher k_v/k_h ratio does not lead to significant productivity increase. Therefore, it has been decided to choose medium shot density of 12. (cost, failure)

The table 4.10 below summarizes the perforation design:

Charge type	Gun conveyance method	Explosive type	Phasing (°)	Shot density (shots/foot)
Metallic Conical Liner	Tubing Conveyed Perforation (TCP)	HMX	45	12

Table 4.10. Perforation Design Summary

REFERENCES

Geology & Formation Evaluation

1. Wills J.M., (1990). North Sea Oil and Gas Reservoir II. Graham & Trotman Limited. 1st edition. Page (26 – 45).
2. “Little about basic petrophysics by Muhammad Zahid” [online] Available at: http://www.carbonet.net/learninggeoscience_Petrophysics.pdf [Accessed: 30 September 2020]
3. “Thickness-weighted arithmetic-average method” [online] Available at: <https://www.uomisan.edu.iq/eng/ar1/admin/pdf/59599443338.pdf> [Accessed: 7 October, 2020]
4. Howard D., Thomas A., (1985). The Fulmar Oil Field (Central North Sea): geological aspects of its discovery, appraisal and development. [Accessed: 7 October, 2020]
5. Gluyas, J. and Hichens, H., 2002. The United Kingdom Oil and Gas Fields Commemorative Millennium Volume. London: Geological Society of London, pp.485-647.
6. Gray, J., 2013. Petroleum Prospectivity of the Principal Sedimentary Basins On The United Kingdom Continental Shelf. pp.10-15.
7. Buller, A., 1990. Proceedings of the 2Nd North Sea Oil and Gas Reservoirs Conference. London: Graham & Trotman, pp.1-25.
8. *The Defining Series: Basic Well Log Interpretation* | Schlumberger. [online] Available at: <<https://www.slb.com/resource-library/oilfield-review/defining-series/defining-log-interpretation>> [Accessed 18 December 2020].
9. Asquith, G. and Krygowski, D., 2004. *Basic Well Log Analysis*. Tulsa: The American Association of Petroleum Geologists, pp.1-20.
10. Raza, A., Gholami, R., Rezaee, R., Bing, C., Nagarajan, R. and Hamid, M., 2017. Preliminary assessment of CO₂ injectivity in carbonate storage sites. *Petroleum*, 3(1), pp.144-154.
11. Ma, S. and R. Morrow, N., 1996. Relationships between Porosity and Permeability for Porous Rocks. International Symposium of the Society of Core Analysts, p.13.
12. Saner, S., Kissami, M. and Al Nufaili, S., 1997. Estimation of Permeability From Well Logs Using Resistivity and Saturation Data. *SPE Formation Evaluation*, 12(01), pp.27-31.
13. Singh, N., 2018. Permeability prediction from wireline logging and core data: a case study from Assam-Arakan basin. *Journal of Petroleum Exploration and Production Technology*, 9(1), pp.297-305.
14. Rasolofosaon, P. and Zinszner, B., 2002. Comparison between permeability anisotropy and elasticity anisotropy of reservoir rocks. *GEOPHYSICS*, 67(1), pp.230-240.
15. Al-Joumaa, J. and Al-Jawad, M., 2019. Calculating heterogeneity of Majnoon Field/Hartha Reservoir using Lorenz Coefficient method. *IOP Conference Series: Materials Science and Engineering*, 579, p.012026.
16. Anyiam, O., Mode, A., Okpala, C. and Okeugo, C., 2018. The Use of Lorenz Coefficient In The Reservoir Heterogeneity Stduy of A Field In The Coastal Swamp, Niger Delta, Nigeria. *Petroleum and Coal*, p.11.
17. Fitch, P., Lovell, M., Davies, S., Pritchard, T. and Harvey, P., 2015. An integrated and quantitative approach to petrophysical heterogeneity. *Marine and Petroleum Geology*, 63, pp.82-96.

18. Cornford, C., 2009. *Source Rocks and Hydrocarbons of the North Sea*. 4th ed. London: Page (376-462)
19. GLENNIE, K., 1998. *Petroleum Geology of the North Sea*. Fourth ed. London: Blackwell Science Page (283-284)
20. Michens, J. G. G. a. H. M., 2003. *United Kingdom Oil and Gas Fields*. London: Geological Society Memoirs. Page (211-217, 311-313)
21. Crain, 2015. *Petrophysical Handbook*. [Online]
Available at: <https://www.spec2000.net/16-netpay.htm> [Accessed: 13 October 2020]
22. University, H.-W., 2018. *Geoscience B*. 4th edition Edinburgh. Page (199-201)
23. University, H.-W., 2018. Formation Evaluation. Page (118-125, 161-170)
24. Dr Peter Fitch, 2010. *London Petrophysical Society*. [Online]
Available at: https://lps.org.uk/wp-content/uploads/2016/05/08_LPS_Petrophysics_101_Fitch.pdf [Accessed: 13 October 2020]
25. Ziegler P.A., 1975, “The Geological Evolution of the North Sea Area in the Tectonic Framework of North Western Europe”, Norges geol unders. 316, The Hague, Netherlands
26. Johnson H.D., Mackay T.A., 1986, The Fulmar oil field (Central North Sea) – geological aspects of its discovery, appraisal and development: Marine and Petroleum Geology, v. 3, pp. 99-125.
27. Heriot-Watt University (2015). *Geoscience B*. Page (159 – 174)
28. Heriot-Watt University (2014). *Reservoir Engineering A*. Page (24 –39)

Reservoir Engineering

1. “Water flooding” [online] Available at: <https://petrowiki.spe.org/Waterflooding#:~:text=This%20is%20accomplished%20by%20%22voidage,oil%20viscosity%20and%20rock%20characteristics>). [Accessed: 10 October, 2020]
2. Kleppe J., (2016). Buckley-Leverett Analysis. Norwegian Science of Technology and Science. [Accessed: 15 October, 2020]
3. Idrees M., (2019). A simple approach to identify the proper relative permeability model. Materials Science and Engineering Conference. [Accessed: 15 October, 2020]
4. “Average Water Saturation” [online] Available at: <https://www.sciencedirect.com/topics/engineering/average-water-saturation> [Accessed: 15 October, 2020]
5. Heriot-Watt University, Introduction to Petroleum Engineering. Gross rock volume calculation
6. Heriot-Watt University, 2018. *Reservoir Engineering B*. pp (242-243)
7. Jahn, F., 1998. *Hydrocarbon Exploration and Production*, Vol. 46. Elsevier Science. Page (208-209), (213-214)
8. Beller, M., Chauvel, A. and Simandoux, P., 1999. The Challenge of North Sea Oil and Gas Fields. *Oil & Gas Science and Technology*, 54(1), pp.105-123.
9. Heriot-Watt University (2014). *Reservoir Engineering A*. Page (98– 122)

Drilling Engineering

1. “Casing Design” [online] Available at: https://petrowiki.org/PEH:Casing_Design [Accessed: 20 October, 2020]
2. Ford J., (2015). *Drilling Engineering* Heriot-Watt University. Page (165-201), (419-447), (227-329).[Accessed: 20 October, 2020]

3. Aslanidis P., (2018). Design of the full casing program in a deviated well. Msc Thesis. [Accessed: 20 October, 2020]
4. Utsalo O., Olamigoke O., (2014). An Excel Based Casing Design Application. SPE 172466. *Nigeria Annual International Conference and Exhibition*. [Accessed: 20 October, 2020]
5. Zvonimir B., Vladimir C., Sanel N., (2014). Selection Casing Material Depending of Wells Fluid Corrosivity. [Accessed: 20 October, 2020]
6. "Casing Design Catalogue" [online] Available at: <https://www.tenaris.com/> [Accessed 22 October, 2020]
7. Minton R.C., (1981). Drilling Fluids and practices for Central North Sea Tertiary Shales. SPE 10386.1. [Accessed 22 October, 2020]
8. "Drilling Fluids" [online] Available at: https://petrowiki.org/PEH:Drilling_Fluids [Accessed: 29 October, 2020]
9. Michael J. S., Kinn S., (2005). Improving drilling performance in the chalk reservoir of the Valhall field. SPE 95238. Annual Technical Conference and Exhibition. [Accessed: 29 October, 2020]
10. Tovar J., (2010). Design and Evaluation of Perforation Performance Using Dynamic Under Balance – North Sea Case Histories. SPE 135712. *Annual Technical Conference and Exhibition*. [Accessed: 30 September 2020]
11. (2016). Production Technology 2. Heriot-Watt University. Page (36-70). [Accessed 22 October, 2020]
12. Cosad C., (1992). Choosing a Perforation Strategy. Schlumberger Testing Services. [Accessed 22 October, 2020]
13. "Perforating Solutions. Halliburton Wireline & Perforating" [online] Available at: https://www.halliburton.com/content/dam/ps/public/lp/contents/Books_and_Catalogs/web/JRC_Catalog/Perforating-Solutions.pdf [Accessed 22 October, 2020]
14. Buller, A., 1990. *Proceedings Of The 2Nd North Sea Oil And Gas Reservoirs Conference*. London: Graham & Trotman, pp.25-30.
15. Daniel, R., 2001. Pressure prediction for a Central Graben wildcat well, UK North Sea. *Marine and Petroleum Geology*, 18(2), pp.235-250.
16. Baouche, R., Sen, S. and Boutaleb, K., 2020. Distribution of pore pressure and fracture pressure gradients in the paleozoic sediments of Takouazet field, Illizi basin, Algeria. *Journal of African Earth Sciences*, 164, p.103778.
17. Jahn, F., Cook, M. and Graham, M., 2011. *Hydrocarbon Exploration And Production*. Amsterdam: Elsevier, pp.40-42.
18. Drillingformulas.com. 2020. [online] Available at: <<http://www.drillingformulas.com/bop-stack-organization-and-bop-stack-arrangement/>> [Accessed 17 December 2020].
19. Grace, R. and Cudd, B., 1994. *Advanced Blowout & Well Control*. Houston: Gulf Pub. Co., pp.3-35.
20. Anon., 2019. Netwas Group Oil. [Online] Available at: <https://www.netwasgroup.us/operations/faults-1.html> [Accessed: 12 November 2020]
21. Anon., 2020. Bentec. [Online] Available at: <https://www.bentec.com/rigs/euro-rigs/skiddable-euro-rig/skiddable-euro-rig.html> [Accessed: 12 November 2020]
22. Frank Jahn, M. C. & M. G., 2003. Hydrocarbon Exploration and Production. 6th ed. UK: Elsevier. Page (32-34)
23. Hampton, 2019. Repsol Sinopec. [Online] Available at: <https://www.repsolsinopecuk.com/decommissioning/fulmar/about-fulmar> [Accessed: 12 November 2020]

24. Heriot-Watt, 2015. Drilling Engineering. 3rd ed. UK: Edinburgh. Page (13-16)
25. Chakrabarti, S. K., 2005. Handbook of Offshore Engineering. 1st ed. New York: Elsevier.
26. Panchal, N., 2012. Attitude control system for directional drilling bottom hole assemblies. [Online] [Accessed 4 December 2020].
27. Zhang, C., 2016. Overview of rotary steerable system and its control methods. [Online] [Accessed 4 December 2020].
28. A. Abelmann, 2016. ODP. [Online] Available at: http://www-odp.tamu.edu/publications/188_IR/chap_02/c2_9.htm [Accessed: 27 November 2020]
29. Hassan, Z., 2018. Common Drilling well problems (Reasons, indications, mitigation and prevention). [Online] [Accessed 27 November 2020]
30. Sabins, F., 1990. SPE 20005: Problems in Cementing Wells. [Online] [Accessed 27 November 2020]
31. Belknap, W., 1969. SPE 2635: Offshore Drilling in North Sea. [Online] [Accessed 11 December 2020].
32. J.A. Noerager, 1987. SPE16164: Drilling Time Predictions from Statistical Analysis. [Online] [Accessed 11 December 2020]

APPENDIX

Appendix A. Geology & Formation Evaluation.

Appendix A1. Composite Well Logs

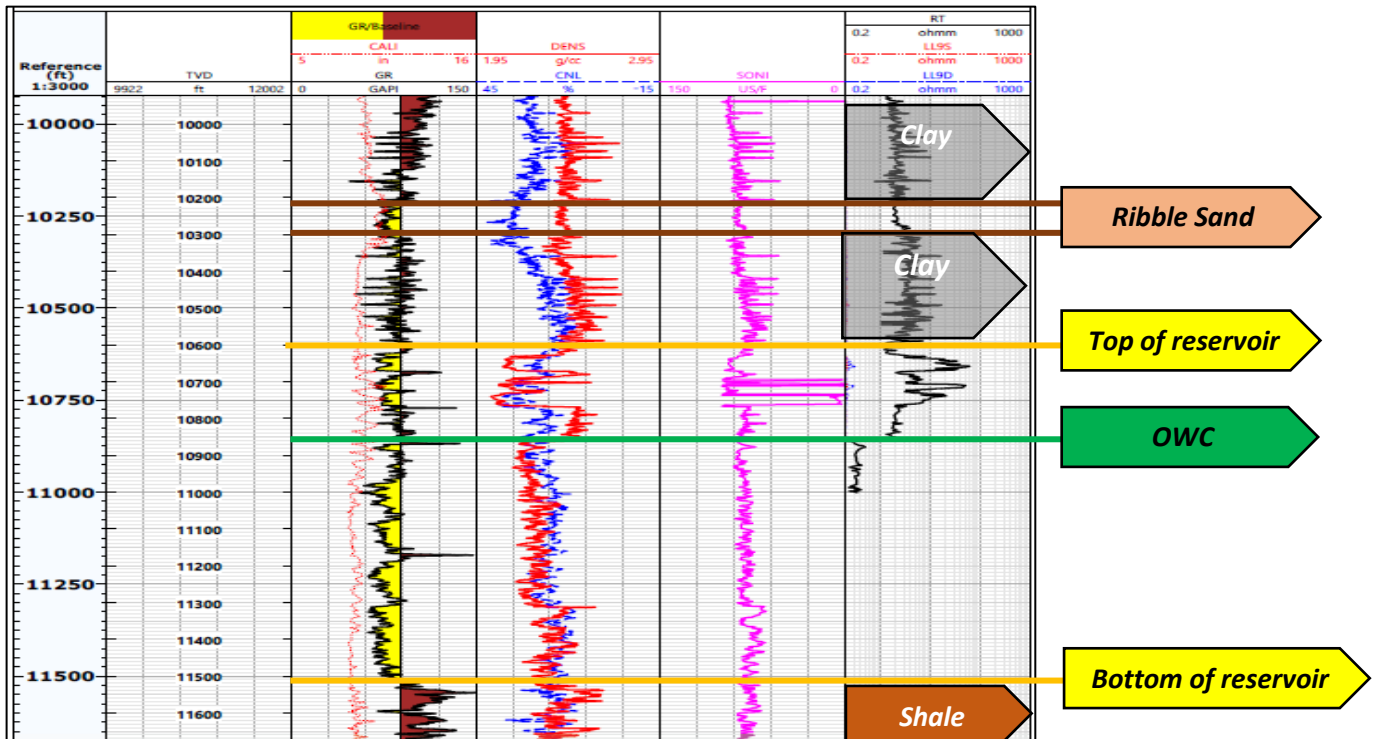


Figure A1.1. Well X-2 logging

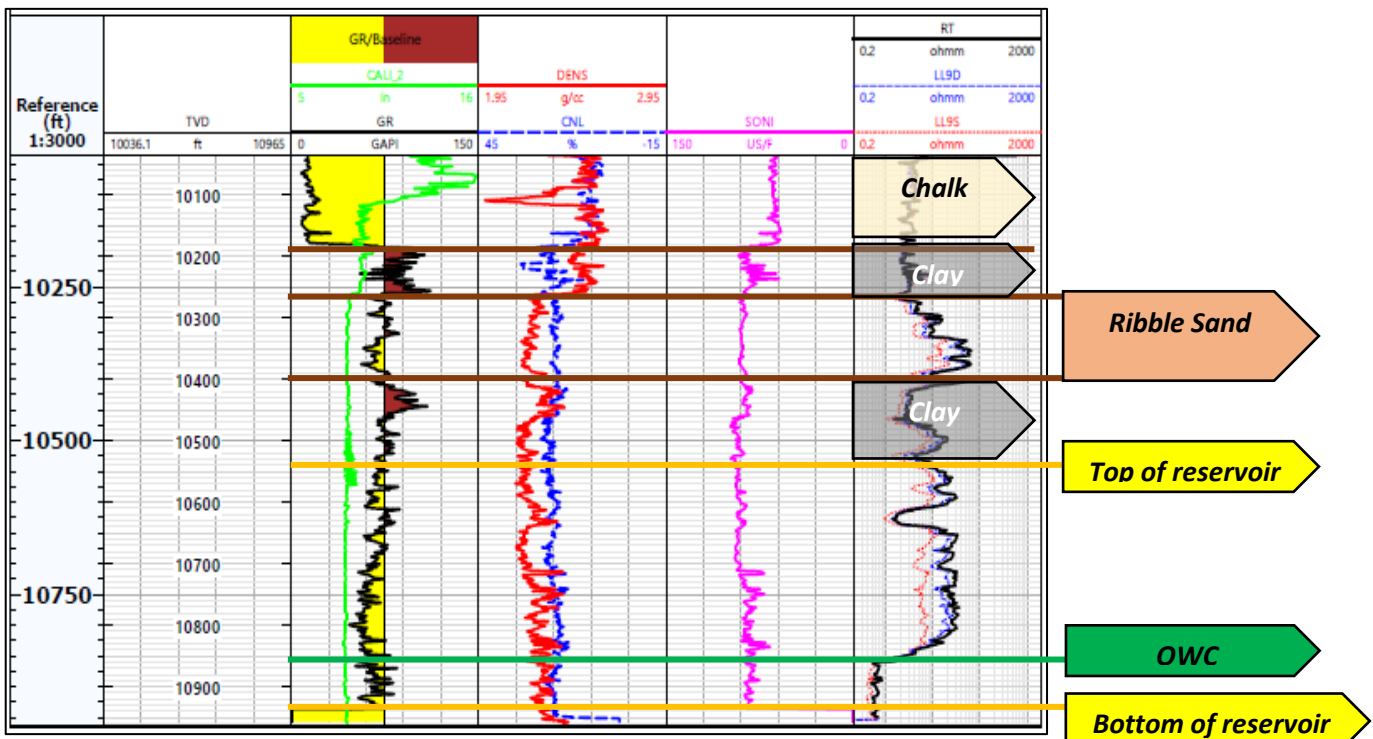


Figure A1.2. Well X-3 logging

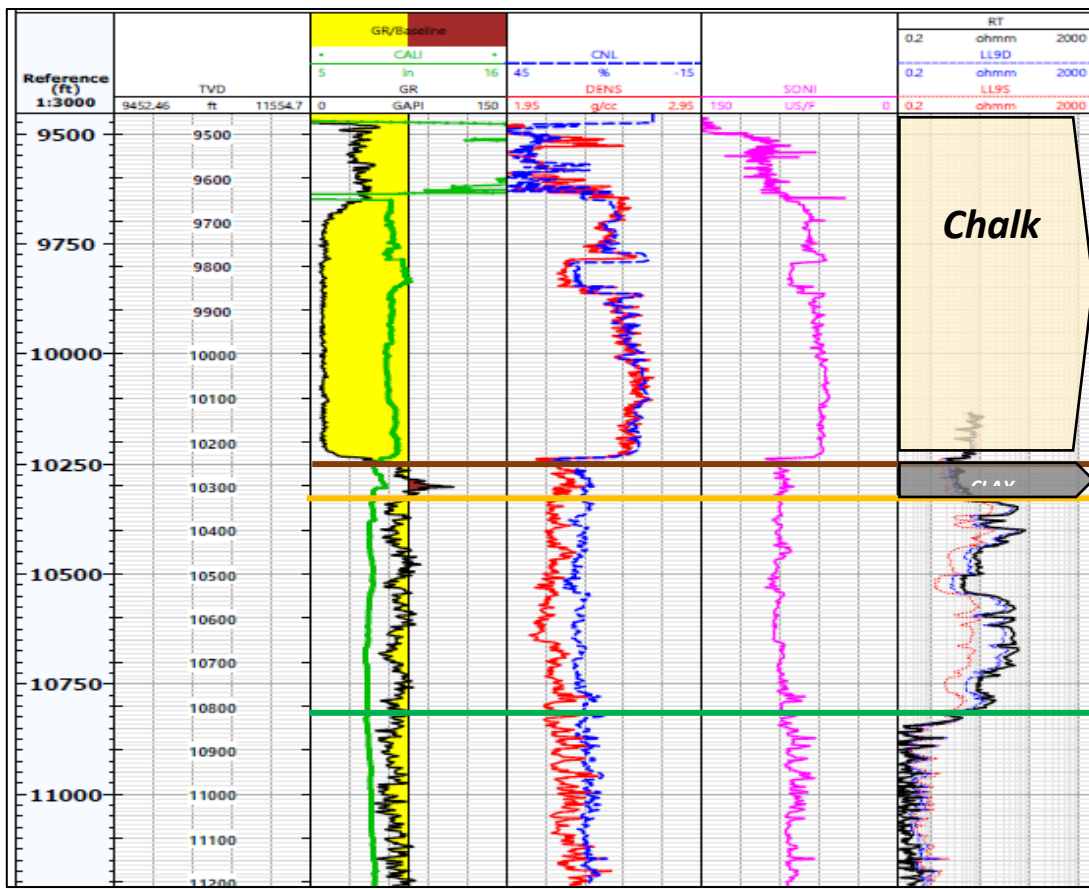


Figure A1.3. Well X-4 logging

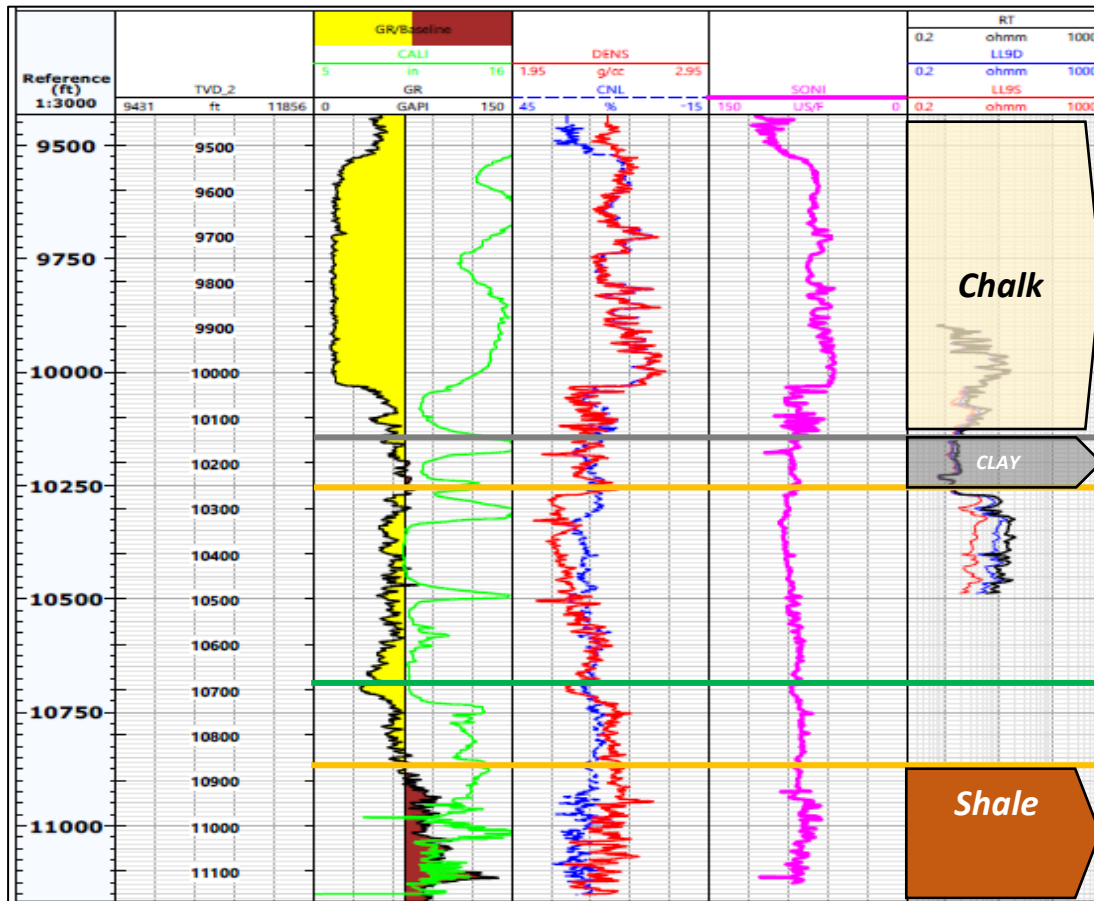


Figure A1.4. Well X-5 logging

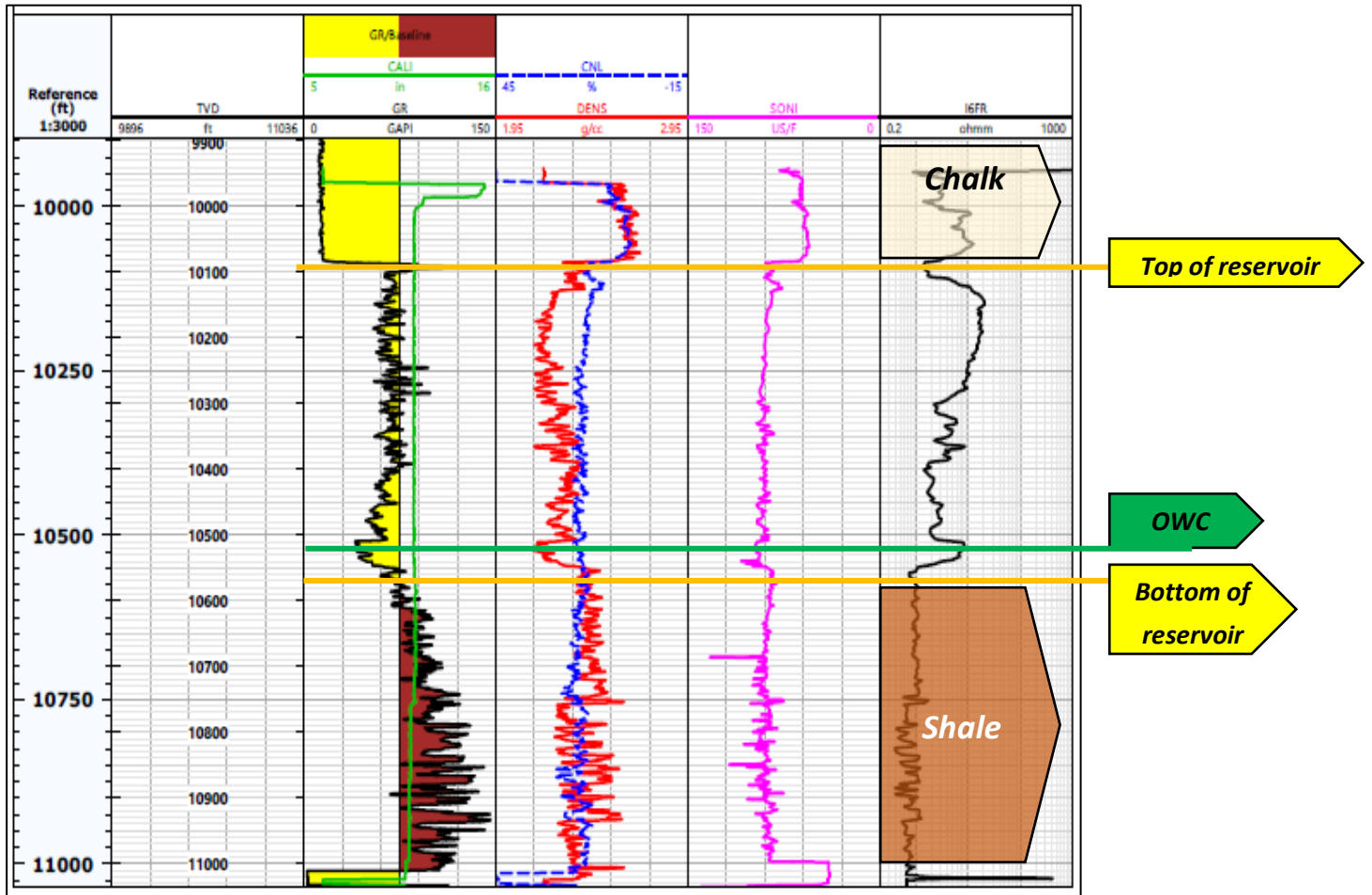


Figure A1.5. Well X-6 logging

Appendix A2. Core Porosity and Permeability graphs

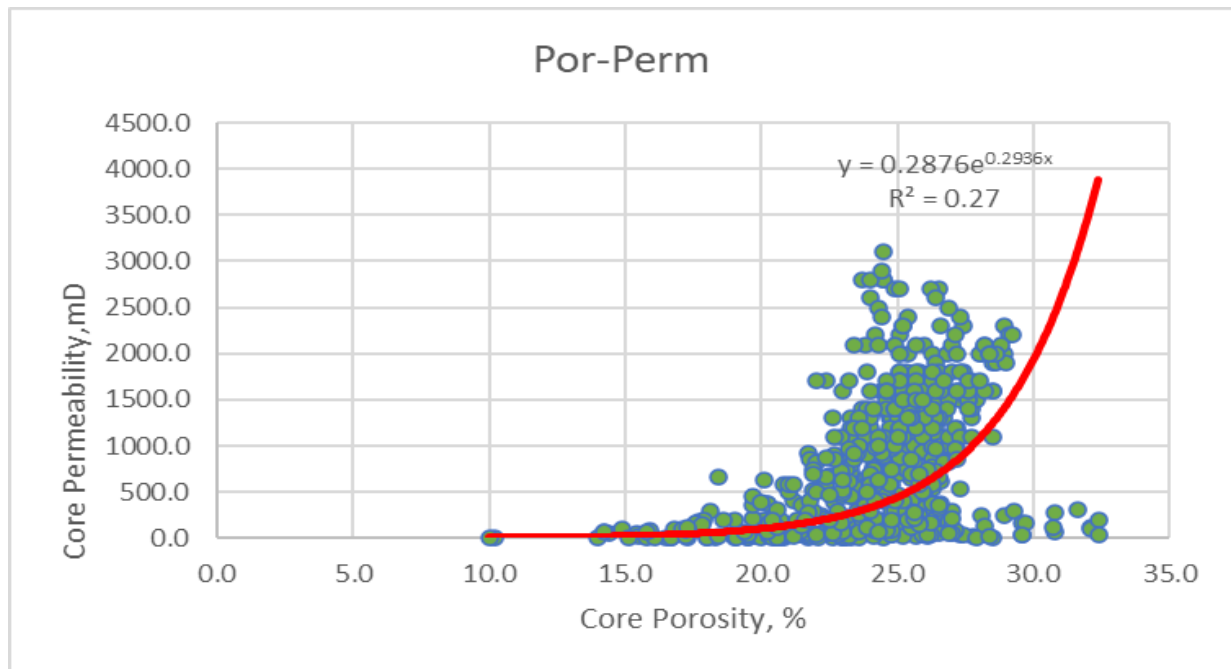


Figure A2.1. Core permeability vs core porosity for well X-4

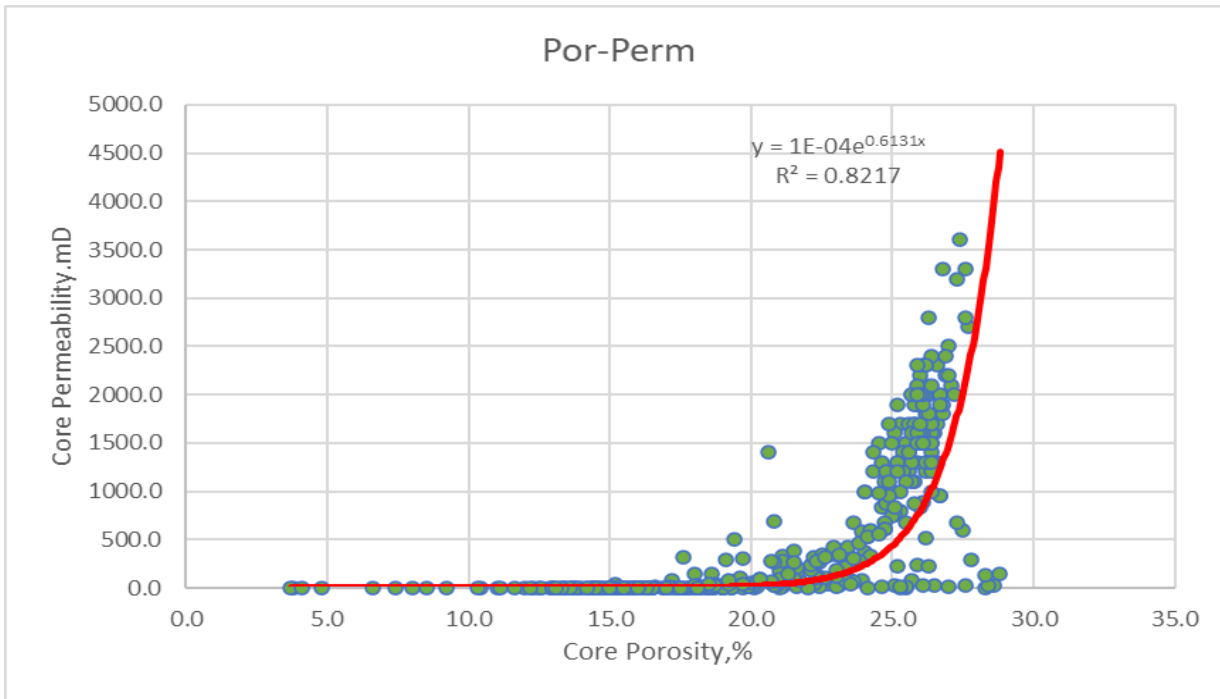


Figure A2.2. Core permeability vs core porosity for well X-5

Appendix A3. Determination of cut-offs (core calibration method)

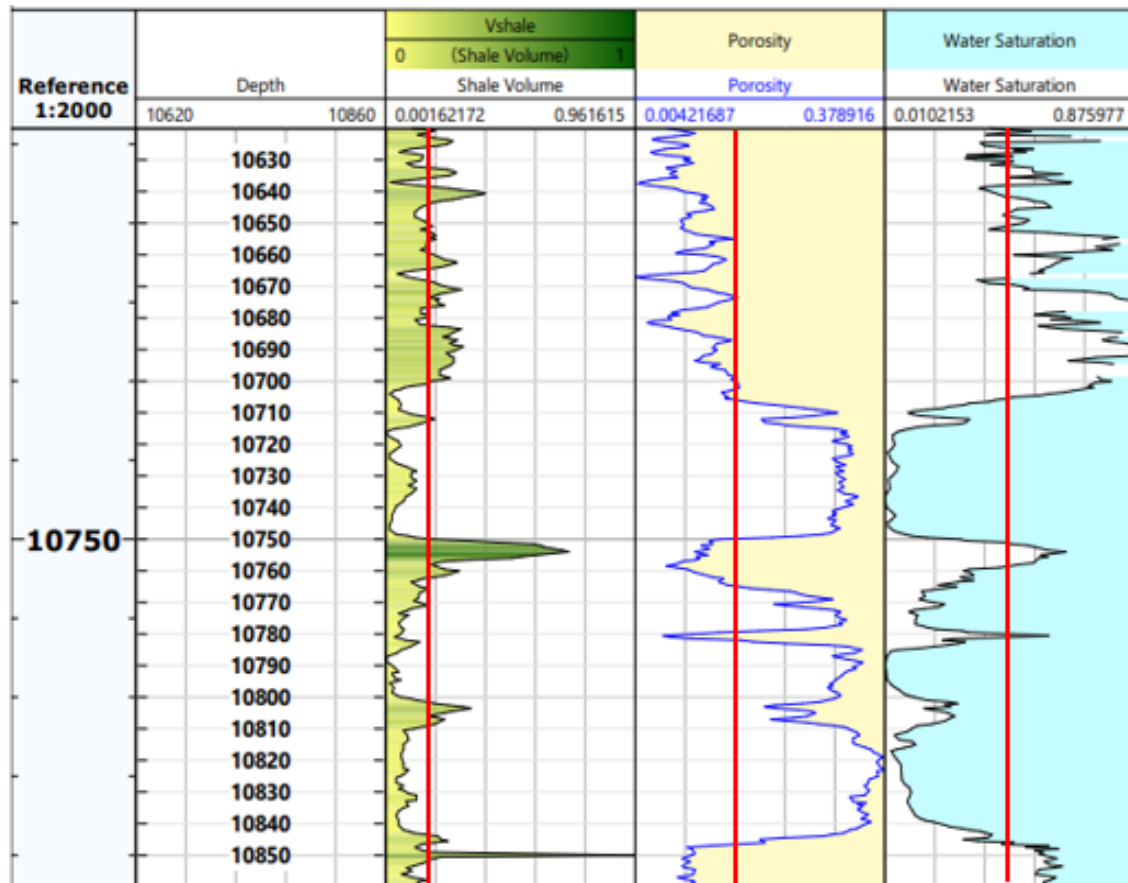


Figure A3.1. Core calibration method – Well X-2

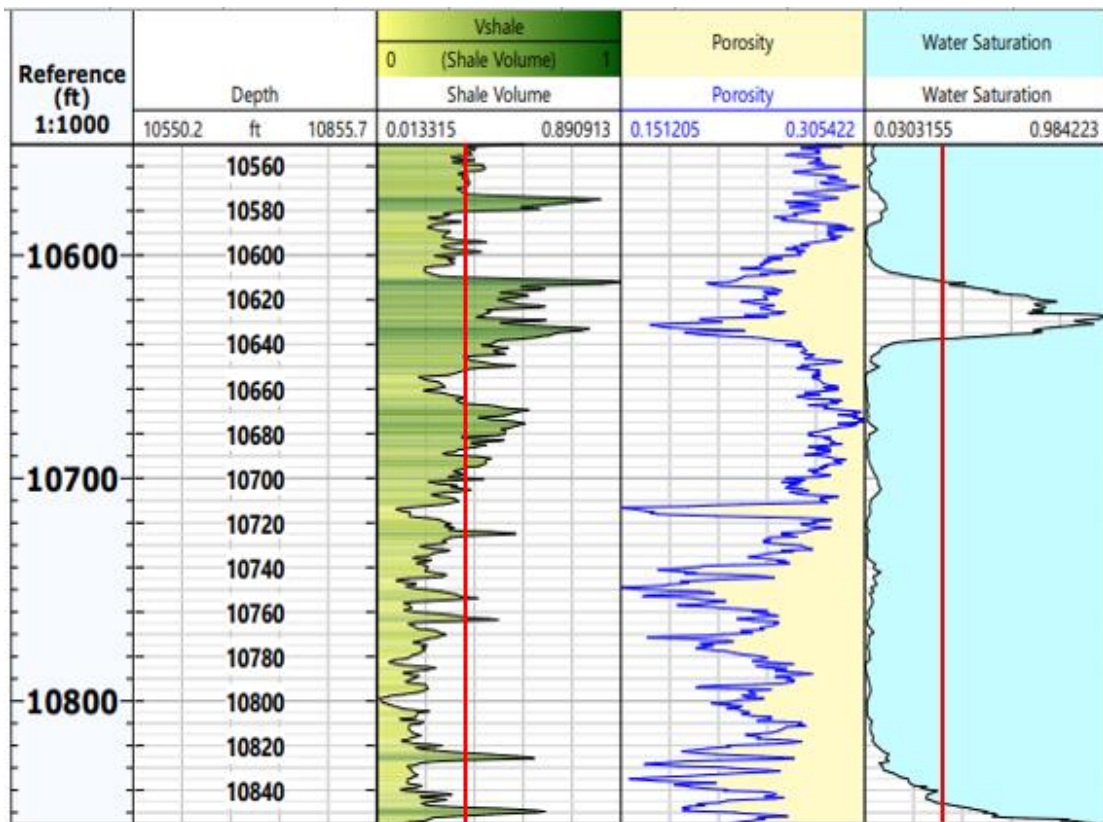


Figure A3.2. Core calibration method – Well X-3

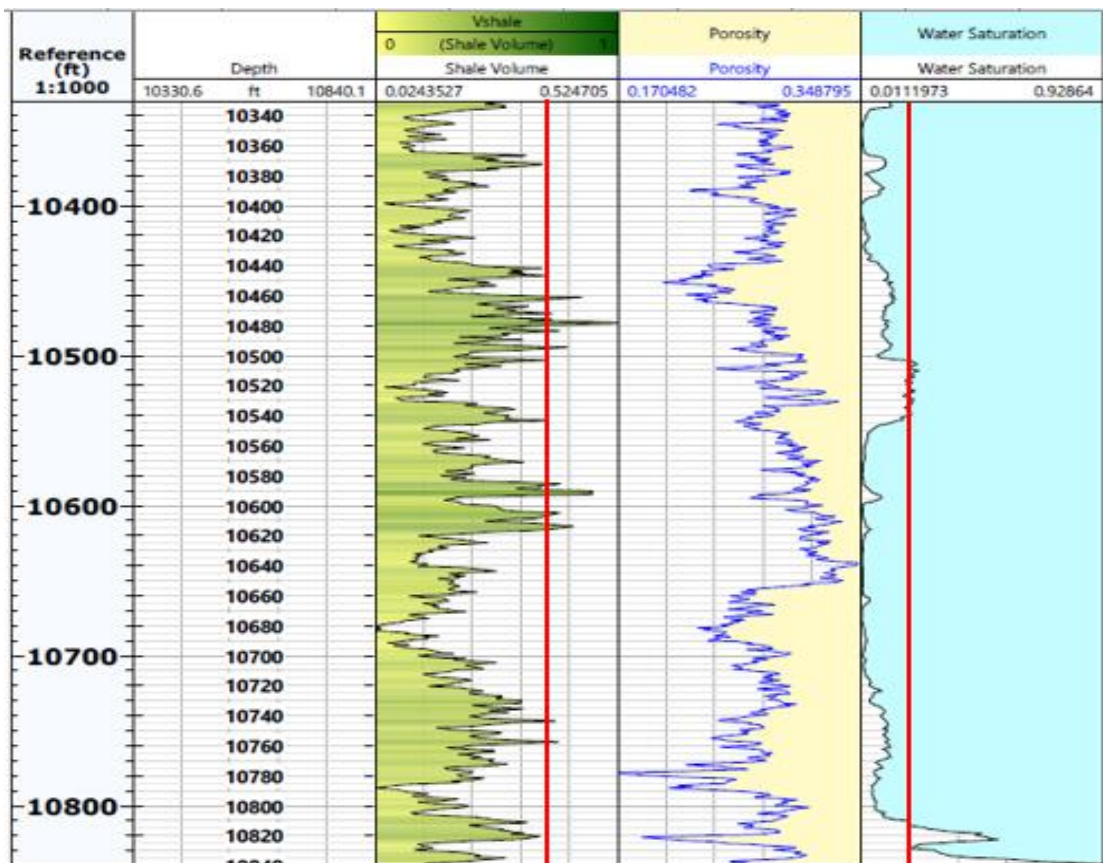


Figure A3.3. Core calibration method – Well X-4

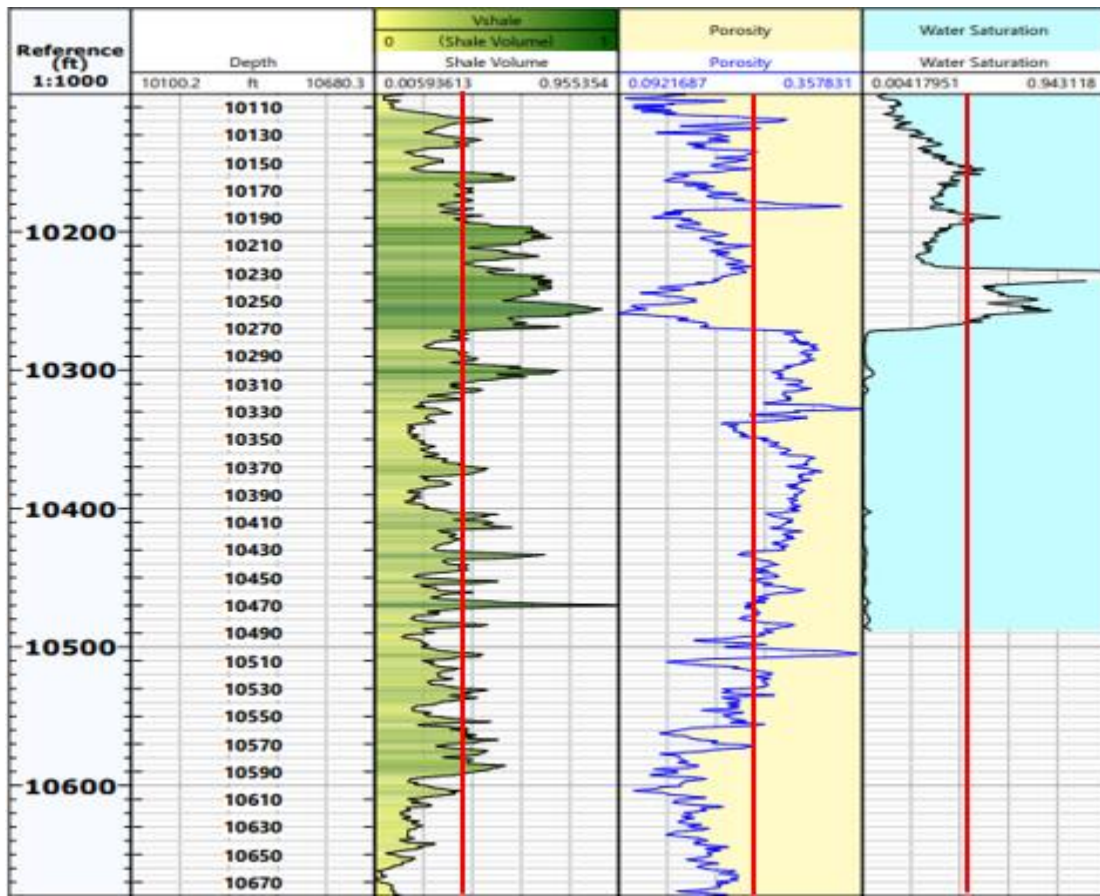


Figure A3.4. Core calibration method – Well X-5

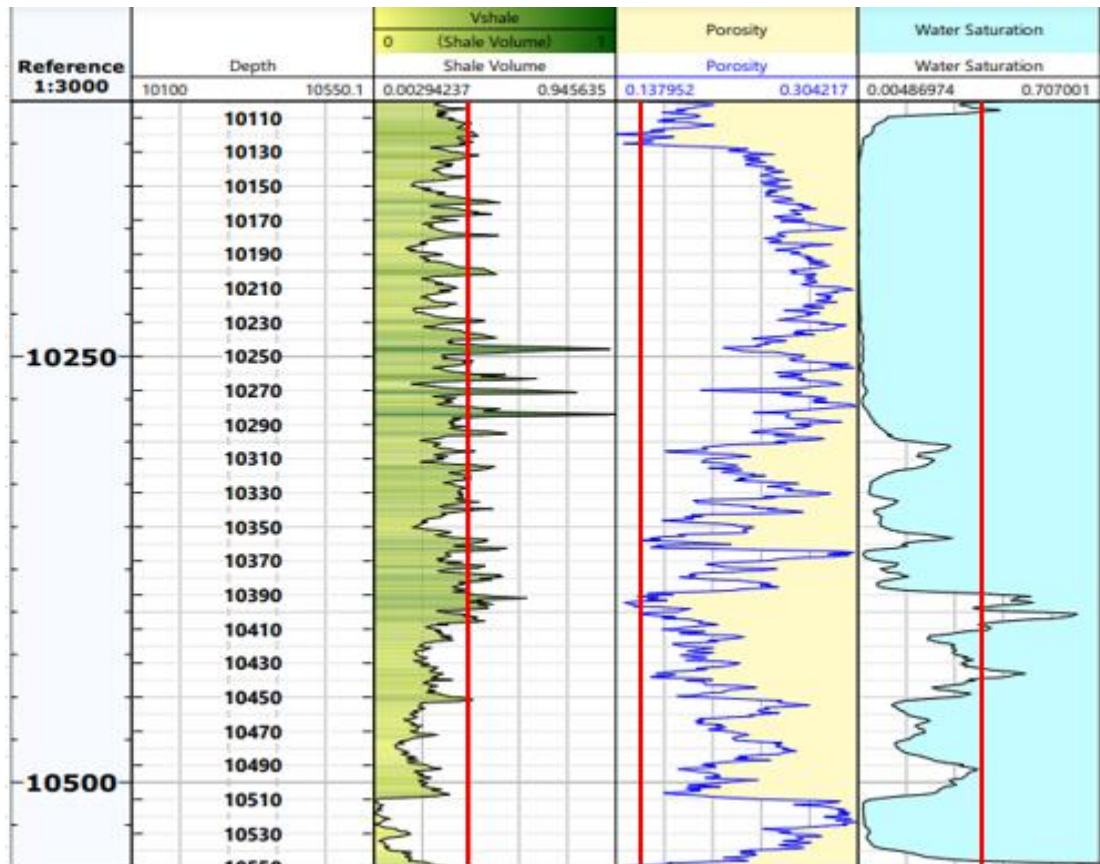


Figure A3.5. Core calibration method – Well X-6

Appendix B. Reservoir Engineering

Appendix B1. STOIP Calculation

Parameters	Well 1	Well 2	Well 3	Well 4
MAX. porosity	0.31	0.35	0.27	0.31
MIN. porosity	0.14	0.1	0.2	0.21
AVE. porosity	0.22	0.24	0.24	0.28
MAX. water saturation	0.164	0.244	0.25	0.23
MIN. water saturation	0.108	0.106	0.17	0.04
AVE. water saturation	0.13	0.147	0.188	0.111
N/G	0.64	0.56	0.62	0.91

Table B1.1. Parameters for the wells of South compartment

South compartment parameters	
MAX. porosity	0.31
MIN. porosity	0.1625
AVE. porosity	0.245
MAX. water saturation	0.222
MIN. water saturation	0.106
AVE. water saturation	0.144
AVE. N/G	0.68
Bo	1.323

Table B1.2. South compartment – averaged parameters

Parameters	Well 5	Well 6
MAX. porosity	0.28	0.27
MIN. porosity	0.16	0.14
AVE. porosity	0.23	0.22
MAX. water saturation	0.35	0.284
MIN. water saturation	0.21	0.204
AVE. water saturation	0.256	0.236
N/G	0.62	0.91

Table B1.3. Parameters for the wells of North compartment

North compartment parameters	
MIN. porosity	0.15
MAX. water saturation	0.317
MIN. water saturation	0.207
AVE. porosity	0.225
AVE. water saturation	0.246
AVE. N/G	0.765
GRV	224294.46
Bo	1.323

Table B1.4. North compartment – averaged parameters

Appendix B2. PVT Analysis Tables

Well 2 (Table 2.1 -2.6)

Well 1(Table 2.7-2.14)

Component	Mol%				Mol%			
	Case B				Case C			
	Reservoir Fluid	Stage 1	Stage 2	Tank oil at 77F	Reservoir Fluid	Stage 1	Stage 2	Tank oil at 77F
C ₁	23.37	6.67	0.51	-	23.61	4.01	0.29	-
C ₂	8.32	5.00	1.59	0.32	8.66	3.96	1.36	0.50
C ₃	8.61	7.21	4.65	2.72	9.56	7.33	5.09	3.85
iC ₄	1.21	1.23	1.09	0.91	1.33	1.34	1.20	1.08
nC ₄	5.00	5.46	5.33	4.83	5.28	5.87	5.63	5.34
iC ₅	1.62	2.05	2.27	2.27	1.71	2.25	2.40	2.41
nC ₅	3.06	3.90	4.37	4.43	3.11	4.16	4.47	4.52
C ₆	3.58	4.87	5.62	5.87	3.82	5.61	6.21	6.38
C ₇	5.66	7.94	9.28	9.75	5.72	8.65	9.66	9.96
C ₈	5.55	7.93	9.33	9.84	5.72	8.87	9.94	10.28
C ₉	4.33	6.25	7.37	7.78	4.54	7.15	8.03	8.31
C ₁₀₊	28.23	41.10	48.55	51.28	25.60	40.67	45.72	47.38
N ₂	0.80	0.11	-	-	0.80	-	-	-
CO ₂	0.66	0.28	0.04	-	0.54	0.13	-	-

Table B2.1. Well 2 Oil Analysis Data (mole %)

Component	Weight%				Weight%			
	Case B				Case C			
	Reservoir Fluid	Stage 1	Stage 2	Tank oil at 77F	Reservoir Fluid	Stage 1	Stage 2	Tank oil at 77F
C ₁	3.35	0.71	0.05	-	3.46	0.41	0.03	-
C ₂	2.24	1.00	0.28	0.05	2.38	0.76	0.24	0.09
C ₃	3.40	2.11	1.19	0.67	3.85	2.05	1.30	0.96
iC ₄	0.63	0.47	0.37	0.30	0.70	0.49	0.40	0.36
nC ₄	2.60	2.11	1.80	1.57	2.80	2.17	1.89	1.75
iC ₅	1.04	0.98	0.95	0.92	1.12	1.03	1.00	0.98
nC ₅	1.98	1.87	1.84	1.79	2.05	1.90	1.86	1.84
C ₆	2.76	2.79	2.82	2.83	3.01	3.07	3.10	3.10
C ₇	5.08	5.29	5.41	5.46	5.23	5.50	5.60	5.63
C ₈	5.68	6.03	6.21	6.28	5.96	6.43	6.57	6.62
C ₉	4.97	5.33	5.50	5.57	5.32	5.83	5.96	6.01
C ₁₀₊	65.81	71.21	73.57	74.57	63.69	70.32	72.05	72.67
N ₂	0.20	0.02	-	-	0.21	-	-	-
CO ₂	0.26	0.08	0.01	-	0.22	0.04	-	-

Table B2.2. Well 2 Oil Analysis Data (weight %)

Component	Mol%			Mol%		
	Case B			Case C		
	Stage 1	Stage 2	Tank gas at 77F	Stage 1	Stage 2	Tank gas at 77F
C ₁	60.01	40.69	9.73	56.94	34.04	8.35
C ₂	15.60	23.86	24.20	16.64	24.92	25.48
C ₃	11.67	21.33	39.21	13.36	25.37	40.07
iC ₄	1.16	1.99	4.28	1.30	2.44	4.39
nC ₄	4.01	6.18	14.08	4.27	7.77	14.02
iC ₅	0.67	0.83	1.95	0.78	1.07	1.98
nC ₅	1.22	1.32	3.04	1.34	1.64	3.01
C ₆	0.76	0.67	1.29	0.78	0.76	1.33
C ₇	0.66	0.52	0.95	0.73	0.54	0.91
C ₈	0.33	0.22	0.34	0.36	0.21	0.36
C ₉	0.11	0.08	0.10	0.10	0.05	0.10
N ₂	2.31	0.73	-	2.17	-	-
CO ₂	1.49	1.58	0.83	1.23	1.19	-

Table B2.3. Well 2 Gas Analysis Data (mole %)

Case	Stage	Separator	Separator	Solution	Oil Formation	Gas gravity	Stock Tank Oil		Bo at Pb	Fluid Density
		pressure	temperature	GOR	Volume Factor, Bo *		Gravity	g/cc		
A	1	100	77	400	1.067	0.853	40.90	0.8208	1.388	0.666
	2	0	77	91	1.008	1.411				
B	1	500	225	358	1.182	0.906	39.96	0.8253	1.390	0.672
	2	40	87	119	1.026	1.079				
	3	0	77	34	1.008	1.504				
C	1	300	200	424	1.143	0.963	40.24	0.8239	1.411	0.676
	2	30	80	82	1.031	1.136				
	3	0	77	22	1.008	1.504				

Table B2.4. Well 2 Separator Test Data

Pressure	Relative Volume	Fluid Density	Bo
psia	VBP at 250F = 1.00	g/cc	RB/STB
6000	0.949	0.706	1.339
5500	0.953	0.703	1.345
5000	0.958	0.699	1.352
4500	0.963	0.695	1.359
4000	0.968	0.692	1.366
3500	0.974	0.688	1.374
3000	0.984	0.681	1.388
2500	0.989	0.677	1.395
2000	0.997	0.372	1.407
1813	1.000	0.670	1.411
1700	1.030	0.650	1.453
1600	1.062	0.631	1.498
1500	1.100	0.609	1.552
1000	1.453	0.461	2.050
800	1.754	0.382	2.475
600	2.294	0.292	3.237
400	3.445	0.194	4.861
200	7.064	0.095	9.967
150	9.528	0.070	13.444

Table B2.5. Well 2 Flash Liberation Test, Density and Bo Data

Pressure	Viscosity
psia	cP
6000	0.50
5700	0.49
5000	0.47
4280	0.45
3570	0.43
2860	0.42
2150	0.40
1863	0.39
1720	0.39
1440	0.41
1150	0.44
870	0.46
585	0.54
300	0.58
160	0.61
14.7	1.26

Table B2.6. Well 2 Viscosity Data

Component	Well Effluent	Separator (1)		Tank	
		Liquid	Gas	Liquid	Gas
		Mol%	Mol%	Mol%	Mol%
C1	26.38	2.84	63.86	0.1	17.42
C2	9.84	4.59	18.2	0.84	24.45
C3	9.45	6.61	10.47	4.07	34.02
I-C4	1.30	1.82	0.79	1.19	3.92
N-C4	4.76	6.36	2.17	5.29	12.13
I-C5	1.55	2.32	0.33	6.36	2.11
N-C5	2.72	4.14	0.46	4.34	3.06
C6	3.89	8.3	0.22	3.09	1.42
C7+	38.73	62.9	0.11	74.71	0.76
CO2	0.40	0.09	0.89	0.01	0.53
N2	0.98	0.03	2.5	0	0.18

Separator	Separator (1)	Tank	Total
Pressure (psig)	100	0	-
Temperature (°F)	77	77	-
GOR (SCF/STB) (relative to tank oil)	436	109	545
Density of gas (g/litre)	1.0196	1.7317	-
Density of tank oil (g/cc)	-	0.819	-
Shrinkage factor (STB/RB)	-	0.7094	-
Oil Formation Factor (B_{ob}) at Pb and 250F (RB/STB)	-	1.4096	-

Table B2.7. Well 1 Separator Combination 1

Component	Well Effluent	Separator (1)		Tank	
		Liquid	Gas	Liquid	Gas
		Mol%	Mol%	Mol%	Mol%
C1	26.38	1.62	59.49	0.12	20.59
C2	9.84	2.97	19.02	1.1	27.02
C3	9.45	6.98	12.75	4.94	33.25
I-C4	1.3	1.48	1.06	1.33	3.38
N-C4	4.76	6.08	2.99	5.78	9.94
I-C5	1.55	2.37	0.46	2.43	1.53
N-C5	2.72	4.27	0.65	4.43	2.17
C6	3.89	6.56	0.3	7.02	0.92
C7+	38.73	67.61	0.15	72.84	0.42
CO2	0.4	0.05	0.86	0.01	0.59
N2	0.98	0.01	2.27	0	0.19

Separator	Separator (1)	Tank	Total
Pressure (psig)	50	0	-
Temperature (°F)	70	60	-
GOR (SCF/STB) (relative to tank oil)	478	46	524
Density of gas (g/litre)	1.082	1.6263	-
Density of tank oil (g/cc)	-	0.8161	-
Shrinkage Factor (STB/RB)	-	0.7174	-
Oil Formation Factor (B_{ob}) at Pb and 250F (RB/STB)	-	1.3939	-

Table B2.8. Well 1 Separator Combination 2

Component	Well Effluent	Separator (1)		Tank	
		Liquid	Gas	Liquid	Gas
	Mol%	Mol%	Mol%	Mol%	Mol%
C1	26.38	2.98	64.9	0.12	19.82
C2	9.84	4.54	18.06	1.1	27.1
C3	9.45	9.14	9.96	5.01	33.72
I-C4	1.3	1.85	0.72	1.36	3.41
N-C4	4.76	6.4	1.96	5.85	10.07
I-C5	1.55	2.35	0.28	2.45	1.56
N-C5	2.72	4.13	0.4	4.46	2.18
C6	3.89	6.14	0.18	7.02	0.92
C7+	38.73	62.23	0.09	72.62	0.42
CO2	0.4	0.16	0.9	0.01	0.61
N2	0.98	0.08	2.55	0	0.19

Separator	Separator (1)	Tank	Total
Pressure (psig)	100	0	-
Temperature (°F)	70	60	-
GOR (SCF/STB) (relative to tank oil)	422	99	521
Density of gas (g/litre)	1.0037	1.6366	-
Density of oil (g/cc)	-	0.8157	-
Shrinkage Factor (STB/RB)	-	0.7185	-
Oil Formation Factor (B_{ob}) at Pb and 250F (RB/STB)	-	1.3918	-

Table B2.9. Well 1 Separator Combination 3

Component	Well Effluent	Separator (1)		Tank	
		Liquid	Gas	Liquid	Gas
	Mol%	Mol%	Mol%	Mol%	Mol%
C1	26.38	6.97	74.12	0.15	25.63
C2	9.84	8.11	14.09	1.11	27.28
C3	9.45	10.91	5.86	4.3	28.97
I-C4	1.3	1.67	0.38	1.19	3.06
N-C4	4.76	6.26	1.02	5.26	9.06
I-C5	1.55	2.12	0.15	2.35	1.41
N-C5	2.72	3.74	0.2	4.34	2.12
C6	3.89	5.43	0.1	7.08	0.95
C7+	38.73	54.47	0.05	74.2	0.43
CO2	0.4	0.25	0.82	0.02	0.81
N2	0.98	0.07	3.21	0	0.28

Separator	Separator (1)	Tank	Total
Pressure (psig)	250	0	-
Temperature (°F)	70	60	-
GOR (SCF/STB) (relative to tank oil)	326	213	539
Density of gas (g/litre)	0.8979	1.554	-
Density of oil (g/cc)	-	0.8181	-
Shrinkage Factor (STB/RB)	-	0.7114	-
Oil Formation Factor (B_{ob}) at Pb and 250F (RB/STB)	-	1.4057	-

Table B2.10. Well X-1 Separator Combination 4

Separator	Separator (1)	Separator (2)	Tank	Total
Pressure (psig)	250	50	0	-
Temperature ($^{\circ}$ F)	70	60	60	-
GOR (SCF/STB) (relative to tank oil)	320	97	88	505
Density of gas (g/litre)	0.8979	1.1716	1.743	-
Density of oil (g/cc)	-	-	0.8135	-
Shrinkage Factor (STB/RB)	-	-	0.7245	-
Oil Formation Factor (B_{ob}) at Pb and 250F (RB/STB)	-	-	1.3803	-

Table B2.11. Well X-1 Separator Combination 5

Pressure	Bo at 245 F and below Pb
psia	RB/STB
1895	1.380
1729	1.354
1444	1.311
1160	1.269
875	1.228
591	1.183
306	1.128
170	1.086
110	1.061

Table B2.12. Well X-1 Bo data

Pressure	GOR at 245 F and below Pb
psia	SCF/STB
1895	539.00
1729	530.49
1444	516.23
1160	502.57
875	488.98
591	474.95
306	458.65
170	448.73
110	442.35

Table B2.13. Well X-1 GOR data

Pressure	Density of fluid	Viscosity	
		centistokes	centipoise
5849	0.6983	0.69	0.48
5419	0.695	0.68	0.47
4995	0.6917	0.68	0.47
4566	0.6882	0.67	0.46
4139	0.6846	0.66	0.45
3712	0.6806	0.66	0.45
3286	0.6765	0.65	0.44
2859	0.6721	0.65	0.44
2432	0.6673	0.65	0.43
2005	0.6622	0.65	0.43
1895	0.6607	0.65	0.43
1579	0.6724	0.65	0.44
1152	0.6883	0.68	0.47
868	0.6997	0.71	0.5
583	0.7121	0.78	0.54
299	0.7269	0.82	0.59
14	0.7566	0.89	0.67

Table B2.14. Well 1 Density & Viscosity

Note: At the above equations, standard conditions are taken as 60 F and 14.7 psia

Bo^* is Oil Formation Volume Factor which is equal to oil volume at separator conditions per volume of stock tank oil at STP (Standard Temperature and Pressure).

Formation Water Analysis

Cation/Anion	Concentration
	mg/l
Na^+	47833.0
K^+	2344.0
Ca^{2+}	7455.0
Mg^{2+}	674.0
Fe^{2+} (total)	43.0
Fe^{2+} (dissolved)	24.0
Ba^{2+}	9.5
Cl^-	90912.0
SO_4^{2-}	295.0
HCO_3^-	220.0

Table B2.15. Cation/Anion Concentration

Component	Mol%
N_2	5.56
CO_2	1.66
C_1	81.73
C_2	7.14
C_3	2.44
iC ₄	0.24
nC ₄	0.65
iC ₅	0.16
nC ₅	0.18
C_6	0.11
C_7	0.10
C_8	0.03

Table B2.16. Liberated Gas Composition Data of Formation Water Sample

Formation water was taken from 10962 to 10982 ft interval of Well 2. In its sample, specific gravity of total gas volume is equal to 0.677 (air = 1), while that of water is 1.103 at °F. Complete separation of gasses from formation occurred at 90 °C and gas/liquid ratio was recorded as 14 SCF/bbl. Hydrogen Sulfide content is close to zero (0.1 ppm). Resistivity was measured at two different temperature values (21.3 and 93.3 C) as 0.067 and 0.023 ohmm respectively, while value of pH and amount of suspended solids were detected like 5.85 and 72 mg/l.

ASTM Distillation	
	Temperature °C
IBP (initial boiling point)	48
5% volume recovered at	79
10% volume recovered at	103
20% volume recovered at	139
30% volume recovered at	182
40% volume recovered at	231
50% volume recovered at	275
60% volume recovered at	319
70% volume recovered at	349
FBP (final boiling point)	350
Recovery = 73%v	Residue = 27%v

Table B2.17. ASTM Distillation Data

ASTM distillation is one type of distillation that it is utilized to determine volume of recovery volume between initial and final boiling points.

Specific gravity at 60/60°F	0.8306
API gravity at 60°F	39°
Water content	0.15%
BS and W content	0.15%
Salt content	0.0008%w NaCl
Kinematic viscosity at 100°F	3.04 cS
Pour point (ASTM maximum)	: -3 °C
Pour point (ASTM minimum)	: -36 °C
Cloud point	: 19.6 °C
Paraffin wax content	6.1%w
Congealing point of wax	-
Sulphur content	0.26%w
Asphaltene content	0.40%w

Table B2.18. Average Reservoir Fluid Properties

Appendix C. Drilling Engineering

Appendix C1. Pressure Profile

Fracture Pressure Calculation: Ben Eaton Method

$$P_f = (P_o - P_p) * \left(\frac{\nu}{1 - \nu} \right) + P_p + S_t$$

Where,

- P_f – fracture pressure (psi)
- P_o – overburden pressure (psi)
- P_p – pore pressure (psi)
- ν – Poisson's ratio
- S_t – tectonic stress which is equal to 0

Poisson's ratio for different lithologies are shown in the table below:

Formation Type	Interval (ft)	Poisson's Ratio
Siltstone, Claystone	200-3000	0.15
Siltstone, Claystone, Marlstone	3000-9000	0.23
Chalk	9000-9525	0.28
Kimmeridge Clay	9525-10350	0.30
Sand	10350-10750	0.15

Table C1.1. Poisson's ratio values of X field formations

TVDSS (ft)	NP (psi)	PP (psi)	Overburden P (psi)	Poisson's Ratio	FP (psi)
0	0	0	0	0	0
265.27	58.97	58.97	264.18	0.15	95.18
459.03	213.29	213.29	457.15	0.15	256.32
652.30	310.27	310.27	649.63	0.15	370.16
893.90	426.58	426.58	890.23	0.15	508.40
1232.13	597.21	597.21	1227.08	0.15	708.36
1570.36	725.19	725.19	1563.92	0.15	873.20
1811.95	853.16	853.16	1804.52	0.15	1021.05
2101.86	981.14	981.14	2093.25	0.15	1177.39
2343.46	1066.45	1066.45	2333.85	0.15	1290.11
2536.73	1151.77	1151.77	2526.33	0.15	1394.34
2778.33	1237.09	1237.09	2766.93	0.15	1507.06
2971.60	1365.06	1365.06	2959.42	0.15	1646.42
3213.19	1450.38	1450.38	3200.02	0.23	1973.00

3406.47	1578.35	1578.35	3392.50	0.23	2120.24
3599.74	1663.67	1663.67	3584.98	0.23	2237.57
3841.34	1748.98	1748.98	3825.59	0.23	2369.27
4034.61	1876.96	1876.96	4018.07	0.23	2516.51
4276.21	1962.27	1962.27	4258.67	0.23	2648.21
4517.80	2047.59	2090.25	4499.28	0.23	2809.83
4662.75	2168.18	2302.15	4643.64	0.23	3001.56
4711.07	2190.65	2558.10	4691.76	0.23	3195.43
4952.67	2302.99	2643.41	4932.36	0.23	3327.12
5387.54	2505.20	3199.36	5365.45	0.23	3846.37
5677.45	2640.01	3284.68	5654.17	0.23	3992.45
5919.04	2752.35	3412.65	5894.77	0.23	4154.06
6015.68	2797.29	3583.28	5991.01	0.23	4302.47
6208.95	2887.16	3839.23	6183.50	0.23	4539.47
6402.23	2977.04	3967.21	6375.98	0.23	4686.71
6643.82	3089.38	4095.18	6616.58	0.23	4848.33
6692.14	3111.85	4308.47	6664.70	0.23	5012.28
6885.42	3201.72	4692.40	6857.18	0.23	5339.02
7223.65	3359.00	4905.69	7194.03	0.23	5589.22
7368.60	3426.40	5033.66	7338.39	0.23	5722.09
7706.83	3583.68	5246.95	7675.24	0.23	5972.28
7948.43	3696.02	5332.27	7915.84	0.23	6103.99
8141.70	3785.89	5460.24	8108.32	0.23	6251.22
8431.61	3920.70	5502.90	8397.04	0.23	6367.38
8769.84	4077.98	5716.19	8733.89	0.23	6617.58
9011.44	4190.32	5801.51	8974.49	0.23	6749.28
9349.67	4347.60	5844.17	9311.34	0.28	7192.51
9542.94	4437.47	5929.48	9503.82	0.28	7319.50
9736.22	4527.34	6014.80	9696.30	0.30	7592.59
10026.13	4662.15	6100.12	9985.02	0.30	7765.08
10122.77	4707.09	5972.14	10081.26	0.30	7733.19
10364.36	4819.43	5801.51	10321.87	0.15	6599.22
10509.32	4886.83	5929.48	10466.23	0.15	6730.08
10750.91	4999.17	5886.82	10706.83	0.15	6737.41

Table C1.2. Pressure values at different depths

TVDSS (ft)	Pore P (ppg)	Fracture P (ppg)	Safety Pore (ppg)	Safety Fracture (ppg)
265.27	4.28	6.90	4.58	6.60
459.03	8.94	10.74	9.24	10.44
652.3	9.15	10.91	9.45	10.61
893.9	9.18	10.94	9.48	10.64
1232.13	9.32	11.06	9.62	10.76
1570.36	8.88	10.69	9.18	10.39

1811.95	9.05	10.84	9.35	10.54
2101.86	8.98	10.77	9.28	10.47
2343.46	8.75	10.59	9.05	10.29
2536.73	8.73	10.57	9.03	10.27
2778.33	8.56	10.43	8.86	10.13
2971.6	8.83	10.65	9.13	10.35
3213.19	8.68	11.81	8.98	11.51
3406.47	8.91	11.97	9.21	11.67
3599.74	8.89	11.95	9.19	11.65
3841.34	8.76	11.86	9.06	11.56
4034.61	8.95	11.99	9.25	11.69
4276.21	8.82	11.91	9.12	11.61
4517.8	8.90	11.96	9.20	11.66
4662.75	9.49	12.38	9.79	12.08
4711.07	10.44	13.04	10.74	12.74
4952.67	10.26	12.92	10.56	12.62
5387.54	11.42	13.73	11.72	13.43
5677.45	11.13	13.52	11.43	13.22
5919.04	11.09	13.50	11.39	13.20
6015.68	11.45	13.75	11.75	13.45
6208.95	11.89	14.06	12.19	13.76
6402.23	11.92	14.08	12.22	13.78
6643.82	11.85	14.03	12.15	13.73
6692.14	12.38	14.40	12.68	14.10
6885.42	13.11	14.91	13.41	14.61
7223.65	13.06	14.88	13.36	14.58
7368.6	13.14	14.93	13.44	14.63
7706.83	13.09	14.90	13.39	14.60
7948.43	12.90	14.77	13.20	14.47
8141.7	12.90	14.77	13.20	14.47
8431.61	12.55	14.52	12.85	14.22
8769.84	12.53	14.51	12.83	14.21
9011.44	12.38	14.40	12.68	14.10
9349.67	12.02	14.79	12.32	14.49
9542.94	11.95	14.75	12.25	14.45
9736.22	11.88	15.00	12.18	14.70
10026.13	11.70	14.89	12.00	14.59
10122.77	11.35	14.69	11.65	14.39
10364.36	10.76	12.24	11.06	11.94
10509.32	10.85	12.32	11.15	12.02
10750.91	10.53	12.05	10.83	11.75

Table C1.3. Pressure gradients at different depths

Appendix C2. Casing Design

Casing Strings	Size (OD,inch)	Hole or Bit Size (inch)	Setting Depth TVDSS (ft)	Mud Density (ppg)
Conductor	30"	-	450	-
Surface	20"	26"	4500	9.9
Intermediate 1	13 3/8"	17 1/2"	6100	12.3
Intermediate 2	9 5/8"	12 1/4"	10000	13.5
Production Liner	7"	8 1/2"	10600	11.5

Table C2.1. Results of preliminary casing design

1ST INTERMEDIATE CASING DESIGN

BURST	TVDSS (ft)	External Load (psi)	Internal Load (psi)	Net Load (psi)	Design Load (psi)
	Surface	0	3697.576	3697.6	4067.3336
	Casing Shoe (6100ft)	1452.776	4307.576	2854.8	3140.28
COLLAPSE	TVDSS (ft)	External Load (psi)	Internal Load (psi)	Net Load (psi)	Design Load (psi)
	Surface	0	0	0	0
	Casing Shoe (6100ft)	3787.368	0	3787.4	3787.368

Table C2.2. Burst & Collapse Load Calculation for 13 3/8" Intermediate Casing

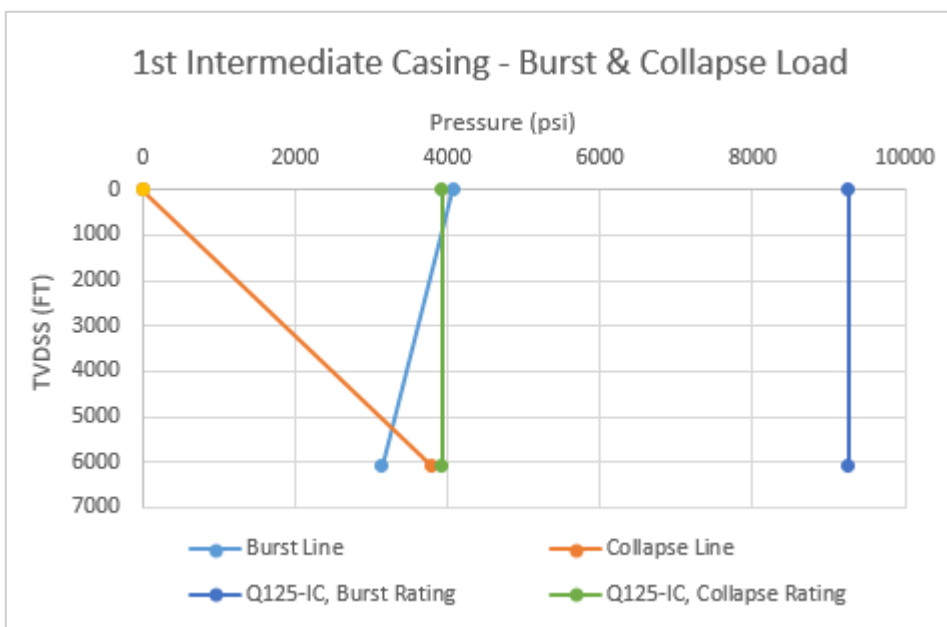


Figure C2.1. Burst & Collapse Load Demonstration for 13 3/8" Intermediate Casing

2nd INTERMEDIATE CASING DESIGN

	TVDSS (ft)	External Load (psi)	Internal Load (psi)	Net Load (psi)	Design Load (psi)
BURST	Surface	0	5019.736	5019.7	5521.7096
	Casing Shoe (10000ft)	2381.6	6019.736	3638.1	4001.9496
COLLAPSE	TVDSS (ft)	External Load (psi)	Internal Load (psi)	Net Load (psi)	Design Load (psi)
	Surface	0	0	0	0
	Casing Shoe (10000ft)	6240	0	6240	6240

Table C2.3. Burst & Collapse Load Calculation for 9 5/8" Intermediate Casing

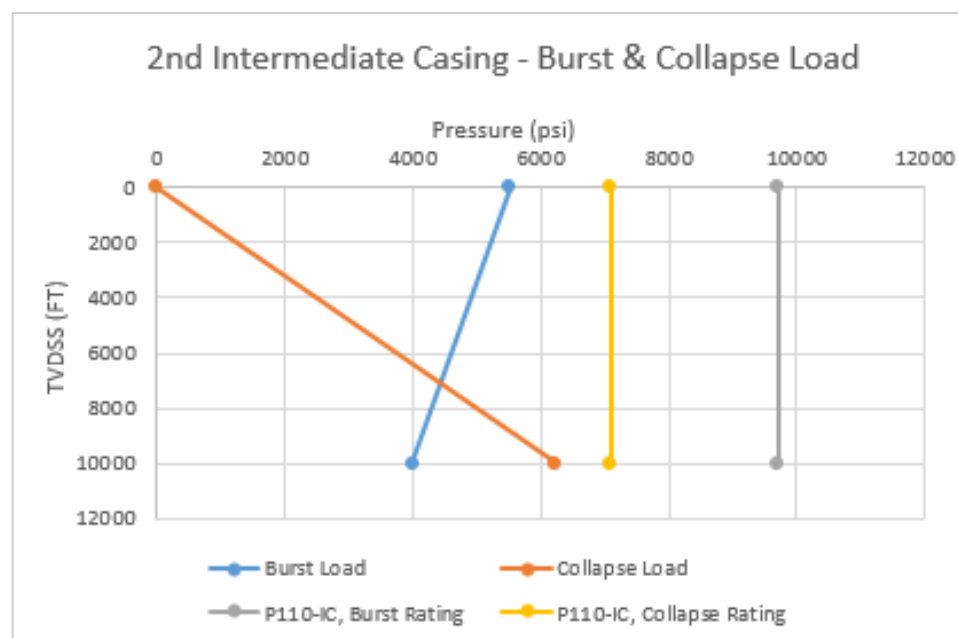


Figure C2.2. Burst & Collapse Load Demonstration for 9 5/8" Intermediate Casing

PRODUCTION LINER DESIGN

	TVDSS (ft)	External Load (psi)	Internal Load (psi)	Net Load (psi)	Design Load (psi)
BURST	Surface	0	3349.6	3349.6	3684.56
	Liner Shoe (10600ft)	4409.6	6300	1890.4	2079.44
COLLAPSE	TVDSS (ft)	External Load (psi)	Internal Load (psi)	Net Load (psi)	Design Load (psi)
	Previous casing shoe	0	0	0	0
	Liner Shoe (10600ft)	6079.736	0	6079.736	6079.736

Table C2.4. Burst & Collapse Load Calculation for 7" Production Liner

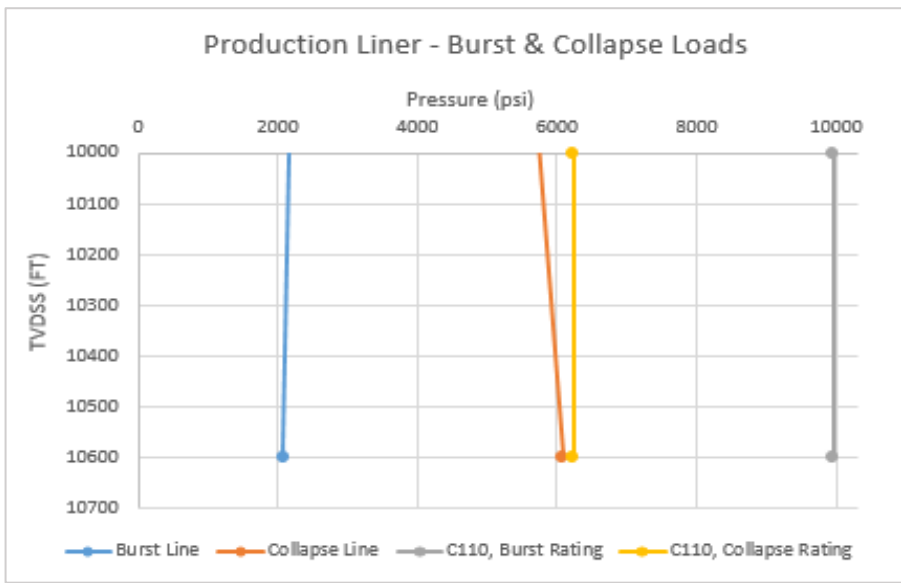


Figure C2.3. Burst & Collapse Load Demonstration for 7" Production Liner

RESULTS OF TENSION LOAD CALCULATIONS

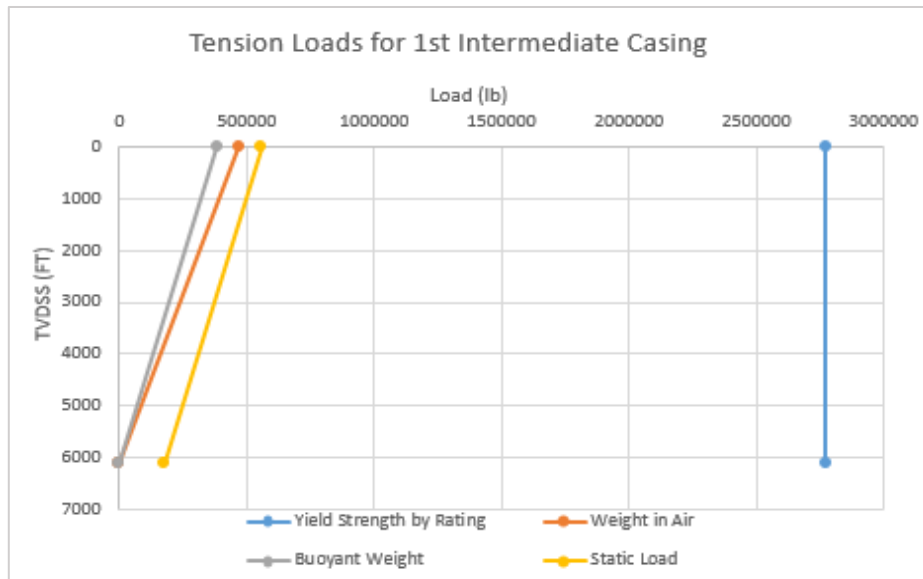


Figure C2.4. Tension Load Demonstration for 13 3/8" Intermediate Casing

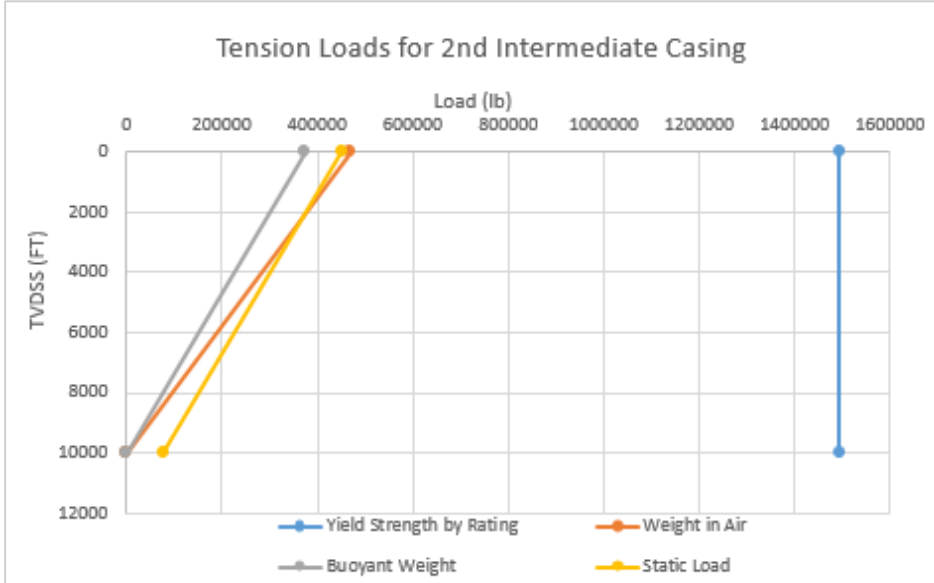


Figure C2.5. Tension Load Demonstration for 9 5/8" Intermediate Casing

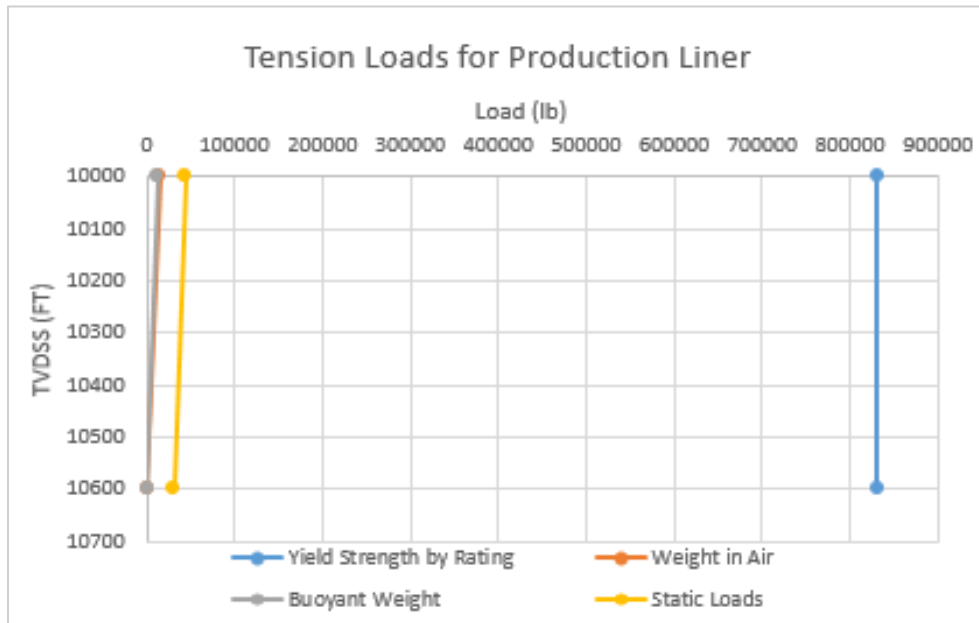


Figure C2.6. Tension Load Demonstration for 7" Production Liner

Appendix C3. Cementing Design

Cementing calculations of 13 3/8" intermediate casing is demonstrated as an example. Figure 1 can be helpful to visualize cementing operation and necessary data for calculations is provided at the Table 1.

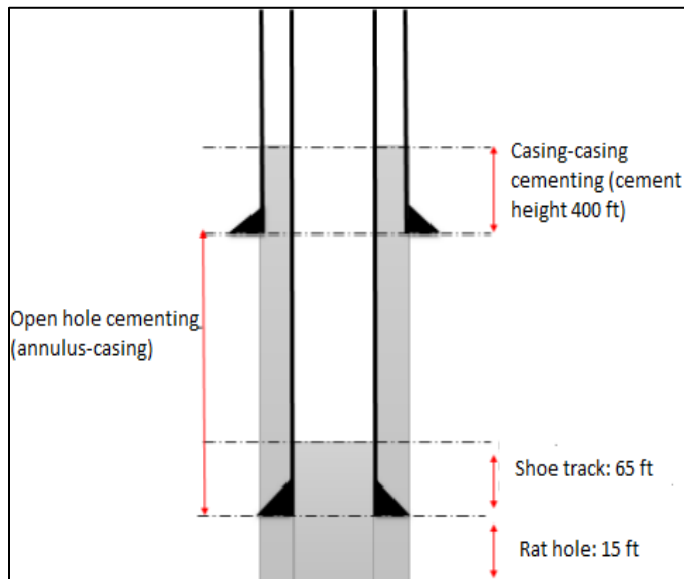


Figure C3.1. Description of cement job

Parameters	Value	Unit
Casing Setting Depth	6100	ft
Previous Casing Shoe	4500	ft
Hole Size	17.5	in
Casing ID	12.275	in
Casing OD	13.375	in
Previous Casing ID	18.376	in
Rate Hole	15	ft
Shoe Track	65	ft
TOC	4100	ft
Excess	20	%
Yield of Class G cement	1.14	ft ³ /sk
Mixwater requirements	4.97	Gal/sk

Table C3.1. Cementing Calculation

1. $V_{\text{Shoe Track}} = 65 * \left(\frac{12.275}{12}\right)^2 * \frac{\pi}{4} = 53 \text{ ft}^3$
2. $V_{\text{Rat Hole}} = 15 * \left(\frac{17.5}{12}\right)^2 * \frac{\pi}{4} * 1.2 = 30 \text{ ft}^3$
3. $V_{\text{Casing-Hole Annulus}} = 1.2 * 1665 * \frac{17.5^2 - 13.375^2}{144} * \frac{\pi}{4} = 1388 \text{ ft}^3$

4. $V_{\text{Casing-Casing Annulus}} = 400 * \frac{18.376^2 - 13.375^2}{144} * \frac{\pi}{4} = 346 \text{ ft}^3$
5. $V_{\text{Total}} = 53 + 30 + 1388 + 346 = 1817 \text{ ft}^3$
6. $\text{Number}_{\text{Sack}} = \frac{1817}{1.14} = 1594$
7. $V_{\text{Mixture Water}} = 1594 * 4.97 = 7922 \text{ Gal} = 188 \text{ bbl}$
8. $V_{\text{Displacement Fluid}} = \left(\frac{12.275}{12}\right)^2 * \frac{\pi}{4} * (6615 - 65) = 5383 \text{ ft}^3 = 959 \text{ bbl}$

Note: In the calculations, TVD (height) is not utilised to determine length of casings, which should be cemented. Because well is deviated and therefore, extra calculations are done to determine the length of casing.

Appendix C4. Directional Drilling

With the help of the following graph (Figure 1), calculation process of different parameters can be easily understood.

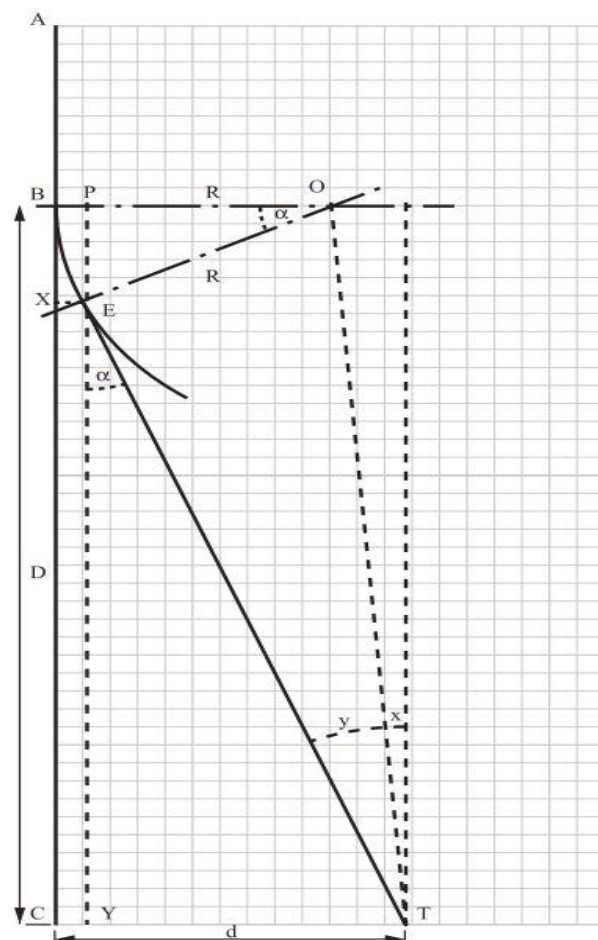


Figure C4.1. Design of Well Trajectory

In this graph, R (or OE) is the radius of Build-up section and with the following calculation (1), it can be determined.

$$R = \frac{100*360}{2*\pi*\gamma^\circ} = \frac{100*360}{2*\pi*2.7} \approx 2122 \text{ ft (1)}$$

At the next step, tangent angle (α) should be determined with the calculations below.

$$D = TVD - KOP = 10600 - 4950 = 5650 \text{ ft (2)}$$

$$\tan x = \frac{d-R}{D} = \frac{4400-2122}{10600-4950} = 0.40 \text{ (3)} \quad x = \tan^{-1}(0.40) \approx 21.8^\circ$$

$$\sin y = \frac{R*\cos x}{D} = \frac{2122*\cos 21.8^\circ}{4400} = 0.45 \text{ (4)} \quad y = \sin^{-1}(0.45) = 26.7^\circ$$

$$\alpha = x + y = 21.8^\circ + 26.7^\circ = 48.5^\circ \text{ (5)}$$

Then, Along Hole Depth was calculated with the next equation.

$$AT = AB + EB + ET$$

In this equation, AB is length of vertical section till KOP point and equal to 4950 ft. However, other two parameters (EB and ET) was determined with in the following form.

$$EB = \frac{2*\pi*\alpha*R}{360} = \frac{2*\pi*48.5*2122}{360} \approx 1796 \text{ ft (6)}$$

$$ET = \frac{D-R*\sin \alpha}{\cos \alpha} = \frac{5650 - 2122 * \sin 48.5^\circ}{\cos 48.5} \approx 6128 \text{ ft (7)}$$

Then

$$AT = 4950 + 1796 + 6128 = 12874 \text{ ft (8)}$$

Horizontal Departure (ft)	TVD (ft)	Inclination Angle($^{\circ}$)
0	0	0
0	4950	0
1	5024	2
5	5098	4
12	5172	6
21	5245	8
32	5318	10
46	5391	12
63	5463	14
82	5535	16
104	5606	18
128	5676	20
155	5745	22
183	5813	24
215	5880	26
248	5946	28
284	6011	30
322	6074	32
363	6137	34
405	6197	36
450	6256	38
496	6314	40
545	6370	42
596	6424	44
648	6476	46
702	6527	48
716	6539	48.5
4400	10600	-

Table C4.1. Well Trajectory Data

Appendix C5. Perforation Design

Explosive type	Wireline conveyed (~1 hour exposure)	Tubing conveyed (100 hour exposure)
RDX	160° C	110° C
HMX	200° C	140° C
HNS	260° C	230° C

Table C5.1. Typical maximum allowable reservoir temperatures for different types of explosives

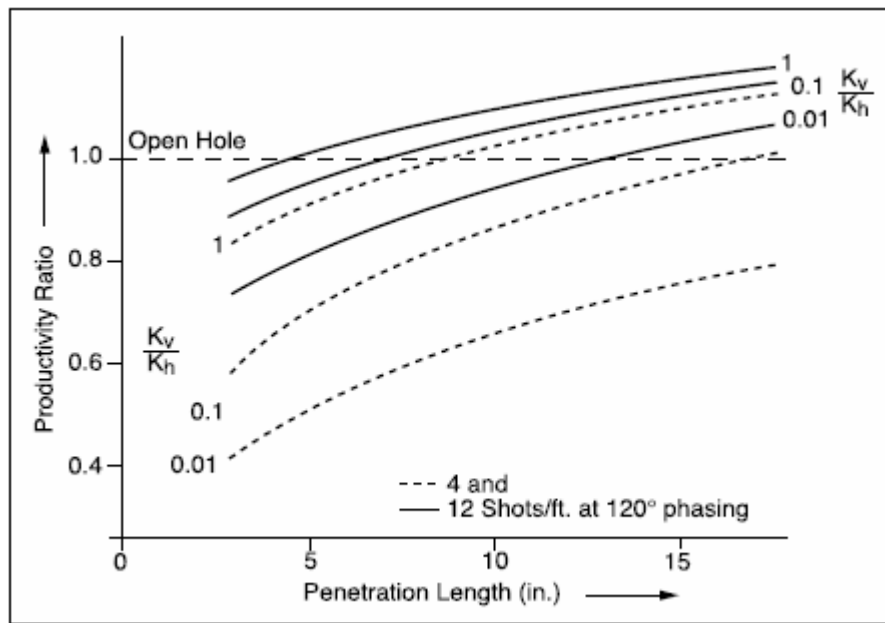


Figure C5.1. Influence of vertical & horizontal permeability and perforation density on productivity